DURBAN UNIVERSITY OF TECHNOLOGY
INYUVESI YASETHEKWINI YEZOBUCHWEPHESHE

Controlled Switching of 11 kV Vacuum Circuit Breaker for Fault Interruption

By

Goolam Hoosen, Nadeem
Student No. 20502637

A dissertation submitted in fulfilment of the requirements for the Master of Engineering Degree in the Department of Electrical Power Engineering, Faculty of Engineering and the Built Environment

Durban University of Technology

Supervisor: Dr Evans Eshiemogie Ojo
Co-Supervisor: Prof Nelson M. Ijumba

June, 2022

DECLARATION

I hereby declare that this dissertation is my work, and each text has been correctly referenced or cited. Moreover, this work has not been previously published in portion or whole for another degree at any other University.

This research was duly supervised by Dr. Evans E. Ojo and Prof. Nelson M. Ijumba at the Durban University of Technology.

Submitted by:

01 June 2022

… …. ……

Goolam Hoosen, Nadeem Date

Student Number: 20502637

Approved for Final Submission by:

18-07-2022

…… . ……

Supervisor: Dr. Evans E. Ojo Date

22 July 2022

…… …. ……

Co-Supervisor: Prof. Nelson Ijumba Date

Dedication

"I am…
Who I am,
Because of ALLAH Subhanahu wa ta'ala my Creator,
our Prophet Muhammad SalAllahoo Alaihi Waa Alihi Wasalam
and my FAMILY,
Who have been in my life, all my life,
Because of all the love,
Because of all the Blessings,
And all the inspiration"
Thank You!

Acknowledgements

I would like to acknowledge the following:

- My supervisor, Dr. Evans Eshiemogie Ojo for the guidance during this research and continuous support throughout every step towards the successful completion of this dissertation. Also, I would like to use this opportunity to acknowledge my supervisor for the knowledge he has imparted onto me and the sacrifices he had made to help me complete this master's programme. Thank you

- My Co-supervisor, Prof. Nelson M. Ijumba for his technical support, the guidance provided and the research articles which assisted me in writing this dissertation. Thank you

Abstract

Fault currents are identified as the reason for the poor quality of supply in a power system. The circuit breakers are the most dynamic and transient equipment in transmission and distribution power systems and they are the main interrupter for the clearing of faults. In the power system, 95% of faults occur in the medium voltage network. If a faults occurs and is not interrupted timeously by the circuit breaker, the entire system ages faster.

It was identified that the arcing temperature during fault interruption is most responsible for the wearing of the circuit breaker arcing contacts, thus, leading to the reduced breaker lifespan. The useful life improvement was dependant on the reduction of the arcing current and power of the arc which is proportional to the arcing energy and temperature. The vacuum circuit breaker was investigated for the controlled switching technologies. A predicted controlled trip time logic equation was derived using the controlled switching methodology with the addition of using input parameter variables relevant to the circuit breaker environment to predict early current zero tripping. The environmental conditions comprised of the ambient temperature, idle time and standard circuit breaker operation time. The advanced controlled circuit breaker logic was also developed using electromagnetic transient simulation software called PSCAD to predict the earlier current zero tripping times based on the vacuum circuit breakers environmental conditions. The software uses the black box modules to mimic operation of each environmental condition namely the idle time logic controller, temperature delay logic controller and predicted current zero controller. The results for the predicted controlled trip time equation was compared to the results obtained using the simulated results on PSCAD.

The results from the predicted controlled trip equation versus the simulated advanced controlled simulated module proved to be within a 0.1% tolerance. The PSCAD software also facilitated the analysis of results for the various interruption phenomena namely the namely arc voltage, arc current, transient recovery voltage, re-ignition, restrikes, dynamism and temperature of arc that occur during the circuit breaker fault interruption. The abovementioned interruption had seen a reduction when compared to the conventional circuit breaker during fault interruption with the average arc current being reduced by 10%. The advanced controlled simulated results obtained for the interruption phenomena was thereafter benchmarked against the simulated conventional vacuum circuit breaker using the Arrhenius equation to determine its impact on the circuit breaker useful life.

The results for the advanced controlled switching circuit breaker had proven an average of 7% improvement in useful life when compared to a conventional circuit breaker. The 7% improvement proved to increase the circuit breaker lifespan for an average of 20 years to 21.4

years. This is a 1.4-year improvement in the circuit breaker lifespan. Thus, the cost of replacement of the circuit breaker may be deferred by 1.4 years but this has a significant impact on the total annual capital expenditure budget due to the number of circuit breakers used.

Table of Contents

List of Figures

List of Tables

Acronyms

A	Amperage
AC	Alternating Current
ACS	Advanced Controlled Switching
ACSS	Advanced Controlled Switching Systems
ACSR	Aluminium Conductor Steel Reinforced
ASEA	Allmänna Svenska Elektriska Aktiebolaget
AP	Apparent Power
BPA	Bonneville Power Administration
CAPEX	Capital Expenditure
CIGRE TF	Conseil International des Grands Réseaux Electriques Technical Forum
CIGRE WG	Conseil International des Grands Réseaux Electriques Work Group
CuCr	Copper-Chromium
CT	Current Transformer
CS	Conventional Switching
CSS	Controlled Switching Systems
DC	Direct Current
EMTP	Electromagnetic Transient Program
RTD	Resistance Temperature Detector
RYB	Red Yellow Blue
RMS	Route Mean Square
HV	High Voltage
IEC	International Electrotechnical Commission
IEEE	Institute of Electrical and Electronics Engineers
MCB	Mini Circuit Breaker
MVAC	Medium Voltage Alternating Current
MV	Medium Voltage
MVA	Mega Volt Amperes
NERSA	National Energy Regulator of South Africa
OPEX	Operational Expenditure
PSCAD	Power Systems Computer Aided Software
SA	South Africa
SAIDI	System Average Interruption Duration Index
SAIFI	System Average Interruption Frequency Indices

Sf6	Sulfur Hexafluoride
SN	Simulation Number
TRV	Transient Recovery Voltage
VCB	Vacuum Circuit Breaker
VT	Voltage Transformer
YNd1	Star Neutral Delta 30°

Chapter 1

Introduction

1.1 General Background

The increase in demand for power is making it more difficult for power utilities to maintain the efficiency of power system generation and distribution, which ranges from the large to the medium industrial users, municipalities, commercial and domestic users. Power utilities are continuously facing challenges of remunerating funds for their capital expenditure (CAPEX) which is required for the upgrading and installing of additional infrastructure to cater for the additional power demand. Another challenge experienced by power utilities is the recuperating of funds for the operational expenditure (OPEX) which is used for maintaining the existing infrastructure, vital for maintaining the existing power demand.

The OPEX is increased when the power system experiences fault currents and power losses. This results in low power quality on the lines which directly impacts the revenue generated by the power utilities. This impact of power quality eventually leads to equipment failure which results in the increase in the CAPEX. In essence both the CAPEX and the OPEX are directly affected by the poor quality of supply.

The supply of power to all aspects of the nation is fundamental and it vital that the consumptions of power is delivered without interruption hence, the quality of power supply needs to be maintained. Quality of power supply parameters within the South Africa electrical network are governed and made to operate within a regulation or standards set by the National Energy Regulator of South Africa (NERSA). However, these standards cannot be achieved when equipment lifespan is reached prematurely due to it not being able to withstand temporary anomalies or surges. Equipment installed on the power system needs to be able to withstand temporary surges in deviation from the power quality parameters so that the equipment replacement is prolonged. This help in mitigating the CAPEX deficits for the power utilises.

The inability of protection systems and circuit breaker to clear faults on time is mostly responsible for power equipment failures such as the transformers failure. This also causes the circuit breakers to fail over time due to effects of inrush currents and arcing. The concept of controlled switching systems (CSS) is a method used in controlling the timing of the pre-strike (for close operations) or contact separation (for open operations) for each pole of a circuit breaker. This is with respect to the phase angle of the system voltage or the current in order to minimize stresses on the components of the power system. In high voltage application,

controlled breaker switching has been developed to control the operation of the circuit breaker, such that it closes the breaker at the earliest currents zero point. This occurrence takes into account the effects of the breaker idle time and temperature when energizing the breaker. This is to ensure that the circuit breaker is energized at a time with the least effects of arcing and inrush currents. Controlled switching technology was also developed with the capability of only energizing at the earliest currents zero without the intelligence to take into account the effects of idle time and temperature when energizing a circuit breaker. In addition, the controlled breaker switching can also be implemented on circuit breaker opening with the combination that it trips quickly and at the earliest currents zero time with the intelligence of taking into account the effects of idle time and temperature. This is to prevent damage to the major electrical equipment and the circuit breakers. The implementation of this concepts are rarely applied on medium voltage applications for fault interruption and this is rarely done using the vacuum circuit breaker.

1.2 Problem Statement

Research indicates that short circuit faults account for 95 % of the electrical faults that occur on a power system [1]. The survey conducted by CIGRE QG A3.06 across 21 countries power systems on the reliability of high voltage equipment, indicated that 36.7 % of circuit breakers on a power system are located on voltages that are more than or equal to 60 *kV*. The survey also indicates that 54 % of the circuit breakers are used for protecting the overhead power lines [2]. This effectively indicates that the majority of the power systems are located at the voltages below or equal to 60 *kV* where majority of the faults occur on power lines. The voltage below 60 *kV* are regarded as the distribution network in South Africa's power system. Thus, Eskom, Municipalities and independent power producers, the voltages such as 33 *kV*, 22 *kV* and 11 *kV* are categorized as the medium voltage systems. Hence, majority of faults in South Africa's power system are located in the medium voltage (MV) power lines. The MV network forms the largest part of the power system and it is considered as the heart of the power system [3].

The application of high voltage circuit breaker protection using controlled switching is a common practice and it is well established in the field of electrical engineering. High voltage circuit breaker applications are where most of the controlled switching research is at an advanced stage. However,the application of controlled switching on medium voltages is not well established as compared to the high voltage switching [4]. This poses a fundamentally challenge as majority of power utilities assets are located in the medium voltage networks.

Most research that are available for the controlled switching applications for the medium voltage circuit are more focused on circuit breaker closing rather than circuit breaker opening

(tripping) for fault interruption. Closing the circuit breaker to an unloaded transformer results in arcing phenomenon that can negatively affects the lifecycle of the circuit breaker. This arcing phenomenon is also present when opening a circuit breaker during fault interruption. The presence of this arcing phenomenon, requires the implementation of the controlled switching technology for fault interruption which is also essential in protecting the circuit breaker [5]. Thus, due to the limited research on medium voltage circuit breaker opening, this investigation explores the implementation of the controlled switching technology for the MV networks using the indoor vacuum circuit breaker.

1.3 Motivation

This research was necessitated by the realization of the common challenge experienced by power utilities where insufficient capital is available for maintenance, upgrades or the replacement of the aged equipment. In an effort to alleviate this challenge, the research was focused on improving equipment useful life and to extend power utilities budget for equipment replacement. In addition, allowing them with adequate time to attend to other network maintenance. The major part of the power grids is the medium voltage networks which accounts for 56 % of the network size and it is prone to faults. The common faults that was identified in the medium voltage network is the line-to-earth faults which account for an average of 95 % of its faults occurrence [2]. These findings have motivated this study and this research is in the direction of the medium voltage vacuum circuit breaker protection which forms an integral part in maintaining the power grid quality of supply. Subsequently, this has led to the investigation on how to improve the lifespan of a vacuum medium voltage circuit breaker for fault interruption. This will be achieved by adopting a protection device using the controlled switching techniques to control the breakers and the circuit switchers more accurately. Consequently, this will protect the circuit breakers which directly help the power utilities to improve their power system and the quality of power supplied. This study investigation, employs both analytical and numerically tools. The goal being, to lower the impact of faults on the MV network by improving its protective system. In conclusion, protecting the circuit breakers from the effects of arcing led by faults, contribute positively in improving the useful life of the equipment in the medium voltage networks.

1.4 Research Aims and Objectives

The aim of this research is to design, develop and model an advanced controlled switching (ACS) 11 kV indoor circuit breaker and simulate it using the electromagnetic transient program (EMTP) in order to improve the circuit breaker useful life. The aim is to model the ACS circuit

breaker while connected to a medium voltage power line during fault interruption. This is to analyze the arcing phenomena in its relation to the equipment useful life, in order to reduce the CAPEX and the OPEX costs for power utilities.

In relations to the aims of the project, the objective of this study will entail the following:

- Modelling the non-controlled or conventional vacuum breaker for fault interruption using an electromagnetic transient simulation program to ascertain the circuit breaker tripping times and interruption phenomena at several fault angles.
- Derive a functional predicted controlled trip logic equation for fault interruption time on the medium voltage circuit breaker to achieve current zero interruption [6].
- Modelling the controlled vacuum breaker for fault interruption by using the electromagnetic transient simulation program using the black box modules to simulate the circuit breaker environmental conditions in order to achieve the current zero tripping.
- Use the controlled simulated model to simulate the vacuum circuit breaker interruption phenomena and analyze its results at several fault angles.
- Implement a comparative study for results from the interruption phenomena. The results extrapolated from simulation of the non-controlled vacuum breaker which will be used as the baseline in comparison to the controlled vacuum circuit breaker results for fault interruption will be used to analyze the circuit breaker useful life and then determine the improvements. The results will subsequently be compared with the predicted controlled trip logic equation to verify its accuracy.

The implementation of the above-mentioned controlled switching logic for the MV indoor vacuum circuit breaker on the MV power line during a fault current will ideally trip the circuit breaker at the earliest current zero. This will be accomplished by using the advanced controlled logic which factors in the environmental conditions of the circuit breaker to provide the least arc energy impact, thereby improving the circuit breaker operations and conversely the downstream equipment lifecycle.

1.5 Research Methodology

The research methodologies employed is this study is both analytical and the numerical coupled with the computer simulations. The functionality of the non-controlled and controlled vacuum circuit breaker tripping times under fault conditions was investigated, to develop the philosophies for the advanced controlled switching implementations on a vacuum circuit breaker. The advanced controlled simulated model, operating on the principles of the advanced controlled logic developed, was simulated using the electromagnetic transient software called

the Power System Computer Aided Design (PSCAD). This software uses the input parameters that are in form of the black box model controllers with embedded logic to calculate the relevant trip time and its impact based on the fault current magnitude and angle changes. A numerical model was developed and implemented for the non-controlled circuit breaker switching for fault interruption using the electromagnetic transient simulation program. This model provided the basis to obtain results which was then used in this study to compare controlled switching applications against the advanced controlled switching technology results in order to ascertain if the advanced controlled switching for fault interruption improves the circuit breaker useful life.

The analytical model of the advanced controlled switching technology for the vacuum circuit breaker fault interruption was completed using a predicted controlled trip logic equation. This equation incorporates the environment factors that influence the circuit breaker current zero tripping abilities. The advanced controlled switching model was developed by modifying the non-controlled switching vacuum circuit breaker model using the electromagnetic transient software to incorporate the currents zero logic, temperature logic and idle time logic for fault interruption. The results from the derived predicted controlled trip equation was compared to the results from simulated advanced controlled switching model of the electromagnetic transient simulation program in order to verify its accuracy.

The overcurrent and earth faults in the simulated model for both the non-controlled and controlled logic circuits was implemented using the instantaneous overcurrent relay pick up, with currents rating which is in line with the simulated fault currents applied. The analysis for fault interruption for all simulations was only tested against phase-to-phase faults with the synchronized breaker pole tripping, operating at no more than half a cycle apart in the Red, yellow, Blue (RYB) sequence.

The measurements of both the non-controlled and controlled logic vacuum circuit breaker simulated model were implemented using the voltage and current transformers. This was completed by the interconnection between the simulated switching circuitry model to provide the processed output measurements of the arcing phenomena at several fault current tripping angles. These results obtained was used to analyze the impact of the interruption phenomena on the circuit breaker for both non-controlled and advanced controlled switching. The energy and temperature of the arc was also calculated with the results transposed into the Arrhenius equation to determine lifecycle improvements of the advanced controlled circuit breaker as compared to the conventional control switching.

1.6 Hypothesis

The operation of a circuit breaker during fault interruption causes electrical discharges within the circuit breaker chamber that result in arcing phenomenon. This phenomenon negatively affects the circuit breaker contact material leading to reduction in the circuit breaker lifecycle. The controlled switching technology is a predetermined control strategy for operating the circuit breaker pole in order to reduce switching transients, prevent equipment failures, and improve power quality.

The medium voltage circuit breaker which accounts for the majority of the power grid's circuits breakers are mostly affected by this phenomenon. Hence, the hypothesis for this study:

"The viability to develop advanced controlled switching for medium voltage alternating current (MVAC) circuit-breakers, in particular for the 11 *kV* network"

1.7 Structure of Dissertation

Chapter 1 discusses the rationale for this study which includes the background, problem statement, motivation, research aims and objectives and the hypothesis.

In Chapter 2, the faults on a power system and its adverse effects coupled with the reasons for the implementation of protection systems are discussed. The initial focus is on the investigation of a conventional circuit breaker and subsequently shift to the more advanced protection systems available namely the advanced controlled switching technology.

Chapter 3 entails the concepts of modelling and simulation of logical flow for the advanced controlled switching. This chapter presents both the electromagnetic transient MV model for both the non-controlled circuit breaker and the advanced controlled circuit breaker together with its related logic flow charts.

Chapter 4 presents the results and analysis of results from the computer simulations. The results from the MV modelled non-controlled vacuum circuit breaker was compared to the advanced controlled vacuum circuit breaker. The results are presented numerically and displayed graphically. This aids in establishing the basis for analysing the effects of the controlled switching technology with relevant to the lifecycle improvements. This analysis subsequently provides an in-depth view of how the circuit breakers are impacted by the faults, which then help to determine if the lifespan of the circuit breaker has improved with the advanced controlled switching technology.

Chapter 5 is dedicated to the conclusion of this study and recommendations for future areas of investigation. Thus, the chapter summarises the research carried out in this study and provides the recommendations for prospect of areas of future study based on the outcomes of this work.

Chapter 2

Literature Review

2.1 Introduction

Power system consist of the network architecture that is designed to transfer power from generations station to distribution network over several kilometers. Thus, the power system from the point of generation to the load centres is split into three areas namely generation, transmission and distribution as shown in Figure 2.1. This division is determined by the electrical characteristics as a function of the level of voltage and current. The effectiveness of the electrical power system is measured by ability of the components in the power system to maintain continuous supply of power.

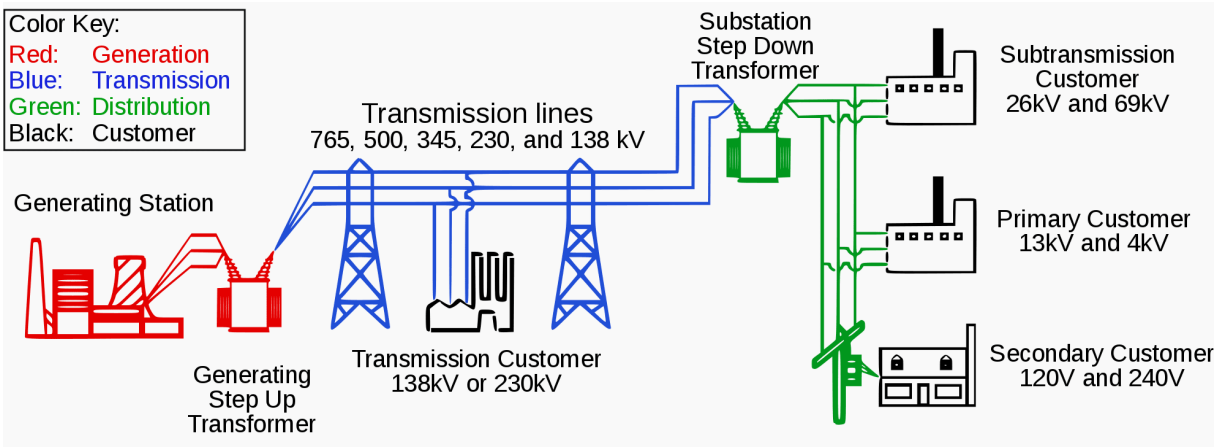

Figure 2.1: The Power Systems Layout [7]

The purpose of the generation network is to generate the power at a lower voltage at approximate 22 *kV*, to reduce cost of the stator winding insulation which increases as the voltage is increased [8]. The lower voltage is stepped up by a transformer in order to transmit the power through the transmission network. The reason for the voltage stepped-up in the transmission grid is to reduce heat losses and the size of the line conductor, thereby making it more economical. The stepped-up voltage also mitigates voltage drop so the power is transported over a long distance. The power is subsequently stepped-down and supply to the distribution network to allow for higher current flow at the medium voltage for the reticulation networks. For the consumption of power by consumers, the distribution voltage is then stepped down further to a lower voltage by a local transformer for domestic customers. The focus of this research was on the distribution power system network configuration at a voltage of 11 *kV*.

The distribution power system configuration incorporates several characteristics that are each important for its functionality. These characteristics consist of the distribution Power system

typology which may be connected in a form of radial network or ring network. The phasing of the power system which forms an important part of the power system configuration can either be connected using the star or delta connection. The medium voltage bus-bar configuration and the supply voltage and frequency are other important characteristics of the network configuration.

2.2 Bus-bar Configuration

Bus-bar are used in generating stations, substations and switch stations as a common coupling point for the feeders which operate at constant voltage [9]. Bus-bars are used in both indoor and outdoor power systems. The indoor medium voltage switchgear which is applicable to this dissertation uses the flat copper bus-bars as a common voltage source to receive power from the incoming feeders and supply power to the outgoing feeders.

The bus-bars configuration may be in a form of a single bus-bar, double bus-bar system or breaker-and-a half. The breaker-and-a-half configuration is usually used in high voltage networks. The single and double bus-bar systems are implemented in both high voltage and medium voltage applications.

The single or straight bus as shown in Figure 2.2 is the most common medium voltage bus-bar configuration used by power unities in both indoor and outdoor bus-bar systems. The configuration is such that the common copper flat bus-bar is divided or sectionalized into two sections using bus-section circuit breakers or a bus section isolator. If a fault occurs on one side of the bus-bar, the other side of the bus-bar is not affected by the fault. The impedance is increased as a result of the bus-bar sectionalizing from the normally opened position resulting from the principles of Ohms law of a parallel circuit, this lowers the fault currents on the bus-bar. This configuration also aids with maintenance where one side of the bus-bar may be isolated for maintenance while the other side is energized, thus, ensuring continuity of supply to consumers. In term of safety during load transfer and uncoupling of the bus-bar, its preferred to use a circuit breaker for sectioning rather than an isolator switch. Single bus-bar systems, as a result of its limited supply flexibility, are implemented when two or less incoming feeders or transformers are supplying power to the medium distribution board [9, 10].

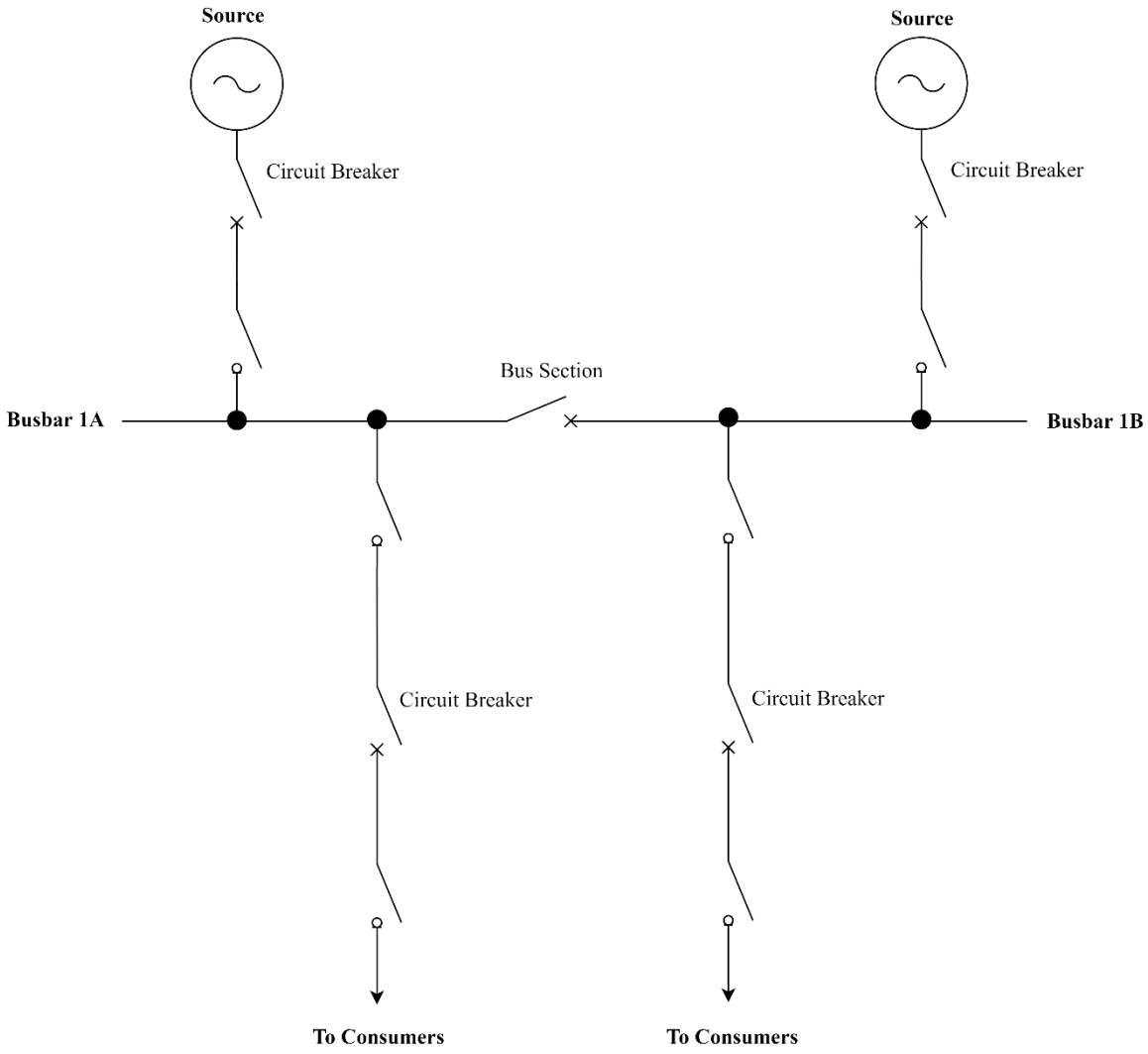

Figure 2.2: Configuration of the Single Bus-bar System [9]

The double bus-bar system is used at supply substations or switch stations where breakdown or interference should have minimal impact on the continuity of supply. The configuration of the double bus-bar consists of two bus bars namely the main bus-bar and the spare bus-bar where the main bus-bar is positioned above the spare bus-bar as shown in Figure 2.3. The main and spare bus-bar are coupled together using a bus-coupler breaker or an isolator similar to the bus section in the single bus-bar configuration. Each incoming feeder or transformer and outgoing feeder is connected to the main and spare bus-bar via isolator switches. The configuration is such that it allows for individual feeders to be continually fed irrespective of the physical position of the feeder on the indoor bus-bar unlike the single bus-bar system which can only feed the feeders on the un-faulted side of the bus-bar [9, 10].

The double bus-bar system, due to its flexibility are applied where three or more incoming feeders or transformers are being used. This is to ensure that any of the incoming feeders or transformers are able to supply any of the outgoing feeders. The costs attributed to installing a

double bus-bar system is high hence the implementation of this configuration needs to be weighted on the criticality of the type of power consumers on the network. This configuration is suited for main substations or switching stations where the power consumers are the large industrial users or a hospital. In areas where space is constrained, the implementation of double bus-bar systems will prove to be difficult.

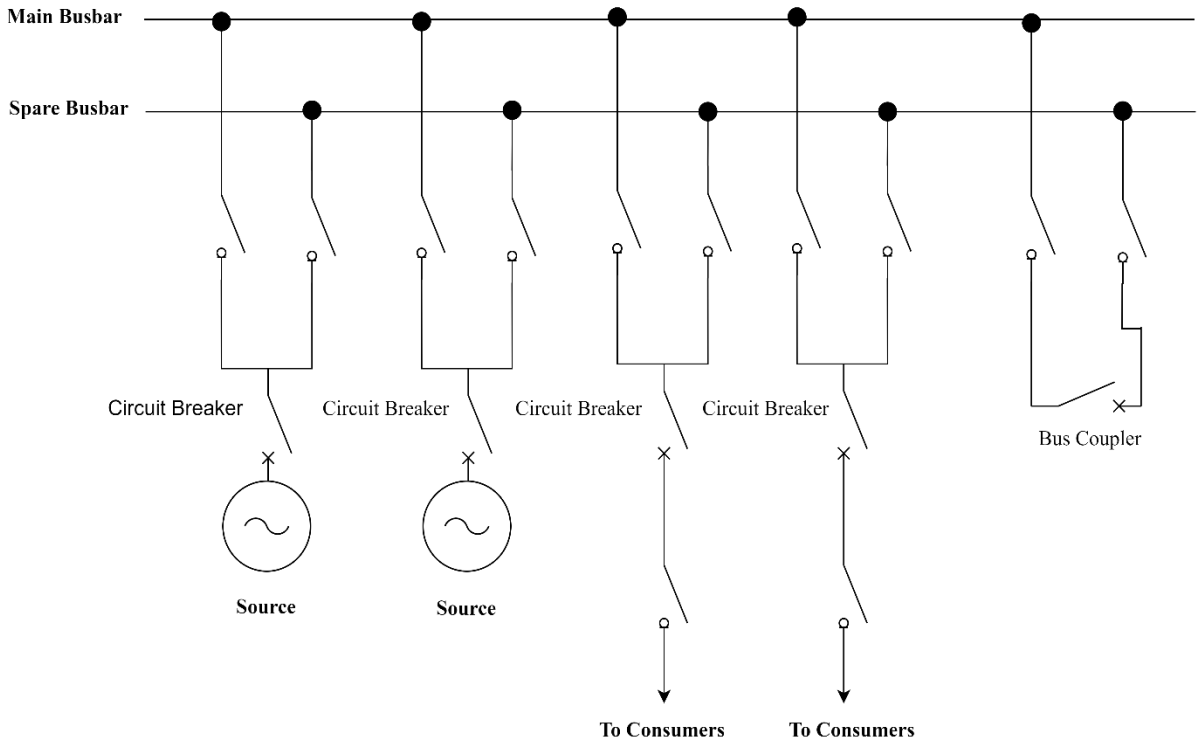

Figure 2.3: Configuration of the Double Bus-bar System [10]

The circuit breakers in the abovementioned bus-bar configurations of both single and double bus-bar systems are the key components to ensure that the system is protected by isolating the fault. In this study, flexibility of incoming feeders to outgoing feeders will not be required as a result of the limited number of incoming and outgoing feeders. The fault currents in this investigation will be limited to the upstream by the neutral earthing resistor, hence, the single bus-bar system configuration will be implemented. The selected system architecture for this dissertation will consist of two incoming feeders, a bus-section breaker and two outgoing feeders as shown in Figure 2.4.

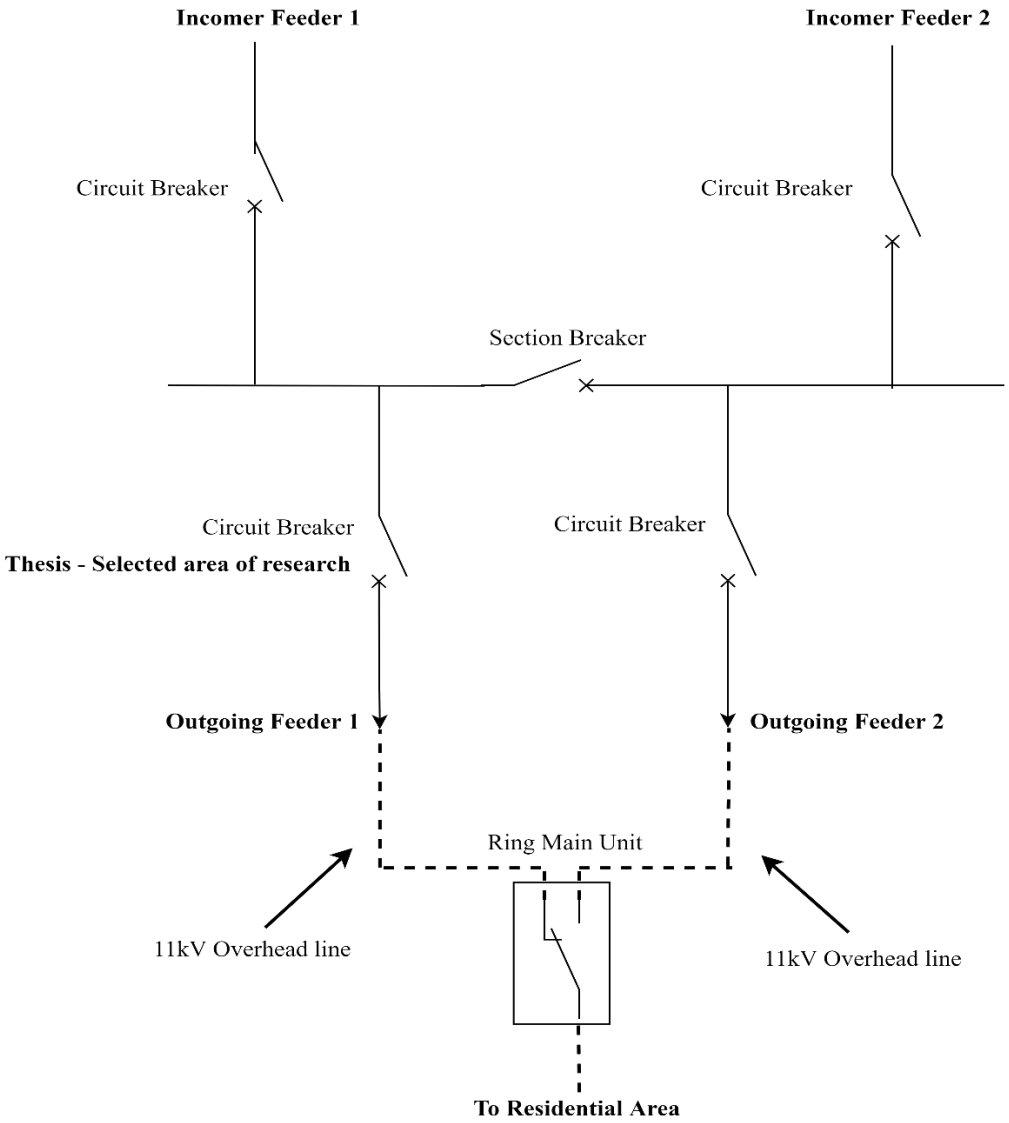

Figure 2.4: Architecture of Single Bus-bar Selected [9]

Reliable power supply is obtained by connecting both the outgoing feeders to the residential area via a ring main unit which will normally be in the open position. In the event that one of the feeders fail, the alternate feeder will be able to provide a back-up supply to the consumers thus, allowing the flexibility of supply to the residential area from both the incomers without the implementation of the double bus-bar system. However only one of the outgoing feeders, namely the outgoing feeder number 2 will be analysed during this dissertation as the results obtained from the circuit breaker specifications and operation of all the circuit breakers in the single-bus-bar configuration will be the same for the current ratings.

2.3 Bus-bar Parameters

The physical characteristics of a bus-bar in terms of the cross sectional area increases as the currents carrying capacity requirements are increased at a specific ambient temperature. This is to allow the bus-bar to withstand both the nominal currents being carried and the short circuit

fault currents. In countries where the ambient temperature is higher, the cross sectional area requirements is higher as a result of the bus-bars thermal rating for the same rated current carrying capacity. The bus-bar during operation dissipates heat from the energy transfer due to the bus-bar resistance which opposes the flow of currents. Hence, this form some of the electrical energy loss by the system in the form of heat and the dissipated heat is absorbed by the surrounding air. The maximum allowed temperature rise the copper bus-bar can operate is at $105\,°C$ and aluminium temperature for bus-bar is at $90\,°C$. The maximum permissible temperature for the bus-bar is calculated using equation (2.1) [11]:

$$M_T = \left(\Delta T + T_A\right) \tag{2.1}$$

Where ΔT = the temperature-rise on the bus-bar and T_A = the ambient temperature of the switch-room. The ambient temperature inside the switch-board used for this study will not exceed $35\,°C$ while the outside temperature of the switchboard which is in the switch-room will not exceed $40\,°C$. This ambient temperature of the switch-room at $40\,°C$ is applicable to the South African temperature conditions. In essence, the copper bus-bar used is able to withstand a temperature rise of $70\,°C$ [11].

The parameters of bus-bar are defined in terms of resistance, reactance and impedance characteristics. The physical characteristic measurements of resistance, reactance and impedance for a 630 *A*, 1250 *A* and 2000 *A* currents rated bus-bar at a rated ambient temperature of $40\,°C$ used for modelling and the link performance analysis is tabulated below in Table 2.1:

Table 2.1: Bus-bar Physical Parameters [11]

Currents levels [*A*]	**Fault currents [*kA*]**	**Resistance [$m\Omega/m$]**	**Reactance [$m\Omega/m$]**	**Impedance [$m\Omega/m$]**	**Weight [*kg* / *m*]**	**Conductor size [*mm* x *mm*]**
630	25	0.121	0.027	0.124	7.9	6.3 x 40
1250	31.5	0.044	0.013	0.046	13.9	6.3 x 110
2000	31.5	0.026	0.008	0.027	21.7	6.3 x 200

The selected bus-bar conductor size for the purpose of this study was the 630 *A* bus-bar using a 6.3 *mm* x 40 *mm* flat copper bar per phase. This bus-bar within the switchboard will be able to provide the currents carrying capacity, with the ability to dissipate the heat adequately thereby preventing any thermal breakdown. The short circuit fault currents rating emanating from the power system on the 11 *kV* board will not exceed 25 *kV* therefore specifying that the fault current rating which is greater than 25 *kV* will not be required. Specifying the equipment with ratings more than the requirements increases the price which is not economically viable hence, 25 *kA* short circuit current rating will suffice.

2.4 Frequency and Quality of Supply

2.4.1 Frequency

The power generated in any of the power system should be equal to or greater than the power demand on the system. If the power demand increase, the power supply available or generated is less, this will cause the frequency to decrease. Frequency deviations can also occur when there are electrical faults on power systems or the disconnection of large loads, this affect the power supply quality.

The effects of frequency deviation during an electrical fault such as the short circuit fault causes an increase in currents which is as a result of the reduction in the inductance on that faulted line that forms part of the system resulting in a voltage drop. During this fault, the protection equipment of that related subsystem of the electrical power system react, causing the protection to operate and the circuit breakers to trip, consequently isolating the fault from the remaining part of the electrical system.

The interrelated voltage, current and impedance deviations will affect the quality of supply power to the consumers due to the decline in power, as a result, there will be a decrease in power that will result in the frequency of the system to drop [12]. Power systems operate at either 50 *Hz* or 60 *Hz* which is dependent on a country's national standard. Frequency is the rate of which current changes over a period of time, the higher the frequency, the longer it takes the cycle to complete a current sinusoidal waveform. The South African national frequency is 50 *Hz*. In a 60 *Hz* power system, a single current waveform cycle is completed in 0.016 *s* compared to a 50 *Hz* supply which completes a current waveform cycle in 0.02 *s*. When a fault occurs on a system in South Africa, the 50 *Hz* system allows the protection equipment a few milliseconds more to reach the current zero as compared to the 60 *Hz* supply. This determines the grading and protection relay response coupled with the use of controlled switching technologies, the protection relays will have more time to react to a fault with little impact on the power system equipment [13]. The heat generated from the 50 *Hz* supply is also slightly lower as compared to the 60 *Hz* supply and this also affects the lifespan of the equipment [13]. The advantages of the 50 *Hz* supply are evident from the abovementioned parameters hence the power supply and equipment used for this investigation will be rated to operate at a frequency of 50 *Hz*. To ensure compliance to the National Energy Regulator of South Africa (NERSA) , the frequency of the system connection will not exceed 2 % or 1 *Hz* of the national regulated frequency of 50 *Hz* [14].

2.4.2 Quality of Supply

Voltage levels and frequency are parameters that affects the power system configuration which have a direct impact on the quality of power supply in a power system.

The quality of supply in distribution system is measured by the sustained interruption indices which are defined as follows [15]:

- The system average interruption frequency indices (SAIFI) which is expressed by the number of customer interruptions per annum over the total number of customers served.
- The system average interruption duration index (SAIDI) is expressed by the number of customer interruption durations per annum over the number of customers served.

The SAIFI and SAIDI calculations for power systems are completed in accordance to NRS-047-1 by power utilities to determine the supply quality. When a medium voltage interruption occurs in the form of a fault on the network for a period greater than $120\,s$, the power utility is penalized by NERSA as a result of its impact on the network reliability indices. This effectively necessitates equipment reliability to ensure quality of supply indices are maintained and penalties are subsequently avoided.

The reliability of protection system is important and the implementation of controlled switching technology to protect the power system equipment from deteriorating, coupled with clearing the fault timeously is equally important. Equipment failure affects the SAFI and SAIDI parameters hence the implementation of technology to assist in reducing the interruptions on the network will effectively improve the overall quality of supply.

2.5 Faults in Power Systems

Faults in power systems are caused due to abnormal conditions that results in energy being wasted. The abnormal conditions may be categorized as either shunt faults or series faults. Shunt faults are primarily caused by short-circuit conditions while series faults are caused by open circuit conditions. The open circuit and short circuit fault conditions are caused by adverse weather conditions, human error, equipment failure etc. The impact of the abnormal conditions result in a deviation from the nominal voltage, frequency and current ratings of equipment or system. These higher current and voltage values create an imbalanced system that causes insulation breakdown of power system apparatus resulting in loss of power flow to consumers, damage to equipment within the power system and even danger to human and animal life [16].

2.5.1 Types of Faults

Faults types are categorized by its fault condition. These fault conditions are either caused by an open or short circuit. Open circuit faults occur when one or more conductor phases are broken or out of circuit therefore increasing the voltage, frequency and decreasing the current. The open circuit fault occurs in series with the line, this is why this type of fault is also called series fault. Short-circuit faults occur due to the insulation failure between phase conductors or between earth and phase conductors or both [17]. The short-circuit fault causes the circuit voltage to decrease while increasing the current. Short circuit faults are further divided into symmetrical and asymmetrical faults. Symmetrical faults are very severe faults but occur less frequently in power systems. The faults are balanced and occur either across all phases only or between all phases and ground.

Asymmetrical faults occur frequently but are less severe and do not involve the entire three phases. These faults occur as a result of single line to ground faults, line to line faults or double line to ground faults. The fundamentals explanations for the open and the short circuit faults are as follows:

- Open circuit: Open circuit faults are the least common faults which include joint failures of cables and overhead lines, and failure of one or more phases of a circuit breakers. The faults also occur due to melting of conductors in one or more phases. Open circuit faults account for 5 % of the electrical faults in a three-phase power system. These are unsymmetrical or unbalanced type of faults except for three phase open fault.
- Short circuit : Short circuit faults are defined as an abnormal connection of very low impedance between two points of different potential [17]. The short circuit fault current in a three phase power systems is divided into three periods namely the initial sub-transient period, middle transient period and the steady state period. The initial sub-transient period lasts for the first few cycles with a very rapid decrement and a high magnitude of short circuit current hence this is the period where most damage is caused. The middle transient period is relatively longer in time with a moderate decrement and the steady state period is where the current reaches a steady value [18].

Short circuit faults are also called shunt faults and accounts for 95 % of the electrical faults on a three-phase power system. These faults are caused due to the insulation failure between phase conductors or between earth and phase conductors or both [17]. These faults may be symmetrical (balanced) or Unsymmetrical (unbalanced) type of faults depending on the fault condition namely three-phase clear of earth, three-phase to earth or phase to phase as shown below in Figure 2.5.

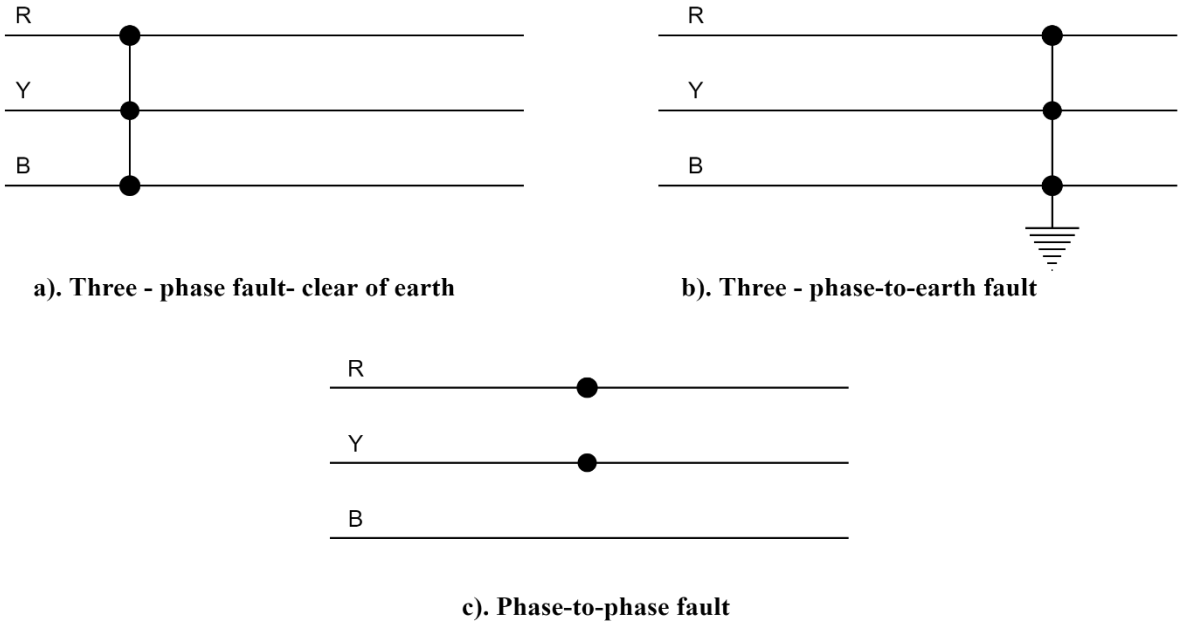

Figure 2.5: Short Circuit Fault Current Types [17]

2.5.2 Analysis of Short Circuit Faults

Short circuit faults are the most common and severe kind of faults, resulting in the flow of abnormal high currents through the equipment or transmission lines. Failure to isolate short circuit faults timeously can lead to an extensive damage of the equipment. It is imperative that the protection equipment that is capable of clearing faults swiftly are required to reduce the risk of equipment damage and maintain the quality of power supplied.

In 1905, ASEA produced one of the first protection equipment which was the relay that picked-up the unsymmetrical faults in the power system by the negative-sequence voltages and the currents that the unsymmetrical faults produce. This protection relays operate such that, after picking up the fault on the system, it subsequently sends a trip signal to the circuit breaker to isolate the unsymmetrical fault.

In [19], Ali et al. describes the nature of the short circuit fault currents having a mixture of symmetrical and unsymmetrical currents, the fault is unsymmetrical during the first few cycles and subsequent to the short circuit, it gradually becomes symmetrical after a few cycles. The unsymmetrical portion of the fault has a direct currents and alternating currents component. The direct currents are short lived and disappears after a few cycles. The decaying nature rate which is known as the “decrement “of the short circuit currents is attributed to the direct currents characteristics.

The short circuit fault currents may be calculated using the impedance method, composition method or conventional method.

The study will focus on implementing the impedance method which is explained as follows: Short circuit fault currents of a power system are calculated using Equations (2.2) – (2.8):

$$I_k = \frac{U_n}{Z} \tag{2.2}$$

Where, I_k = the fault currents, U_n = the applied voltage and Z = the summarised impedance [20]. The fault currents equation above may be manipulated to suite the type of faults on the power system namely, phase to phase, 3 phase and phase to earth [20]. This dissertation will focus on phase to earth faults using the equation (2.3):

$$I_k = \frac{\sqrt{3}U_{LN}}{2Z} \tag{2.3}$$

Where, I_k = the fault currents, U_{LN} = the applied line to neutral voltage and Z = the impedance. The impedance (Z) is the sum from the source of supply to the point at which the fault occurs [21]. In this dissertation, the sum of the transformer, the cable to the MV breaker and the MV overhead line impedance will add up to obtain the impedance (Z). The impedance of the transformer is calculated using the sum of equation (2.4) – (2.5) [19]:

$$\text{Resistance : } R_T = \left(\frac{U_r}{100}\right).\left(\frac{\left(\frac{U_n}{S_n}\right)^2}{S_n}\right) \tag{2.4}$$

Where, U_r is the percentage resistance, U_n is the applied voltage and S_n is the apparent power.

$$\text{Reactance : } X_T = \left(\frac{U_X}{100}\right).\left(\frac{\left(\frac{U_n}{S_n}\right)^2}{S_n}\right) \tag{2.5}$$

Where, U_x is the percentage reactance, U_n is the applied voltage and S_n is the apparent power. The impedance of the MV line or cable is calculated using the sum of equation (2.6) – (2.7) [19]:

$$R_T = p\frac{l}{A} \tag{2.6}$$

Where, l = the length in km, A = the area in mm^2 and p = 1.7 x 10^{-8} Ω is for copper and p = 2.6 x 10^{-8} Ω is for aluminium.

$$X_L = k\frac{l}{1} \tag{2.7}$$

Where, l = the length in km and k = 0.4 for copper and aluminium.

The total magnitude of impedance for the above transformer, line resistance and reactance is calculated using the equation (2.8):

$$Z = \sqrt{(R^2 + X^2)} \tag{2.8}$$

The fault currents are limited by the impedance in the power system and the impedance limiting the fault currents are largely attributed to the reactive components of the power system such as transformers and reactors. During the faults, the reactance of the power system is low hence the low fault conditions here may lead to high currents faults. The circuit breaker specified is to be able to withstand the maximum possible fault currents [9].

The results from the above-mentioned fault currents equations are used for the selection of specification for the circuit breaker and related equipment to prevent equipment failure and possible risk of personnel's safety. The equipment rating for medium voltage 11 *kV* circuit breakers must be specified to accommodate short circuit fault currents of 25 *kA* and 31.5 *kA*.

2.6 Three Phase Network Fault Analysis

The 3-phase faults namely symmetrical faults and the unsymmetrical faults are investigated using quantitative analysis to determine the effects it has on the power system. The analysis of these 3-phases faults on a power system is an important step to ensuring a safe operation of each power apparatus and to accurately determine the settings of the protection devices hence ensuring a swift operation of circuit breakers to clear a fault under each condition applied [22].

2.6.1 Symmetrical Faults Analysis

Symmetrical or balanced faults on a power system results in a short circuit condition due to the fault currents occurring across the entire three phases. The phase currents are equal in magnitude with a 120° phase displacement among them hence, no mutual coupling exists between them. The 120° apart balanced three phase vectors consist of a positive-sequence, negative-sequence and zero sequence of vectors as shown in Figure 2.6. Research indicates that symmetrical faults account for only 5% of the fault occurrence on a power system which is the least occurring fault [19].

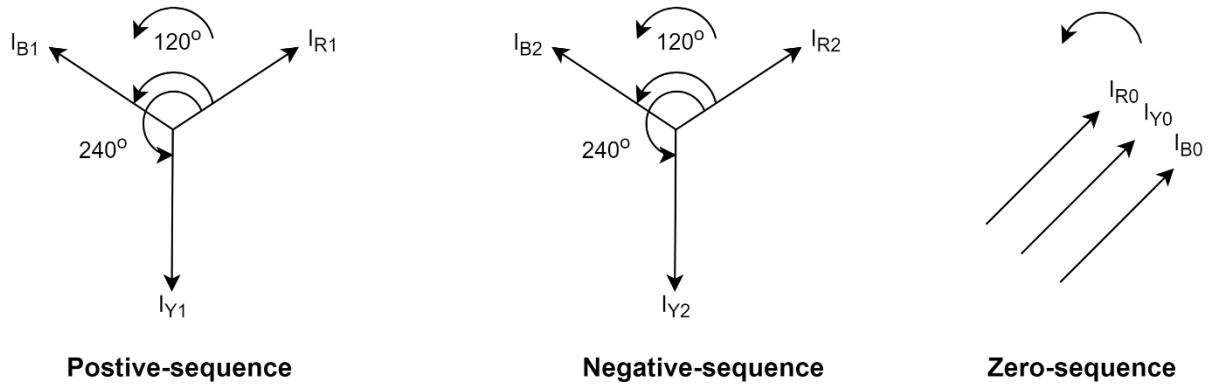

Figure 2.6: Balanced Three Phase Vectors [9]

Symmetrical faults currents on three phase systems is calculated using Thevenins equivalent circuit theorem or short circuit apparent power method as shown in equation (2.10). The fault current calculation only needs to be completed for one phase as the remaining two phases has the equivalent magnitude [23].

Faults in a power system will have a value that is limited to the total impedance in a power system. The impedance is therefore an important part of the equation in determining the symmetrical fault currents. The impedances are largely attributed to the reactive components in the power system namely the generator, transformer and the line. The positive phase sequence impedance is identical to the sum of the impedance in the system namely the conductor, overhead lines and transformer [24]. The faults in the symmetrical three phase system will therefore load the entire network symmetrical with only the positive phase sequence element hence only the positive phase sequence is required to analyze the fault. The impedance may be expressed in a percentage and calculated using equation (2.9):

$$\%X = \frac{Isc.X}{V}.100 \tag{2.9}$$

Where, I_{SC} = the full load current, V = the phase voltage, and X = the reactance in ohms per phase. The reactance of each component will need to be calculated to determine the total reactance in the circuit based on a common apparent power rating. The equation (2.9) is applicable for applications where only the line impedance is considered while in applications where transformers and generators also form part of the circuit being calculated, the percentage with base kVA using per unit system applications is preferred [9].

The short circuit current for a symmetrical fault is determined using equation (2.10):

$$I_{SC} = \left(\frac{V}{X}\right).\left(\frac{100}{\%X}\right) \tag{2.10}$$

Where, I_{SC} = the short circuit current, V = the phase voltage, and X = the reactance in ohms per phase. The rare occurrence of these faults negates the implementation of symmetrical faults

on a power system for controlled circuit breaker tripping hence the symmetrical faults will not be calculated nor simulated for this dissertation.

2.6.2 Unsymmetrical Faults Analysis

Unsymmetrical faults do not involve the entire three phases, these faults occur as a result of single line to ground faults, line to line faults or double line to ground faults [25]. The unsymmetrical faults are such that the currents in the three lines become unequal with a phase displacement between them. The unsymmetrical components are only referred to the fault and line current with phase angles since the source voltage and impedance of the power system always remain symmetrical. The unsymmetrical fault also has a positive, negative and zero phase sequence component similarly to the symmetrical fault. However, it loads the network unsymmetrical.

When an unsymmetrical three phase fault occurs the positive sequence voltage continues to drive the positive sequence currents during the fault while the remaining un-faulted phases continue to maintain the air-gap flux. When the most common fault namely single line to ground fault occurs, the magnetic flux in the air gap is maintained by the remaining un-faulted lines which is smaller than normal and unbalanced. The short circuit fault current in the single line to ground fault will continue to flow until the circuit breaker removes the fault from the circuit. Similarly, line-to-line and line-to-line-to-ground faults also maintains the air gap flux during the fault thus allowing the short circuit current to flow until the circuit breaker removes the fault [26]. This illustrates the reliance of the power systems protection on the correctly selected circuit breaker parameters. Single pole tripping circuits are more responsive than three pole circuit breakers thus the single pole tripping circuit breaker will be applied to this dissertation as a preferred option to ensure that a fault current, is picked up early and trips the faulted phase in an attempt to clear the fault before affecting the related phases and subsequently damage the interconnected electrical equipment

The method to calculate the unsymmetrical faults called symmetrical components of the original unbalanced system was proposed by Dr. D.L. Fortescue in 1918. The principles to the methodology of symmetrical components functions such that any unbalanced system of currents, voltage or other sinusoidal quantities is resolve into their balanced system of phasors and subsequently transferred to its unbalanced system of actual circuit condition by super position of these quantities [25].

$$\begin{bmatrix} I_0 \\ I_1 \\ I_2 \end{bmatrix} = \frac{1}{3} x \begin{bmatrix} 1 & 1 & 1 \\ \vdots & \text{a} & a^2 \\ 1 & a^2 & a \end{bmatrix} x \begin{bmatrix} I_R \\ I_Y \\ I_B \end{bmatrix} \tag{2.11}$$

The symmetrical current components may be expressed in a matrix form as shown in equation (2.11) for the three phases namely, I_R, I_Y and I_B with an operator 'a' that represents $120°$ phase shift between phases and operator 'a_2' that represents a $240°$ phase shift between phases, where the red phase I_R is taken as the reference phase. I_0 represents the zero phase sequence, I_1 represents the positive phase sequence while I_2 represents the negative phase sequence of the unsymmetrical fault currents in symmetrical components [27]. When the fault does not include the ground or earth phase namely any line to line, the current I_0 is always taken as zero thus only negative and positive phase sequence are calculated during non-grounded fault occurrences.

The unbalanced phasors of the system are represented in the terms of its symmetrical components of zero, negative and positive phase currents as a result of the phase relationship which exists between these sequences. The phasor relationship permits the current components of the zero, negative and positive sequences to be transposed in a matrix's form as shown in equation (2.11) to derive the equations for fault currents of each unsymmetrical component to its symmetrical form as shown in equation (2.12 to 2.14):

$$I_0 = \frac{1}{3}.\left(I_R + I_Y + I_B\right) \tag{2.12}$$

Where, I_0 = Zero sequence currents , I_R = the zero sequence current in the red phase, I_Y = the zero sequence current in the yellow phase and I_B = the zero sequence current in the blue phase.

$$I_1 = \frac{1}{3}.\left(I_R + aI_Y + a^2 I_B\right) \tag{2.13}$$

Where, I_1 = Positive sequence currents , I_R = the positive sequence current in the red phase , I_Y = the positive sequence current in the yellow phase is flowing $120°$ out of phase with the red phase, I_B = the positive sequence current in the blue phase is flowing $240°$ out of phase with the red phase.

$$I_2 = \frac{1}{3}.\left(I_R + a^2 I_Y + aI_B\right) \tag{2.14}$$

Where, I_2 = Negative sequence currents, I_R = the negative sequence current in the red phase I_Y = the negative sequence current in the yellow phase is flowing $240°$ out of phase with the red phase, I_B = the negative sequence current in the blue phase is flowing $120°$ out of phase with the red phase.

An unsymmetrical short circuit fault current not exceeding $25\,kA$ will be simulated for this dissertation using the symmetrical component logic in the electromagnetic transient simulation

program derived from the equations (2.12 to 2.14). This fault will allow for the testing of the 3-phase single pole circuit breaker using both the controlled and non-controlled logic sequence technology.

In [26], Gevorgian et al. investigates the short circuit fault current behavior for both symmetrical and unsymmetrical fault using both PSCAD and Cyme software while a more detailed investigation was concluded on the differentiation between the different types of unsymmetrical fault currents. The results for both transient software packages produced was very close to the approximation. The faults were simulated in a system where the impedance was the same for all tests, this enabled the research of the various types of faults to be completed on the same parameters since it is known that impedance limits the fault in any power system. The symmetrical fault current for each phase was as a result of the time of the fault which occurs at different phase angle for each phase. The variation for each sequence component was negligible yet not exactly the same as the theory proves. The unsymmetrical single line-to-ground fault when compared line-to-line fault proved to have a major differentiation, the zero sequence current was zero for the line-to-line while it had high current reading for the line-to-line-to-ground fault. The negative sequence current had a higher current leading for the line-to-line fault when compared to the line-to-line-to-ground fault and the positive sequence current had a higher current reading for the line-to-line fault when compared to the line-to-line-to-ground fault [27].

In [25],V. Ogboh, and T. Madueme, state that the analysis of faults in the unsymmetrical systems of each phase is completed by taking the unbalanced voltages and currents of each phase and analyzing it as three separate set of composed balanced vectors namely the balanced three phase sequence currents of the positive , negative and zero sequence. The symmetrical component methodology is integrated with the artificial neural network algorithm which learns the network operation patterns therefore assisting in diagnosing the network faults. The artificial neural network was implemented on the Nigerian power system transmission line. This technology picked up the type of faults experienced in each protection zone namely zone1, zone 2 and zone 3 of the transmission line thus providing the utility with a better understanding of the faults on the network [22].

2.7 Interruption Phenomena Associated with Faults

2.7.1 Arcing

When a short circuit fault current occurs on a power system, an interruption by the circuit breaker leads to an arc that is formed between the circuit breaker fixed electrode and movable electrode as they are separated. The arcing is a result of the high impedance dielectric medium of the circuit breaker being ionized by the fault current thus allowing a path of conductivity for the formation of the arc. The short circuit fault is classed as a parallel arc fault as its initiated by bringing two phases together or a phase and ground. The arc has a resistive, current and voltage characteristic which determines the arcing intensity. The main effects from an arc is the heat level and pressure produced from the arc power characteristics thus making it hazardous if not contained [28].

The arcing times are longer in larger air gap therefore resulting in thermal stress while the arcing times are shorter in smaller air gap but results in restrikes. Its therefore important that the interruption optimum point for current interruption must be applied to prevent both of the extreme conditions namely restrikes and thermal stress [29]. The average arcing time for a 11 kV vacuum circuit breaker is in the region of 5 *ms* to 10 *ms* [27]. The circuit breaker selected for this dissertation will be able to withstand an arcing time of 15 *ms*.

The detailed research on arcing and its characteristics are covered in the latter part of this chapter.

2.7.2 Re-ignition

Re-ignition occurs when a circuit breaker with a low dielectric strength trips near a current zero point due to a short circuit fault current or normal interruption of a capacitor bank thus causing the current to re-ignite and re-establish within one-eight of the power frequency cycle. Re-ignition as a result of the over voltage over a period of time can damage electrical equipment connected to the circuit breaker.

Re-ignition only occurs if the transient's recovery voltage exceeds the dielectric strength of the circuit breaker such that there is a breakdown in the air gap which emanates from the cooling of the hot gases between the two contacts of the vacuum circuit breaker. This subsequently leads to high frequency currents which exceed the magnitude of the power frequency currents thus breaking down the dielectric medium of the circuit breaker resulting in re-ignition.

When the changing rate of high frequency current in the zero point is smaller than the high frequency current quenching capability of a circuit breaker, the high frequency current will be

extinguished thus preventing re-ignition from occurring. The changing rate of high frequency in the current zero point is calculated using is the equation (2.15) [30]:

$$\frac{di}{dt} = C\left(t - t_{open}\right) + D \tag{2.15}$$

Where, $\frac{di}{dt}$ = the changing rate of current , C = the rate of rise of breaker high frequency quenching capability, D = the breaker quenching capability just before its contact separation, t = the internal time of software (Duration of open time), and, t_{open} = the opening time of the breaker (At contact separation).

The abovementioned standard rated values of C and D for the vacuum circuit breaker is provided by the vacuum circuit breaker manufacturer, the changing rate of the current is subsequently calculated using the equation (2.15) and it varied depending on the circuit breaker internal time (t) and opening time (t_{open}).

The 17.5 *kV* rated voltage vacuum circuit breaker with an applied voltage of 11 *kV* selected for this dissertation requires a high frequency current quenching capacity in the range of 600 $A/\mu s$ and a rate of rise of vacuum breaker high frequency quenching capability of 0 $A/\mu s$ to ensure the circuit breaker has the ability to quench the high frequency at current zero. Surge arresters connected line to neutral are recommend to suppress the re-ignition voltage levels and protect the connected system [31] .

There are other elements which affect the re-ignition in a circuit breaker. In [32] ,Bennendijk et al. concluded from their experiment that the value of re-ignition voltages increase in a smaller gap length between contacts while in larger air gap lengths, the re-ignition voltages are lower. However, the arcing duration is longer. In [33], Yan et al. conducted an experiment to determine the parameters that effects re-ignition in a vacuum circuit breaker, it was revealed that the contact type of material, electrode structure type, and the separation distance of the electrode has an impact the value of the re-ignition. The common copper-chromium (CuCr) material found in vacuum circuit breaker contact materials was tested using three different copper-chromium element compositions namely CuCr50/50, CuCr50/25 and CuCr75/25. The CuCr75/25 element composition proved to have the lowest re-ignition probability. The two structure types namely the half coil and the cup-shaped axial magnetic structure was tested under the same supply voltage, current and an applied short circuit fault current of 25 kA where the half coil structure proved to offer a lower re-ignition value. The recommended electrode separation after the experiments to increase field strength hence lower re-ignition was proven to be in the range of 5 to 10 *mm* for a 17.5 *kA* rated breaker rated at a short circuit fault current

of 25 *kA* [34]. The electrode gap spacing for the vacuum circuit breaker selected for this dissertation is 10mm, this selection of electrode gap distance will ensure an adequate field strength is available and to prevent arcing time extension.

2.7.3 Prestrikes

The prestrikes phenomena occur when the electric filed strength exceeds the dielectric strength between the contacts of the circuit breaker during the closing operation. Prestrikes tend to produce a current and voltage which flows to the load and the reflected waves of the current and voltage returns to the circuit breaker terminals. The reflected current returns as a high frequency current flow arc across the closing gap while the reflected voltage across the contacts will breakdown the dielectric strength of the decreasing gap during closing operation thus leading to a prestrike. The adverse effects of inrush current arcs within a circuit breaker also has a negative impact on the circuit breaker contact surface condition such that as the contact resistance increases from the effects of arcing, so does the probability of prestrikes.

In [35], Wang et al. indicates that prestrikes are more likely when circuit breakers are used for the purpose of switching capacitor banks because of the modification to the contact surface. The research further indicates that phase controlled switching has the ability to effectively reduce the pre-arcing times and the magnitude of inrush current therefore improving the condition of the contact surface hence reducing the probability of restrikes. However, the phase controlled switching is dependent on the prestrike electric field characteristics. Tests results for arc gaps that are greater than 12 *mm* in a 12 *kV* vacuum circuit breaker proved that the prestrike electric filed characteristic is proportional to the type of material used and the gap distance which effectively has an impact on the prestrike voltage infiltration ability. Arc gaps greater than 12 *mm* with the contact surface material of copper-chromium greater than CuCr5050 proved to provide adequate prestrike voltage infiltration results. The results also proved that the type of contact materials doesn't not have any effect on the voltage infiltration when the arc gap is lower than 12 *mm*.

The vacuum circuit breaker used for this dissertation will be a single pole operated circuit breaker which operates on the principles of phase controlled switching. The contact gap will remain at 10mm with the contact material of CuCr75/25. The aim of this dissertation is to provide circuit breaker interruption rather than closing hence the effects of prestrikes on the simulation will not form part of this research.

2.7.4 Current Chopping

Current chopping occurs when the magnetizing currents causes the current to come to zero before the natural current zero during circuit breaker interruption. The instantaneous current is a few amperes at this point of interruption prior to the current zero point which results in the arc becoming unstable as a result of the current being interrupted abruptly and prematurely. The initial stages of the abrupt current behavior for the chopping current commences at the point of interruption. The probability of the chopping phenomena increases when interrupting an unloaded transformer or high rapturing fuse before current zero which is effectively due to the small inductive currents such has transformer magnetizing currents which is completed just before current zero. This is a result of the stored energy from the inductance that triggers additional voltage transient at the circuit breaker [30].

In [36], Lanen et al. indicates in his research that current chopping in vacuum circuit breakers are generally higher than other types of circuit breakers. The simulated results from Lanen et al also indicates that the probability of current chopping is decreased coupled with the arc remaining in an unstable situation for less time when high current interruption is achieved at steep current slopes at current zero. This dissertation aims to achieve tripping at the current zero point using advanced controlled switching technology which aims to reduce the current chopping effects on a circuit breaker. The default current chopping current will be set to not exceed 5A as recommend by circuit breaker manufacturer during simulations [37].

2.7.5 Transient Recovery Voltage

When the circuit breaker interrupts a fault prior to the current zero point, the phenomena succeeding current chopping is termed the transient recovery voltage. The increased current spike after the 1st current chopping waveform leads to the reduction in the following cycles current therefore increasing the voltage which is known as the transient recovery voltage [38].

In [39] , A.H. Soloot and H.K. Hoidalen, indicates from their experiment that the transient recovery value is dependent on the type of load connected to the power system. In a power system where there are highly inductive loads such as transformers and induction motors, the transient recovery voltage is higher. The experiment also revealed that the shape of the transient recovery voltage has an impact on the circuit breakers ability to successfully interrupt. The higher steepness in the shape of the transient recovery voltage had reduced the arcing times and prevented restrikes during short circuit current interruptions by the vacuum circuit breaker.

In [40] , the authors, research indicates that in existing modern power systems, the high rate of rise in transient recovery voltage of up to a few kilovolts per second tend to occur more

frequently when compared to older power systems. The major change in the power system which have given rise to the transient recovery voltage is attributed in the implementation of local generations. An example of this is gas/fuel operated peaking plants which are implemented by independent power producers. The transformers in the local generation stations constructed by independent power producers are installed in close vicinity to the generators which are coupling it to the power network therefore reducing the capacitance in the power system thus leading to high-frequency transient recovery voltage. Another case of high values of transient's recovery voltages are from the short circuit faults that occur on shorter lines that are a few hundred meters from the circuit breaker where the traveling waves from the faulted section of the faulted line results in a very high rise in the transient's recovery voltage. Surge arresters are applied between the line and the neutral to limit the transient recovery voltage but they do not have the ability to limit the rate of rise of recovery voltage. However, the limiting of restrikes can limit the rate of rise of recovery voltage requirements of the circuit breaker.

The 17.5 *kV* rated vacuum circuit breaker selected for this dissertation will comply to IEEE C37.04-199 standard, the peak voltage will not exceed 30 *kV* while the rate of rise of recovery voltage(RRRV) will be below $0.43\,kV/\mu s$.

2.7.6 Restrikes

Restrikes is a an extreme phenomenon that occurs when the current is interrupted at current zero and its re-established after 1 quarter or longer of the cycle followed by the transient recovery voltage [29].The origin of restrikes is the negatively charged macro-particles that are formed between the contacts within the interrupter medium if the transient recovery voltage exceeds the dielectric strength of the circuit breaker. The increased negatively charged particles are not an adequate condition for restrikes as a result of the increased ability of the spark discharge between the macro-particles and the negative contact thus leading to fires. Research on the quantitative characteristics of occurrence in medium and high voltage vacuum circuit breakers have revealed that no less than 95% of possible restrikes occurs in time 0.3 *s* from the moment of arc starvation [41].

The shorter arcing times give way for restrikes to occur due to the shorter gap distances between the contacts. The larger gaps reduce the ability for restrikes to occur but extends the arcing time thus resulting in thermal stresses hence it is concluded that the re-ignition of a vacuum circuit breaker occurring is directly proportional to the probability of restrikes which is affected by the gap distance between the electrode [29]. The optimum gap distance of 10 *mm* for a 17.5 *kV* rated vacuum circuit breaker as outlined in the research from [34] to ensure minimal or no re-ignition and restrikes will be applied to this dissertation.

The institute of electrical and electronic engineer's standard and the international electro technical commission standard recommends reducing of the restrikes by using a stray capacitance connected between the vacuum circuit breaker and the overhead line to facilitate a time delay (t_{dL}) of 0.2 μs in the interruption time which allows for the arcing gap recovery before the onset of the restrikes and subsequently transient recovery voltage. The value of the required stray capacitor is determined based on the load impedance on the line (Z_L). The value of the capacitor is calculated using equation (2.16) [40]:

$$C_{dL} = \frac{td_L}{Z_L} \tag{2.16}$$

Where, C_{dL} = the stray capacitance delay in pf, t_{dL} = the time delay for the circuit breaker μs and, Z_L = the load impedance of the line in Ω. The capacitor value between the vacuum circuit breaker and overhead line for this dissertation to limit the probability of restrikes will be calculated using equation (2.16) and will integrated into the simulated model [37].

The energy produced by the restrike is defined by the voltage step of the load side which lasts for some microseconds. The energy produced by the restrike is the difference in energy stored by the magnetic field of the inductive load prior to the restrike occurring from the energy stored by the electrical field of the stray capacitance. The equivalent circuit representative of the restrike circuit is shown in Figure 2.7 [42].

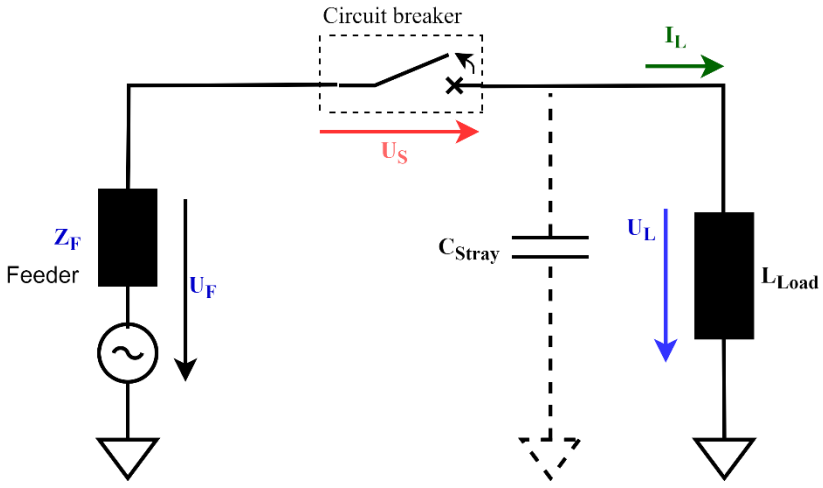

Figure 2.7: Equivalent Circuit Diagram of Restrike Circuit [42]

This restrike energy is calculated using equation (2.17) – (2.19) [42]:

$$W_L = \frac{1}{2}.L\,.\,I^2 \tag{2.17}$$

Where, W_L = the energy from chopping the load current, L = the inductance of the load, and I = the load current (<1).

$$W_C = \frac{1}{2} \cdot C_{Stray} \cdot U^2_{Load} \quad (2.18)$$

Where, W_C = the energy stored from the electrical field of stray capacitance, C_{stray} = the stray capacitance, and U^2_{Load} = the peak ignition voltage. The energy stored from the electrical field(W_C) from equation (2.18) is calculated for each restrike that occurs namely from restrike "n" to restrike (n-1) where "n" is the total number of restrikes occurred hence the total energy stored from the electrical field of stray capacitance for the total restrikes is represented by W_{Csum} [42]. The total oscillating energy of the restrike W_{osc} is the difference in the inductive energy W_L from the stray capacitance of the circuit as shown in equation (2.19):

$$W_{osc} = W_L - W_{Csum} \quad (2.19)$$

Where, W_{osc} = the restrike energy produced.

The electromagnetic transient simulation software used in this dissertation uses the implemented logic from equation (2.17) – (2.19) to determine the total oscillating energy produced from the entire arc including which includes the energy attributed to the restrikes.

2.8 Electrical Contact Resistance

Fault interruption is achieved by the separation of contacts found in a circuit breaker which breaks the continuity of current flow in a power system. During the separation, an arc is formed as a result of the ionized particulars that forms after fault currents has occurred, the current tracks through air via the ionized air particulars thus causing an arc across the contact points namely anode and cathode which generates heat energy that causes thermal expansion of the contacts within a circuit breaker [43].

The contacts are manufactured with a specific resistance which varies from medium to high voltage circuit breakers depending on their voltage and current carrying capacity. Medium voltage circuit breaker contact resistance range from 10 $\mu\Omega$ to 350 $\mu\Omega$.

When arcing occurs across the contacts, the phenomena of fretting corrosion occurs on the circuit breaker contacts. Fretting corrosion on circuit breaker contacts is the friction of the circuit breaker contacts when exposed to electrodynamic forces or thermal expansion that emanate from short circuit fault currents during fault interruption of a circuit breaker. The effects of fretting corrosion results in the formation of an oxidation layer which increases the contacts thickness after being exposed to the heat energy from the arc. The fretting corrosion also causes micro-displacement from the effects of thermal expansion of the copper or silver plated copper contact material. The effects of fretting therefore increase the contact size and

reduces the contacts conductive properties hence opposing the flow of current thus increasing the resistance of the contact materials [44].

2.9 Contact Resistance Measurement Methods

The practical measurement of the contact resistance to ascertain the circuit breakers reliability of the circuit breaker is accomplished using either the static, dynamic test method or black model.

2.9.1 Static Measurement Method

The Static resistance measurement is completed while the circuit breaker contacts are closed at an instantaneous point which is effectively the average of the contact resistance. Static measurement is done using either the 2-wire, 3-wire or 4-wire method. The 2-wire method is applied using a Multimeter which provides accurate measurement between $10\,\Omega$ to $10\,M\Omega$. The 3-wire method is applied on higher voltage breakers where the resistance is more than 10 $M\Omega$. The 4-wire method is the most accurate method where the resistance is below $10\,\Omega$. The 4-wire is applicable to medium voltage circuit breaker since the resistance values are in micro-ohms. The 4-wire method uses two current leads and two sensing leads which eliminates the voltage drop in the leads further by injecting current greater than 10 A [45].

2.9.2 Dynamic Measurement Method

The dynamic test resistance measurement is completed while the breaker is in the open position such that current is injected for a few milliseconds before the close command is given to move the contacts into the closed position. The current and voltage feed, divided, will provide a dynamic resistance through the circuit breaker operation at every millisecond of the circuit breaker close operation. The dynamic resistance measurement unlike the static resistance measurement has the ability to provide further insight into the arcing contact and the eroded parts of the contacts [45].

2.9.3 Contact Resistance Measurement Method

The conventional approach to measuring the contact resistance using either the static or dynamics method requires a DC current injected in across the circuit breaker contacts either from batteries, a capacitive bank or a DC power supply which is usually from 100 A for a medium voltage breaker or 10 % of the rated current as per IEC 60494. The DC injected and voltage is used to determine the resistance of the contacts by connecting a Multi-meter through test leads that operates using the principles of ohms' law [46].

The 1939, the 1st unorthodox approach in simulating the arc dynamics was introduced which led to an era of black model simulations to calculate various arc parameters including the arc resistance. The details of the varies arc conductance models will be discussed in the later part of this chapter. The unorthodox approach in simulating the arc dynamics lead to the introduction of the Mayr model in 1943. The Mayr model measures the dynamic resistance of the arc during the simulated operation using an electromagnetic transient software [47]. It is eminent that the heat effects of the arcing on a circuit breaker results in the contact resistance being increased due to fretting as mentioned earlier [44]. The Mayr model determines the arc resistance measurement using the arc voltage and arc current similar to the conventional measurement of contact resistance which uses the principle of ohms' law. When applying the Mayr arc model, the power of the arc in watts can also be calculated using the baseline values of voltage, current and time of the arc that's available [47]. This power of the arc relative to the energy of the arc during the circuit breaker operation is calculated from the equation (2.20) – (2.21) [48]:

$$E = R.I^2.t \tag{2.20}$$

Where, t = the time duration of I, R = the resistance, I = the current.

The energy of the arc is also represented as:

$$E = \lambda.T \tag{2.21}$$

Where, λ = a function of heat dissipation rate I^2t also known as hysteresis losses, T = the temperature.

The above equations (2.20) – (2.21) demonstrates that for a constant current, if the resistance increases then the energy output will increases thus leading to an increase in temperature.

Therefore, the energy in relation to the power is presented as:

$$E = P.t \tag{2.22}$$

Where, P = the power flow, t = the time duration.

The relationship from the above energy equation (2.22) also proves that the power flow is directly proportional to the amount of energy dissipated [48].

In this research, the active and reactive power of the arc will be measured using the electromagnetic transient simulation software. It is also eminent from the law of physics that for every 1 *J* of energy produced per second, 1 *W* of energy is created hence the amount of power produced by an arc during a fault will assist in determining the amount of energy the arc produced [49]. Research also indicates that the more energy produced for longer duration will negatively impact the circuit breaker by increasing its contacts resistance as a result of thermal displacement and fretting [50].

One can safely conclude that to determine the effects of the circuit breaker arc during a fault current, the Mayr model in conjunction with the integration of the power in relation to energy of arc during the opening operation of the circuit breaker will facilitate in determining the arc's impact on the circuit breaker during operation over a period of time. This will subsequently assist in determining if the circuit breaker contact points resistance will increase.

2.10 Electrical Arc Phenomenon

An electrical arc is a thermal source which generates energy. Electrical arcing requires a potential difference between two conductors to form. Unlike a spark which is only momentary, the electrical arc discharge is continuous since it is fed from a continuous electrical current source. The electrical arc is extinguished when the electrical current source is removed.

The electrical arc in power systems are formed generally on a transmission line or a bus-bars when short circuiting of the phase to phase or phase to earth connections occur, leading to an electrical fault. Electrical arcing is also formed in direct current systems such as photovoltaic panel systems which are used in the generation of power [51]. The electrical arc in the direct current system which is commonly known as DC arcing does not form part of this research scope. The electrical arc phenomena also occur within the circuit breaker chamber during opening or closing of a circuit breaker during normal operation while much larger arc are formed in the circuit breaker chamber during fault interruption.

The electrical arc intensity is dependent on several factors, some of which are the system voltage, fault duration, fault current magnitude, arc length and gap distance. The selected specification by the engineer during manufacturing of the circuit breaker in relation to its power system application is therefore important since the circuit breaker appropriate ratings assist in mitigating arc explosion.

The electrical arc produces heat between $7000\,^{\circ}C$ and $35000\,^{\circ}C$ and an intense light lux level between 108000 lux to 249000 lux at 3 *m*. The pressure produced by an electrical arc is in the region of 2711.64 $N.m$ while the sound produced by the arc is around 150 $d.b$. The above mentioned arc characteristics are not tolerant by personnel or any object is its vicinity. The electrical arc flash over may lead to blindness of personnel's as a result of the bright luminosity emitted and the heat produced from the arc can result in severe injury or death to personnel's who are in close vicinity to the arc. Damage to equipment and property is another compromising situation faced when arching leads to explosions hence responsive protection equipment is required to disintegrate the arcing effects swiftly [52].

Taking the above into consideration, it is evident that electrical arcing when created in an uncontrolled environment can lead to extremely dangerous situations. However, when the

electrical arc is harnessed correctly and created in a controlled environmental, the electrical arc can be beneficial. The electrical arc has facilitated the development of modern day technologies such as the arc in the camera flashes which produce the light that enables the image to be captured in surroundings with sufficient lighting. Electrical arc is also used for spotlights and in fluorescent lightning to assist producing a desired lux level of lighting when no natural light is available. Electrical arc in cutting is also used where the compressed air is combined with a power electrical arc and converted into a plasma that have the ability to cut through steel.

2.10.1 Arc Characteristic

The electrical arc has a resistance which is inversely proportional to the currents that flows through the arc. The arc resistance is dependent on three high level characteristic which is inversely proportional to the arc intensity. These characteristics are as follows [53]:

- The degree of ionization: This is effetely the amount of ionized particles present between the contacts. The lower the ionized particles will result in a decrease in current flow thus forming a high arc resistance. The ionized particles are also responsible for maintaining the arc since it provides a conductor current path flow.
- Length of the arc: The greater the length between the contacts during separation will increase the arc resistance. The length of the arc is inversely proportional to the potential difference between the contacts since the elimination of the voltage potential across the contacts is of a higher magnitude when the contacts are in close proximity.
- Cross-section of arc: The smaller the medium of which the arc travels through, results in the current flow in the medium being restricted hence increasing the resistance of the arc. The cross sectional area during manufacturing of a circuit breaker may be manipulated to suite the reduction in the arcing.

The electrical arc resistance is inversely proportional to the current flow as outlined above. It also is eminent that the thermal energy of the arc is increased with the increase in current of the arc hence we can conclude that the resistance of the arc is inversely proportional to the thermal energy of the arc [53, 54]. The heat intensity of the arc is determined by the thermal energy produced which in relation is the amount of heat flux produced. The heat flux of the arc is broken up into predominately radiant or predominately convective which can be generalized into four type as follows:

- Moving high heat flux which occurs in open air overhead lines
- Stationary directional high heat flux which occurs at transformer bushings
- Directional hot air exhaust from low heat flux which occurs on low voltage switchboards.

- Ejected directional high heat flux arc which occurs in medium voltage switchgear breakers

This research will be limited to the arc effects of the ejected directional heat flux arc in medium voltage switchgear. The ejected directional heat flux arc is dependent on the time of the exposure. The time of the exposure directly related to the fault clearing time. The arc dissipates the heat energy outwards through opening, radiant and convective heat with superheated air. Several of the ejected directional high heat flux arc characteristics which determines the arc intensity is as follows [54]:

- Fault current level : The arc thermal energy is represented in the form of electrical energy ($E = V \times I \times t$). Increase in current will effetely increase the energy out hence reduction in the fault current will increase the arc resistance. In [54] the behavior of the arc in relation to the increase in fault current was investigated using high speed video analysis. The results of the findings over a period of 0.02 *s* using 50 *Hz* frequency proved that the arc accelerates and decelerates as the fault currents are increasing and decreasing for every cycle that being in a sinusoidal manner. The arc is extinguished at every instant of the fault current reaching the current zero point on the cycle.
- Duration of the arc: The duration of the arc is increased as the fault current increases or as the fault current angle changes. This indicates that the high fault currents will make extinguishing of the arc more difficult hence increasing the duration of the arc. The delay in fault interruption by the protective equipment also results in the arc duration increasing. The relationship between current and time is expressed as $\frac{di}{dt}$ where di is the current differential and dt is the time differential. The increase in the $\frac{di}{dt}$ will result in the fault current interruption ability decreasing. Timeously tripping using reliable protection systems to interrupt the fault current is therefore essential to avoid the increased fault current magnitudes.

The relation of the circuit breaker arc characteristics from above, forms a basis of our investigation on the extinguishing of a circuit breaker arc, both timeously and with the least impact using controlled switching technology.

2.10.2 The Electric Arc Initiation

The nature of an arc is like that of a lightning strike. Arc may be initiated in several ways. Some of the arc initiation formations include the touch method, exposing conductors to air and "Glow to arc" transitions. The "glow to arc" transition is formed in medium-low voltage power systems which is the arc initiation formation which forms part of this research investigation.

The "Glow to arc" forms such that the first stage encompasses a "Townsend discharge" where the free electrons are accelerated by an electric field between two separated conductors of opposite electrical charge in a gases area with relatively low potential difference thus resulting in ionization. The ionization causes the current to rise rapidly for a very little increase in voltage which results in a discharge process thus emitting a glow formation. This discharge glow results in a dramatic step change increased voltage which accompanies an incremental current. This subsequently triggers a release of large number of electrons from the cathode that leads to a continuous breakdown of air. The fault currents on the system or the nominal operating currents travel through the ionized conductive path between the conductors which transitions the glow into an arc [50].

The arc phenomena explained above describes the physics of the arc in general that occurs in transmission lines or bus-bar etc. The circuit breaker arc which is based on the arc principles explained above is initiated when the fixed electrode and movable cathode, is separated resulting in the contact area being reduced. This reduction in contact area increases the electron density which subsequently increases the temperature of the medium near the contacts within the circuit such has oil, air or gas therefore forcing the heated medium to ionize and act as a conductor layer to allow for electron flow. This ionization of the medium particulars phenomenon is called the plasma effect. The heated conductive layer with electrons allow for the current to flow from the fixed electrode to the movable cathode thus creating an electrical spark also known as the plasma arc [52]. The technical term "plasma arc" within a circuit breaker is referred to "arc" throughout this dissertation.

The arc within a MV vacuum breaker is concentrated about 2 *ms* after contact separation around the point where the ignition occurs; the arc luminosity is the most when the arc reaches its concentration points. The concentration levels near the anode area is more in comparison to the cathode surface. Once the peak of the arc is reached, the luminosity of the arc decreases together with the decrease in arc concretion thus leading to the extinguishing of the arc.

2.10.3 Arc Interruption

The arc resistance factors responsible for maintaining the arc is the focal point in ensuring successfully arc interruption in a circuit breaker. Arc extinction is broken up into two methods namely the high resistance method and zero current method.

The high resistance method which entails increasing the arcing resistance to provide arc extinction by manipulating the arc characteristics. The several characteristics that can increase the arc resistance thus providing arc extinction is as follows:

- Increasing the length of the arc: Increasing in the contact points distance, results in an increased arc resistance to an extent where the arc is extinct. The circuit breaker trip command which will open the circuit breaker which will effectively increase the spacing of the contract points during a fault.
- Geometry of the cathode and electrode: The electrode gap separation length increase results in an increase in the arc voltage and an increase in noise amplitude. However, the potential difference of the arc between the electrode and cathode after contact separation exceeds a specified distance, prevents the arc to persist. The appearance of the arc tends to distort with an increase in arc gap and results in the arc peak current reducing. The specified gap separation during the open state of the circuit breaker between the electrode and cathode contacts for a 11 kV circuit breaker that will be applied for this dissertation is 10 mm [55].
- Medium of the arc: This refers to the dielectric medium the arc is surrounded by in the circuit breaker chamber. The arc resistance increases with an increase in the dielectric strength of the medium. The medium is dependent on the type of circuit breaker used namely air, oil, Sf6 and vacuum. Each circuit breaker chamber medium possesses different dielectric strengths which assist in extinguishing the arc by de-ionizing the charged particles. The air medium emits radiant heat energy in all direction which hampers its ability to extinguish the arc from the plasma effect thus making it a weak dielectric medium. The oil medium quenches the arc yet the risk of a fire as a results of the arc igniting the oil makes this medium unsafe. The vacuum and Sf6 has good dielectric properties which can reduce the arc plasma effect more efficiently. However, Sf6 gas is not environmental friendly and has less dielectric strength when compared to the vacuum medium, hence the vacuum medium is a more suitable option for extinguishing an arc which will be adopted in this dissertation [54].

The high resistivity characteristics described above is implemented by circuit breaker manufacturers to increase the gap of the contact and use a deionizing Sf6 gas to ensure the ions

are de-ionized to facilitate arc extinction [53]. However, the speed in the clearing time using this method is slower and the extinguishing point of the arc is at a higher current hence causing the lengthy existence of a high current arc that impacts the circuit lifespan as a result of increased contact resistance.

The current zero method operates such that it extinguishes the arc naturally at the point when the fault current reaches the zero point on the current cycle. In spite of the potential rising voltage across the circuit breaker contacts with a small dielectric strength which can lead to voltage breakdown known as restriking voltage, the current zero method eliminates restriking voltage provided that the current is extinguished exactly on current zero point. The extinguishing of the arc at current zero neutralizes the ions in the contact chamber hence increasing the dielectric strength of the medium. The current zero method as a result of circuit breaker idle time and ambient temperature fails to trip the circuit breaker at the exact current zero but rather near current zero hence this method also impacts the circuit breaker lifespans as a result of high current arcing effects [54, 56].

Modern day circuit breakers have adopted both the current zero method and high resistance method which complement each other to reduce the arc impacts on the circuit breaker. However, the circuit breaker idle time coupled with the temperature within the circuit breaker medium together with the protection tripping delays prevents the circuit breaker from tripping at the exact current zero point. Tripping at the exact current zero point rather than the near current zero point has a difference in arc fault current. This will impact the circuit breaker lifespan [50, 53].

This research will focus on implementation of the arc resistance and current zero method that trips the circuit breaker exactly at current zero point by using a circuit breaker technology which will predict the future current zero times to prevent tripping delays. The extinguishing of the arc will be accomplished quicker with a lower arc fault current magnitude and duration therefore, preventing incremental damage to the circuit breaker contacts and related equipment. This will be achieved by using a technology that will have the ability to take into account the idle time, temperature of the circuit breaker to allow for circuit breaker tripping lag time compensation. The implementation of this method with the ability to compensate for the circuit breaker lag times is called controlled switching. The controlled switching technology will compliment a vacuum chamber that has a higher natural dielectric medium hence the rate of de-ionization is higher [56]. The controlled switching will allow the circuit breaker to trip at the exact current zero point therefore lowering the impact duration of the arc fault current thus preventing circuit breaker contact damage. The principles and methodology of the control switching technology will be explained in the latter part of this chapter.

2.11 Power System Protection

The protection of major power equipment together with the maintaining of quality of supply is crucial in any power system. However, it is also important that circuit breakers are also protected in the process since circuit breakers are the key protection component in a power system which is required to interrupt a fault current, overvoltage or to merely isolate a network from the entire power system. Circuit breakers generally fail over a period of time from the effects of arcing from switching operations which causes contact erosion therefore putting the entire power system protection under risk.

Circuit breakers coupled with protection relays increases the power system supply reliability as a result of the intelligent logic embedded into the protection relays. However, the logic of the protection relays is designed to protect the holistic power system by isolating the fault swiftly to improve the quality of the supply. This protection relays logic neglects the effects of the fault onto the circuit breaker during the fault switching applications, hence the focus should be aimed at developing different technologies to improve the circuit breaker reliability. An evaluation of the various circuit breaker interrupting mediums with ancillaries coupled with the controlled switching protection technologies and testing methodologies for controlled switching of a circuit breaker during fault interruption will be reviewed in this chapter in an effort to improve on circuit breaker reliability.

2.12 Circuit breaker Operation

Indoor circuit breakers are designed to interrupt the continuity of current flow in an electrical circuit. The indoor vacuum circuit breaker which is applicable to this dissertation consists of several components which individually contributes to the circuit breaker functionality. The components and its operation that will be covered are as follows:

- Operating Mechanism
- Main current components
- Closing shaft and connecting links
- Breaker Springs
- Racking Mechanism

2.12.1 Operating Mechanism

The operation of the circuit breaker is achieved manually or electrically. The manual operation is primarily for maintenance or when the there is no power available to perform the close

operation of the circuit breaker electrically. The manual operation is achieved by compressing the closing spring with a manual closing spring charging device such as a charging rod.

The circuit breaker is operated electrically by either a closing solenoid or stored energy mechanism. The circuit breaker can also be operated using hydraulic, magnetic and pneumatic mechanism which are primarily used in high voltage circuits which does not form part of the dissertation scope.

The solenoid design is operated using a closing coil where the coil is energised therefore actuating the closing mechanism of the circuit breaker thus achieving a circuit breaker closing operation. The solenoid is an older method which has been replaced by the stored energy method.

The stored energy design operates such that the circuit breaker utilizes a spring rewind motor to charge a closing spring to the closed position of the circuit breaker. The close button energizes the closing coil thus unlatching the closing spring holding latch, which discharged the spring closing the breaker contracts.

In 2005, CIGRE CB survey results indicates that the major failures on power systems are a result of circuit breakers and the major failures in circuit breakers which account for more than 70 % of the faults are from operating mechanism failure [57]. Survey results in [2] indicate that the failures have reduced between 1984 to 2003. The results also depict an increased implementation in stored energy mechanism from 18 % to 29 % hence the implementation of stored energy mechanism designs using a spring rewind motor has proved to be more reliable than the other operating mechanism methods. The more reliable and current stored energy design will be implemented in this dissertation.

2.12.2 Main Current Components

The main current carrying components are the phase or pole of the indoor circuit breaker which varies in thickness depending on the carrying requirements of the application. The phase or pole consist of primary disconnects, primary bushings, moving contact arm and contacts which operate as follows:

- Primary disconnects: The primary disconnects are a set of silver plated copper fingers held together with a spring on each phase of the circuit breaker which are permanently mounted to the breaker bushings that forms the point of contact between the circuit breaker and the switchboard bus-bar. When the circuit breaker is racked into the switchboard, the fingers expands thus causing the springs to exert pressure on both the breaker and cubicle pole thus making a closed circuit between the circuit breaker and switchboard bus-bar.

- Primary bushings: The bushings are a solid copper bus-bar with a silver plating at both ends of the breaker. Each phase will have a supply side and load side of the bushing. The load side is coupled to the moving contact arm while the supply side is connected to the stationary contact.
- Moving contact Arm: The moving arm is silver plated copper conductor which is held by a contact spring that exerts pressure on the bus-bar for a good connection to the primary pivot point on the load side of the primary bushings. The moving arm is connected to one end of the contact and the other end is connected to an insulated push link that connects the moving arm to the operating mechanism.
- Contacts: The contacts vary from air, vacuum and Sf6 circuit breakers. The air and Sf6 circuit breaker has an arcing contact which makes contact first when the circuit breaker is closed and breaks last when the circuit breaker is opened thus is a sacrificial contact that is exposed to the arc to protect the main contracts. The main contacts consist of a silver plated copper body with a silver cadmium oxide material that is attached at the connection point of the moving and stationary contact which carry the circuit breaker load. The vacuum circuit breaker consists of only main contacts that are made from either copper-bismuth or copper chrome allows within a vacuum sealed bottle that's in the shape of a cupped axial magnetic design or slotted design. The vacuum circuit breaker using the copper chrome will be adopted for this dissertation as it assures for lower chopping currents than with a designs employing copper-bismuth. The shape will be an axial magnetic field design, which will be used in this dissertation since it offers a high interrupting current rating as the current flows create magnetic field along the longitudinal axis of the vacuum interrupter which constrict the arc and forces it to remain in diffuse mode thus preventing overheating and contract erosion [58].

2.12.3 Closing Shaft and Connecting Links

The operating mechanism is connected to the insulated links via the closing shaft which operate the moving contacts. The names of the closing shaft vary from suppliers, some of the names are Crank shaft, Main shaft and Jack shaft. When the circuit breaker is closed, the closing shaft is turned by the drive lever which is actuated by the cam disc of the charging shaft that is engaged by the closing spring when the circuit is closing. The opening sequence of the circuit breaker operates in the same sequence as the closing except for the jack shaft which is turned by the opening spring.

2.12.4 Breaker Springs

The circuit breaker has four springs namely the closing spring, opening spring, contract spring and the mechanism springs. Each of the springs function serves as an important part of the circuit breaker operation with details as follows [59]:

- Closing spring: The closing spring is the largest spring on the circuit breaker which is mechanical charged by the spring rewind motor such that it provides energy to close the circuit breaker.
- Opening spring: The opening spring assist the breaker when a trip signal is issued to open the circuit breaker. The operating time of the circuit breaker is reduced in milliseconds when the stiffness coefficient of the opening spring is increased
- Contact springs: The contact springs make the necessary compression to provide a tight connection between the moving and stationary contacts.
- Mechanism springs: The mechanism springs consist of several springs which facilitate the latch actuation and resetting operations that are found in the trip latch, close latch and prop latch.

2.12.5 Racking Mechanism

The circuit breaker is removed from the switchboard compartment by racking it out, the racking out position also signifies that the specific feeder is isolated form the network. In switchboards, there are no isolator so the racking out facilitates is a safety mechanism for maintenance. The racking out of the circuit breaker always allows for easy accessing of the circuit breaker for the required repairs on the circuit breaker to be carried out. The racking is facilitated by a leveler which is turned to either racking the circuit breaker in or out. A more modern system used is called the racking truck system which allows for the circuit breaker to be racked in and out while the door of the cubicle is closed unlike the conventional racking system. This effectively reduces the risk of personnel's being directly exposed to arcing explosion and incorporates an interlock such that the earthing switch is to be on prior to racking out the circuit breaker [60]. The circuit breaker chosen for this dissertation will have a truck system rack out mechanism.

2.13 Circuit-breaker Classification

The classification of circuit breakers may be categorized into several criteria's. The method of classification is dependent on the criteria chosen [61]. The criteria for the classification of circuit breakers is detailed as follows [61]:

- Voltage Class: In South Africa's power systems, circuit breakers with voltages up to

1 *kV* is classified as low voltage circuit breakers, while circuit breakers with voltages from 11 *kV* up to 33 *kV* are classified as medium voltage circuit breakers and voltages above 33 *kV* are classified as high voltage circuit breakers [62]. The medium voltage circuit breaker voltage class will be applied for the purpose of this dissertation.

- Interrupting medium: The circuit breaker interrupting medium is classified as a vacuum, air blast, gas or oil. The medium refers to the arcing quenching medium used to extinguish the arc [63]. The interrupting medium applied for this dissertation will be vacuum.
- According to service : The circuit breaker service is classified as an indoor or outdoor circuit breaker [62]. The service applied for the purpose of this dissertation will be an indoor circuit breaker.
- Type of current: The circuit breaker current type is classified as direct current or alternating current. The application of the circuit breaker in a power system aids in the classification of the circuit breaker current type. In traction substations, namely rail applications, direct current is mainly used while power grids for the purpose of transmitting and distributing power to consumers makes use of alternating current. There are instances where transmitting of power is completed using direct current. However, this forms a minimal part of the power grid. The alternating current circuit breaker will be applied for in this dissertation.
- Way of operation: The circuit breaker way of operation is the methodology used to design the circuit breaker opening and closing. The way of operation is classified into gravity open, gravity close or horizontal breaker [63]. The indoor circuit breaker chosen for the application of this dissertation will make use of a loaded spring which is open by gravity hence the methodology of gravity open will be applied.
- Method of control: The circuit breaker method of control is the method used to open or close the circuit breaker which may be classified as either locally or remotely [62]. The indoor circuit breaker for this dissertation will make use of both the local and remote circuit breaker control method.
- Way of mounting: The way of mounting is the mounting position of the circuit which is classified into front panel mounted, rear of panel or remote panel mounted. The front panel mounted will be applicable to this dissertation.
- Tank construction: The arcing medium is embedded within the tank chamber of the circuit breaker. The tank construction is classified into a separate tank for each pole or one tank for all 3 poles of the circuit breaker. In single pole tripping circuit breakers, the tanks are separated while the 3-pole tripping circuit breakers makes use of one tank. The tank

construction in the outdoor circuit breakers are also termed either dead or live tank. The dead illustrates that the current carrying components are covered while a live tank illustrates are current carrying components are visible. The single pole with 3 individual tanks will be the classified tank construction applied to this dissertation.

- Arcing medium: The method used to extinguish the arc that is formed during the circuit breaker opening or closing operation is generally the common classification referred to when classifying this type of circuit breakers. The arcing medium of a circuit breaker is classified has oil, air, vacuum or Sf6 [63]. The vacuum arcing medium circuit breaker will be applied to this dissertation. The arcing medium also assist in identifying the type of circuit breaker.

2.14 Types of Circuit-breakers

The quality of supply is affected when fault currents occur on a power system which effectively affects the ability the power utility has to deliver power to consumes continuously. The fault currents that occur on a power line or electrical equipment such as a generator or transformer has an ability to damage electrical equipment such as transmission lines, substation and subsequently switch-station, resulting in poor quality of supply and risk of personnel's safety. It is for this reason that protective systems are an important component of an electrical network to ensure that quality of supply is maintained and electrical equipment are protected. One of the key components to any protective system is the circuit breaker. This is required to break a power circuit in an event of a short circuit fault currents, overvoltage or to merely isolate the circuit from the holistic power system.

Circuit breakers are found in low voltage systems (400 *V*) to high voltage systems (up to 800 *kV*). Circuit breakers coupled with protection relays, provide safer switching (opening or closing) to allow protection of major power equipment such as a shunt capacitor bank, shunt reactor, transmission line and transformer [6]. Circuit breakers with only the standard protection relays which are used to pick up on system faults that lead to overcurrent, earth-faults and Under voltage etc. are labeled as conventional circuit breakers which have no integrated intelligence.

2.14.1 Air Circuit-breakers

Air breaker circuit breakers are indoor type circuit breakers which use the atmospheric pressure air as an air interrupting medium. The length of the arc is increased using an arc runner which increases the resistance of the arc as the circuit breaker main contacts are separated. The increase in arc resistance, increases the voltage drop of the arc making it larger than the supply voltage therefore extinguishing the arc. The air circuit breakers are used in both alternating

current and direct current applications ranging from 3.3 *kV* to 12 *kV* with a current range of 400 *A* to 3500 *A*. The air circuit breaker has two sets of contacts namely the main contacts which consist of the fixed and moving contact that is made from a low resistance silver plating and the arcing contacts which are made from copper alloy that is very hard and heat resistance [61]. The principle operation during a fault current is such that the arc is drawn between the main contacts while the air gets ionized, the arc is cooled to reduce the diameter of the arc while the main contacts are separated. The current is then shifted to the arcing contacts where arc between them are forced upwards by the electromagnetic forces provided by the blow out coils and thermal stroke thus allowing it to travel through the arc runners which increases the arc resistance and subsequently the splitter plate which cools the arc therefore extinguishing the arc by deionization with removal of the heat. The disadvantage of the air circuit breaker is the interrupting medium used is air which has low arc extinguishing properties and the operating voltages are limited to 12 *kV* [61].

2.14.2 Vacuum Circuit-breaker

In [29], J. Kaumanns investigates the interruption of the vacuum circuit breaker at different arcing times. The longer arcing times increases the thermal overload hence increasing the ion density at current zero therefore leading to a slower extinguishing of the ion. The results also proved that the voltage shape determines the probability of the restrike which may be related to the metal particles in the gap which react to both the voltage integral and steepness. The higher transient recovery voltage steepness had reduced post arc currents during the simulation. The vacuum circuit breaker will be adopted for this dissertation with the implementation controlled switching technologies which aims to reduce the effects of current chopping within the circuit breaker on unloaded networks [61].

2.14.3 Sulphur Hexafluoride Gas Breakers

Sulphur hexafluoride (Sf6) gas is an electronegative gas which has the ability to absorb free electronics. The properties of the non-inflammable Sulphur hexafluoride gas is such that it remains in the gaseous state up to 9 *kV* and liquefies during low temperatures and is five times denser than air. The principles of operation for the Sf6 gas breaker is such that the moving and fixed contacts of the breaker are open to a high pressure flow of Sf6 gas when the arc is struck between them, the gas captures the electrons from the arc to form immobile negative ions which increases the dielectric strength of the medium thus extinguishing the arc. The Sf6 breaker is suited for high power and voltage applications ranging from 33 *kV* to 760 *kV* [64].

The Sf6 gas breaker has two construction types namely the non-puffer type and pressure puffer type. The only circuit breaker that comes close to the effectiveness of a vacuum circuit breaker in switching applications is the Sf6 gas breaker but its limitation is the greenhouse gas released during operation [65]. A comparison outlying the vacuum circuit to the Sf6 in switching applications is tabulated in Table 2.2. The comparison indicates the vacuum to be the preferred interrupting medium over Sf6 [66,67].

Table 2.2: Vacuum Vs Sf6 Switching Application Comparison [66]

Criteria (Switching)	Sf6 Circuit Breaker	Vacuum Circuit Breaker
Short circuit current with High DC component	Suitable	Suitable
Short circuit current with High RRV	Suitable under certain conditions (RRV>1-2 *kV/ms*	Very Suitable
Transformers	Suitable	Suitable
Reactors	Suitable	Suitable. Steps to be taken when current <600 *A* to avoid over voltage due to current chopping
Capacitors	Suitable. Re-strike free	Suitable. Re-strike free
Capacitors back to back	Suitable. In some cases current limiting reactors required to limit inrush current	Suitable. In some cases current limiting reactors required to limit inrush current
Arc furnace	Suitable for limited operation	Suitable. Steps to be taken to limit over voltage.

2.15 Concepts of Switching

The high voltage switching operations for shunt reactors, capacitor bank, transformer and a power line encapsulate the two types of operations namely “open state” for de-energization and “close state” for energization [68]. The switching operation is either triggered manually or via a relay trip signal. This dissertations scope will focus on switching the circuit to an open state during fault interruption. The interruption of current flow through a power system requires a break in the power circuit which is completed using the older fuse technology which has limitation. The fuse interrupts with increased temperature, that is triggered by the increased power driven by increased current flow from the fault current. The superseding technology for current interruption is the circuit breaker which is a safer alternative to perform switching known as non-controlled switching. Non-controlled or conventional circuit breaker switching has no intelligence and rely upon manual operation or a protection relay signal input to the circuit breaker trip coil to interrupt a fault in a power system. The protection relay in the system uses secondary current and voltage inputs to determine overcurrent and earth faults thereby initiating a trip signal to the circuit breaker. The limitation of conventional circuit breaker

switching is its inability to achieve interruption at current zero. Hence, a technology called controlled switching was later developed. Controlled switching functions such that when a fault is detected by the protection relay, the controlled switching device through a continuous monitoring of current and voltage input from the connected system together with previous interruption time data logs aids the controlled switching device in deriving a logical algorithm to intercept the trip signal to the trip coil with a time delay that enables the circuit breaker to achieve near current zero interruption. Another technology was later developed called synchronized switching. It works on the principles of conventional controlled switching. However, the difference is that the circuit breaker connected can vary the speeds of the contacts opening or closing to achieve the required tripping time near the current zero crossing [69]. The pitfall of this technology is that it causes contact bouncing which causes wear on the circuit breaker contacts that increases the resistance of the contacts thus reducing the reliability and lifespan of the circuit breaker [70]. A recent switching technology improvement to controlled switching was introduced called advanced controlled switching. It uses the principles of the conventional controlled switching technology with the addition of sensors within the circuit breaker which monitor the ambient temperature, idle time and control voltage to enable it to factor these values into the logical calculation for the tripping compensation times of the circuit breaker during fault interruption to achieve accurate current zero interruption [71, 72].

2.15.1 Non-controlled Switching

The non-controlled circuit breakers have only one characteristic for switching a circuit breaker which limits its ability to achieve tripping near current zero crossing, hence hampering its ability to mitigate transient in some switching applications therefore impacting the circuit breakers lifespan.-The switching applications where these various transients occur is as follows [72, 73]:

- Inrush currents and voltage transient are a result of energizing reactive loads at the incorrect instant while restrikes occur when de-energizing shunt reactors with inadequate arcing times thereby affecting the reliability of the equipment.
- In transformers, during energization, the inrush current leading to the arc current within the circuit breaker is caused by residual flux which is the sum of the voltage component caused by the flux plus the nominal voltage input to the transformer.
- During capacitor bank energization in large power networks where active power compensation is required, the unsystematic switching of the capacitor banks generate transients caused by the potential difference between the capacitor and the power system voltage also resulting in an arc displacement within the circuit breaker.

- In shunt reactors which are used for reactive compensation on large power networks, during de-energizing, the inductive characteristics of the reactor causes opposition to the sudden current adjustment therefore leading to circuit breaker arcing and subsequently restrikes as a result of the load current deceasing.

When the de-energization of a line occurs as a result of fault current interruption at an instant deviating from the current zero point, the fault current produces high inrush currents within the circuit breaker which produces an arc current with high thermal stress followed by a voltage restrike after current interruption. The high inrush current and the voltage restrike causes wear on the breaker contacts which impacts the circuit breaker reliability and lifespan [6].

In aid of mitigating the above transient effects and stresses on the power system electrical equipment, power utilities have realized various switching technologies such as synchronized switching, controlled switching(point-on-wave) which all aims to reduce premature circuit breaker wear by taking into account the transients parameters and some also the environment conditions therefore tripping the circuit breaker near current zero [72].

2.15.2 Controlled Switching

In 1995, a survey conducted in CIGRE TF 13.00.01 indicates that controlled switching have been the accepted technology by power utilities for shunt capacitor, shunt reactor, power lines and transformer applications. However, research indicates that circuit breakers using controlled switching technology in power lines are the least from the other applications used and only account for 2% of the power line circuit breakers installed [74].

In the last 30 years, since the initial development of controlled switching technology in circuit breakers, there have been extensive research which investigates the use of controlled switching in high voltage applications that are greater than $200\,kV$ yet the amount of circuit breakers at power utilities in high voltage systems greater than $200\,A$ only account for 26.7% as per CIGRE WG A3.06 survey completed in 2007 [75].

The survey by CIGRE WG A3.06 also indicates that the circuit breaker failures since the previous survey have reduced marginally. The is attributed to majority of the research being aimed at controlled switching of high voltage networks and it being aimed at shunt capacitor, shunt reactor and transformer applications. This only accounts for less than 36.7 % of circuit breakers installed on power systems rather than medium voltage networks on overhead power lines which account for majority of circuit breakers on a power system [75]. In the recent years, an improvement incorporating additional logic processing to the conventional controlled switching technology was introduced called advanced controlled switching. It uses the

principles of the conventional controlled switching technology with the addition of sensors. The sensors within the circuit breaker monitor the ambient temperature, idle time and control voltage to enable it to factor these values into the logical calculation for the tripping compensation times of the circuit breaker during fault interruption. The controls initiate the trip for the faulted phase rather than the entire three phases therefore current is interrupted at a target instant. The tripping at current zero prediction times are improved therefore reducing the transients caused during switching and also improving the quality of supply and reducing electrical and mechanical stresses on the circuit breaker and related electrical equipment [71, 72]. Should the zero crossing not occur within a pre-set time, the circuit breaker will trip conventionally provided no failures are detected. This modern advancement to the controlled switching technology will be implemented in this dissertations. The parameters embedded into logic of the advanced controlled switching technology namely the ambient temperature and circuit breaker idle time will provide an advancement to the controlled switching technology are detailed as follows:

- Ambient temperature: The circuit breaker ambient temperature is the measure of the temperature accumulated within in the circuit breaker from the thermal stress during operations which is a transformation of electromagnetic energy to heat coupled with the natural ambient temperature outside of the circuit breaker. The temperature accumulated impacts the coil resistance which influences the coil current thus leading to the change in the operating characteristics of the circuit breaker hence increasing the switching time. The temperature of the circuit breaker will be factored into the logic of the controlled switching logic to ensure the operating characteristics of the circuit breaker is adapted to the next tripping operation [71]. The ambient time will be implemented in this dissertation using a mathematical logic that will assist in determining the controlled switching device compensation to achieve current zero tripping.
- Idle time: The idle time in circuit breakers which uses hydraulic operated mechanism rather than spring or electromagnetic mechanism showed a distinct differentiation in idle times greater than 72 hours, this saturates the circuit breaker therefore increases its opening times by 2 s as a result of air bubbles dissolved in the hydraulic fluid which influences the speed of the hydraulic pistons. In addition, mechanical fatigue of the metal components of the breaker due to insufficient lubrication is also a contributing factor to the lag. The idle time logic also factors in the delays from historic switching and incorporates a compensating variable in the pre-set time which continuously changes as the breaker idle times lapses [71, 72]. The spring operating mechanism for the vacuum circuit breaker applied to this dissertation will be used to ensure the idle

times are minimal. The idle time will be implemented in this dissertation using a mathematical logic that will assist in determining the controlled switching device compensation time to achieve current zero tripping.

- Control voltage: The control voltage which effectively influences the current through the coil is only applicable to the closing operation of the circuit breaker since the operating times from simulations in [71] proved that the times remain the same irrespective of the applied control voltage hence this will not be incorporated into the logics of this dissertation.

The protection relay preforming the overcurrent, earth fault or differential protection logic operations for fault interruption is embedded in the LV compartment of the switchboard that is completely isolated from the circuit breaker compartment. The same LV compartment where the protection relay is embedded is where the controlled switching device is installed which has sensors connected to the controlled switching device to form the advanced controlled switching device. The logic and pre-set parameters are loading onto the controlled switching device which uses arithmetic processing logics operations to predict pre-set operating times during faults taking into account the temperature, idle time and the natural current zero point.

The advantages of controlled switching are improvement in the power quality on the power network, decrease in electrical and mechanical stresses, therefore decreasing equipment failures. Controlled switching technology for circuit breakers are mainly found in high voltage applications that exceeds 132 kV and are commonly used with Sf6 Gas, oil and Air type breakers [6].The evolving controlled switching technology have been proven to decrease the risk of electrical equipment failure, improve quality of supply and reduce maintenance costs on high voltage networks hence the benefits of this have been realized and subsequently implemented onto medium voltage application. However, advanced controlled switching was never implemented with a medium voltage vacuum circuit breaker.

2.15.3 Principle of Controlled Switching

Conventional controlled switching uses logical algorithms which determine the time that the circuit breaker requires to interrupt or switch on a power system to achieve near current zero tripping. The principles of operation of conventional controlled switching are that the logarithms are dependent on the electrical inputs to the controlled switching device such as current and voltage parameters. The current input to the controlled switching device is transmitted via a current transformer and the voltage input is transmitted via a voltage transformer. The input current and voltage per phase enables it to calculate the opening time and compensation time to determine the optimum tripping or switching on time based on the

connected network parameters. The opening time is the time between input instant of the tripping command from the protection relay and the instant of opening. The compensation time is difference between the target opening time and the earliest zero-crossing point. When a fault is detected by the protection relay, to achieve fault interruption, the protection relay sends the trip signal to the controlled switching device. The controlled switching device then starts a timer when the earliest zero-point crossing is detected based on its analyses of the input electrical parameters and phase angles, once the time has lapsed, the opening command is sent to the circuit breaker from the controlled switching device to start opening the circuit breaker. The current phase angle is measured for opening while the voltage phase angle is measured for closing for controlled switching applications. The opening time is stored within the controlled switching device as a predicted time to assist in predicting the next tripping time [4]. The conventional controlled switching proved to be a major improvement to the non-controlled circuit breaker operations. However, the accuracy of the predicted times is low since the circuit breakers previous closing time would have been performed at a different environmental conditions to that of the next tripping time hence the predicted times would differ for each interruption.

2.16 Rate of Change

The Arrhenius equation is used to measure the rate of change relevant to the circuit breaker lifespan with reference to the temperature and energy of the arc [76, 77]. The equation is a formula for temperature dependence of reaction rates. The Arrhenius equation is commonly used in the evaluation of the thermal endurance of electrical insulating materials within circuit breakers as recommend by IEC 60216-8 [78].

$$k = e\frac{E_A}{RT} \tag{2.23}$$

Where, E_A = the energy produce by the arc in $kJ\ mol^{-1}$, R = Constant at 8.31 $J\ K^{-1} mol^{-1}$., T = Temperature of the Arc in k and K = Kinetic Rate constant in $M^{-1}.S^{-1}$.

2.17 Reasons for Choosing Advanced Controlled Switching for Fault Interruption

Majority of the research conducted focuses on the high voltage closing applications with the use of Sf6 Gas circuit breakers using conventional controlled switching to reduce inrush currents and transients during energizing (breaker closing) of transformers, shunt reactors and shunt capacitors. The most recent research on medium voltage applications was published in the year 2015 by M. Andre et al. in [74]. However, the research conducted doesn't describe the type of circuit breakers used in the medium voltage closing applications and only controlled switching is implemented rather than the advanced controlled switching technology. The research also did not evaluate fault interruption. The most recent research focusing on circuit breaker opening for fault interruption was published in the year 2007 by R. Thomas in [79] who presents fault interruption implementation on a 420 *kV* high voltage network power line using a Sf6 gas circuit breaker. Thomas develops an algorithm to clear the simulated faults on an EMTP namely phase-to-Phase and phase-to-Earth faults with and without earth connection by synchronizing the trip commands of each phase of a 3-phase breaker with its respective currents zero times. However, the research did not evaluate medium voltage fault interruption using a vacuum circuit breaker. Thomas applies the $R-L$ model using the conventional controlled switching equation (2.24) which is based on Laplace transforms that is applied when calculating the instantaneous fault time for a high voltage power line.

$$\Delta T_{IF}\left(t\right) I_F.\left[\, sin\left(\omega \cdot t + \alpha - \varphi\right) - sin\left(\alpha - \varphi\right) \cdot e^{(-t/\tau)}\right] \tag{2.24}$$

Where, ΔT_{IF} = the fault current logic instantaneous time, I_F = the fault current time, t = the time, ω = the power system frequency, α = the phase angle of the phase voltage when the fault is initiated and τ = the time constant of the symmetrical transient component of fault current.

The equation (2.24) illustrates the voltage phase angle has more influence on the fault current zero trip times during the transient stage than the time constant(τ). The equation provides insight to the current zero tripping times which serves has one of the input parameters to the controlled switching device to predict the holistic compensation times of the circuit breaker.

The literature reviews on the controlled switching of a 11 *kV* vacuum circuit breaker switchboard for fault interruption was challenging due to previous studies not investigating fault interruption using advanced controlled switching on a medium voltage indoor vacuum breakers. Each literature source. However, provided an insight into the individual components of the research which aided with direction on this research topic. Currently there is no published research on implementation of advanced controlled switching on Medium voltage power lines using a single phase indoor vacuum circuit breaker for fault interruption. This leaves one with

unanswered question on the impact the vacuum breaker technology coupled with the advanced controlled switching technology will have, on Medium voltage power lines for fault interruption. The arc extinguishing times and inrush currents effects may possibly be reduced further by using this technological combination. The benefits of this implementation may increase the lifespan of equipment and improve the quality of supply of the power network. This dissertation will focus on implementation and analysis of an advanced controlled switching technology on a 11 kV switchboard vacuum breaker of a medium voltage power lines for fault interruptions to find the results in this uncharted area.

Chapter 3

Modelling and Simulation

3.1 Introduction

Circuit breakers used in industries and power utilities are subjected on a daily basis to the effects of arcing during energizing and circuit breaker interruption. The effects of the circuit breaker arcing, reduce the lifespan of the circuit breaker and related power system equipment. If the magnitude or duration of the arc is reduced, this reduces the impact on the circuit breaker and subsequently improves the circuit breaker and related equipment's lifespan. The ways of reducing the effects of arcing are investigated in this study using the advanced controlled switching technology on a circuit breaker. Documented in this Chapter, the tools, components with specifications, the simulated model and its process workflow used to achieve the advanced controlled switching. The 3-phase Line-to-Earth fault interruption was explored using the conventional controlled switching as defined by equation (2.24). The results obtained was compared with the results from the PSCAD electromagnetic transient simulation software simulated model to determine how well the results agrees. The impact of the non-controlled circuit breaker during a fault interruption relevant to the interruption phenomena were obtained using the PSCAD electromagnetic transient simulation results only.

The non-controlled switching simulated results was subsequently used as the basis of comparison for the exploration of the advanced controlled switching circuit breaker results when exposed to the 3-phase Line-to-earth fault. The advanced controlled switching 3-phase Line-to-Earth fault interruption time results were obtained using the predicted time, controlled switching logic equation which takes into account the effects of near current zero timing, ambient temperature, and idle time. The 3-phase Line-to-Earth fault interruption time results as presented in this next Chapter for the advanced controlled switching circuit breaker and this was firstly compared with the non-controlled circuit breaker, then subsequently compared with the results from the PSCAD simulated model for verification. The interruption phenomena result for the faulted phase for both the advanced controlled and non-controlled were obtained using the PSCAD electromagnetic transient simulation.

3.2 Analytical Modelling

3.2.1 Arc Models

Arc models are used for the modelling the arc fault current and the arc conductance. The arc models are classified into different models based on graphics, physical models and the black box models. These models can incorporate equations with design parameters as attributed to the expression to obtain the arcing characteristics. The physical form is the actual testing of the circuit breaker in real time under laboratory conditions [80]. The black box model is a simulation model using the electromagnetic transient software which describes the relationship between the input and output signals. The logic of the arc is described by differential equations as related to the arc characteristics. The arc model types available are the Cassie arc model, the Mayr arc model and the Schavemaker arc model.

The Cassie arc model has a fixed temperature parameter that is cooled by forced convention. This implies that the cross-section area of the arc is proportional to the current with the arc voltage constant. This model is only suitable for high current time intervals when the plasma temperature of the arc is more than $7726.25\,°C$ [81]. The Cassie model equation for arc conductance is defined as:

$$\frac{1.dg}{g.dt} = \frac{1}{\tau}.\left(\frac{u^2}{Uc^2} - 1\right) \tag{3.1}$$

Where, g = the arc conductance, τ = the arc time constant, Uc^2 = single phase voltage constant and u = the arc voltage across the breaker.

The Mayr model, the time constant and cooling power can either be a constant function of electrical quantities namely conductance, current or voltage. The Mayr model is suited for arc modelling near the current zero point when the plasma temperature is less than $7726.25\,°C$ [82]. Hence, based on this characteristic, this is the preferred model for this study. The time and cooling power was kept constant during the simulations. This was completed to limit the interference of the arc characteristics by varying the manufacturers rating. This model provided the basis of comparison between the controlled and non-controlled switching. The Mayr arc model equation is defined as:

$$\frac{1.dg}{g.dt} = \frac{dIng}{dt} = \frac{1}{\tau}.\left(\frac{u^2}{Uc^2} - 1\right) \tag{3.2}$$

Where g = the arc conductance, τ = the arc time constant, u = the arc voltage across the breaker and i = the arc currents.

The Schavemaker model is based on the Mayr model but modified with the addition of the total cooling. The power constant used is split into two parameters namely the cooling power constant and the cooling constant [81].

$$P = P_o + P_1 \tag{3.3}$$

Where, P = total cooling power constant, P_0 = the cooling power constant in Watt and P_1 = the cooling constant. The cooling constant P_0 is the cooling power of the circuit breaker. The cooling constant P_1 represents the regulation of influence of the electrical power inputs on the circuit breaker cooling power therefore, it also represents the pressure built-up in the breaker caused by ohmic heating of the extinguishing medium by the arc. The cooling constant and cooling power constant in this study was not varied during simulations but rather kept at the specified rating predetermined by the manufacturer. The Schavemaker arc model is presented as [83]:

$$\frac{1.dg}{g.dt} = \frac{dIng}{dt} = \frac{1}{\tau}.\left(\frac{ui}{P_0 + P_1 \mid i} - 1\right) \tag{3.4}$$

Where g = the arc conductance, τ = the arc time constant, P_0 = the cooling power constant in Watt, P_1 = the cooling constant, u = the arc voltage across the breaker and i = the arc currents. The goal of this study with reference to the power characteristic is to ascertain the energy output of the arc during the non-controlled circuit breaker switching fault operation and the controlled circuit breaker switching operation under the same cooling power constant and cooling constants. Thus, varying the cooling power constant and cooling constant was not favourable as it will result in multiple variables with inconstancies in the simulated results. Hence, the additional splitting of the total power constant in the Schavemaker model proved to be unsuitable for the purpose of this study.

3.2.2 Arc Voltage Model

The flashing and dynamic behaviour of the arcing is attributed to the voltage characteristic of the arc [50]. The sustenance of the arc in a medium voltage system is dependent on a large voltage drop across the contact points since the voltage potential increases the ionizing potential of the air near the contacts. The higher ionizing potential at the contact points results in a large part of the voltage appearing across the contact points region. The gap length and the cross sectional area between the contact points also has an impact on the voltage drop, the larger the gap, the lower the potential difference across the gap hence reducing the ionization potential thus increasing the arc resistance [50]. It is evident from the abovementioned characteristics which depicts that the voltage and resistance are dependent on the length of arc. The representation of the Mayr arc model of the arc voltage is mathematical represented using equation (3.5) [84]:

$$\frac{d\upsilon}{dt}=\left[\left(\frac{\upsilon}{i}\right)\frac{d}{dt}\right]-\left[\frac{\upsilon}{\phi}\left(\frac{\upsilon i}{P}-1\right)\right] \tag{3.5}$$

Where, $G=\frac{i}{\upsilon}$ = the arc conductance, P = the cooling power constant, u = the arc voltage across the breaker and i = the arc currents. The arc voltage is calculated using equation (3.5) which is further broken into the anode and cathode total fall voltage The increase in the arc voltage (U_{arc}) is defined as follows:

$$U_{arc}=U_{oa}+U_{os} \tag{3.6}$$

Where, U_{oa} = the total fall voltage and U_{os} = the increase in arc voltage.

In [85], the authors, inferred from their research that the arc voltage produced during a short circuit fault current is dependent on the arrangement of the electrodes and is directly proportional to the arc power produced. The research also indicates that the arc voltage is dependent on the initial pressure in the electrical installation. Thus, installation of arc pressure chutes on indoor switchboards are recommend to decrease the gas density thereby reducing the effects of arcing. The medium voltage arc behaviour magnitude is dependent on the relationship between the electric input power and the power lost through heat dissipation of the arc. Using the parameters from the Mayr arc model, the power loss to the arc is calculated using:

$$P_{Arc}=(U_0+r_0.|i_{arc})l.i_{arc} \tag{3.7}$$

Where, P_{Arc} = the power lost to the arc, U_0 = the contact voltage per arc length, r_0 = the resistive component per arc length, i_{arc} = the instantaneous arc current and l = the time-dependant arc length. The power loss of the arc which transposes to heat energy impacts the contact points resistivity as a result of the heat flux therefore leading to inefficient equipment which subsequently results in equipment failure.

It's evident that the initiation of any arc is highly dependent on the potential difference between contacts points and the length of the arc hence circuit breakers are used to assist in maximizing the contact distances thus reducing the potential difference. The disadvantage of using the circuit breaker only for contact separation is its limitation on contact distance and its lengthy time required to reach contact separation hence additional methodologies in conjunction with the circuit breaker are required to extinguish arcing.

3.2.3 Arc Fault Current Model

The electrical arc fault current produced in a circuit breaker chamber when exposed to a short circuit fault current is determined using IEEE 1584 arc evaluation method as defined by equation (3.8) [86] :

$$Ig(Ia) = 0.00402 + 0.983Ig(IB) \tag{3.8}$$

Where, $Ig(Ia)$ = the arc fault current and $Ig(IB)$ = the short circuit fault current.

The short circuit fault current of the power system increases over a period of time as the power system network expands with additional equipment being installed. The short circuit rating of the circuit breaker is specified based on a 20-year forecasted period which is the average lifespan of a circuit breaker. This is to ensure that the short circuit rating of the circuit breaker is adequate to withstand the increased short circuit fault currents on the power system as the grid expansion occurs [87].

The calculation of Ig(Ia) using the forecasted 20-year short circuit fault current value is therefore important to ensure that the circuit breaker arc fault current of 20 years 'may be endured by the circuit breaker. The short circuit fault current is obtained from the circuit breaker manufactures rated short circuit fault current data. This ensures the short circuit current rating of the circuit breaker used was adequate to withstand the initial arc fault current and future arc fault currents. This prevents protection failure and subsequent damage to equipment. Hence, the arc fault current was calculated using equation (3.8) for this study.

3.3 Component specifications

3.3.1 Circuit-breaker Specification

The MV vacuum circuit model *3AH373* was selected for this dissertation. The specification of the MV vacuum circuit breaker is tabulated in Table 3.1 which complies with the IEC 62271-100(2012) standard.

Table 3.1: Circuit Breaker Specifications

Circuit breaker Characteristic Description	**Rated**	**Simulated**
Rated voltage	17.5 *kV*	11 *kV*
Asymmetrical breaking currents	73 *kA*	25 *kA*
Chopping Currents	-	5 *kA*
Rated operating currents	4000 *A*	211 *A*
Short circuit currents rating for 3 seconds (I_{sc}):	50 *kA*	25 *kA*
Rated short duration currents (I_r)	3 *s*	0.05 *s*
Pole tripping	Segregated pole tripping	-
Breaker open resistance	1.e6 Ω	-
Breaker closed resistance	1e-6 Ω	-
Frequency	50/60 *Hz*	50 *Hz*
Rated lighting impulse within voltage (Up)	110 *kV*	-
Rated short-duration power frequency within voltage	50 *kV*	-
Short circuit breaker currents operation sequence	CO-30min-CO	-
Temperature Operating range	-5 °C to +40 °C	-5 °C to 40 °C
Rated Supply Voltage for coil	110 *V*	110 *V*
Closing time	75 *ms*	N/A
Opening time	30.01 °C	30.0 *ms*
Arcing time	10.5 *ms*	10.05 *ms*
Idle time	Not specified	Variable
Clear fault without opening breaker	Not specified	N/A
Electrode spacing	10 *mm*	10 *mm*
Capacitance connected between breaker and line value	$2.9e^{-8}$	$2.9e^{-8}$
Vacuum Pressure	$p \leq 10^{-5}$ *Pa*	$p \leq 10^{-5}$ *Pa*

The breaker timings are explained as follows:

- The closing time of the breaker is the period between the command of the closing and the point of contact of all the poles
- The opening time refers to the period between the command and the opening of the last pole.
- Arching time is the period from the start of the first arc to extinction of all the arc.
- Break time refers to the opening time plus the arcing time.

The chopping current of the selected MV vacuum circuit breaker is in the region of 5 *A* which is the maximum rated chopping current specified by vacuum circuit breaker manufacturer [37]. The simulated model on PSCAD allows for 5 *A* chopping current cycle to occur.

3.3.2 Power Supply (Source) Specification

The simulated power source chosen comprises of the source feed from the power utilities using a YNd1 88/11 *kV* transformer, hence, the phase angle shifts HV/MV winding configuration of the source is 30°. The power factor chosen is 1 pf which is taken to be an ideal source which means no reactive component exist:

Table 3.2: Power Supply Specifications

Source Description	Specification	Applied
Source Voltage	11 *kV*	11 *kV*
Power Factor (p.f)	1	1
True Power (P)	4000 *kW*	4000 *kW*
Apparent Power (S)	4000 *kVA*	4000 *kVA*
Reactive Power (Q)	0 *kVAr*	0 *kVAr*
Frequency	50 *Hz*	50 *Hz*
Vector Group	YNd1	-
Voltage Ramp Up	0 *s*	0 *s*
Voltage phase angle	30°	30°

3.3.3 Conductor Specification

The feeder network from the outgoing tested circuit breaker to the loaded area is via an overhead network. The cable network has a better aesthetics and requires less maintenance when compared to the overhead line. However, the overhead line has a cheaper installation when compared to the cable network due to the area of the conductor being smaller hence less copper is being used. Cable networks are recommended for the urban areas while overhead networks are preferred for rural areas. This dissertation result on the circuit breaker is applicable to the cable and overhead network as this does not have a significant effect on the simulation parameters and results. However, for the purpose of testing, the overhead line is selected. The MV line conductor code name HARE is selected for the conventional and controlled PSCAD simulation process with characteristics shown in Table 3.3.

Table 3.3: Conductor Specifications

Conductor Characteristics	Specification	Applied
Overall area	122.48 mm^2	122.48 mm^2
Conductor outer radius	0,00708 m	0,00708 m
Conductor thickness	0.00 003342 m	0.00 003342 m
Ultimate tensile strength	36000 N	<36000 N
DC resistance at 20°C	0.2733 Ω / km	0.2733 Ω / km
DC Resistance at 50°C	0.3063 Ω / km	0.3063 Ω / km
Conductor Relative Permeability	1.0	-
Currents rating	360 A	300 A
Currents rating at 50°C (Normal)	292 A	<292 A
Currents rating at 50°C (Emergency)	380 A	<380 A
Conductor type	ACSR	-
Voltage	33 kV	11 kV
Length of line	N/A	25 km
Cores	Single Core	3x single cores

The outgoing feeder network selected for the purpose of this dissertation, is a 3-phase hare conductor that connects at the circuit breaker on the source end, and subsequently connect at the ring main unit on the load end.

3.3.4 Stray Capacitance

The stray capacitor is connected between the vacuum circuit breaker and the overhead line to facilitate a time delay of 0.2 s in the interruption time which allows for the arcing gap recovery therefore reducing the effects of transient recovery voltage. The stray capacitance is only used on the advanced controlled switching circuit breaker circuit in efforts to reduce the probability of restrikes due to the current zero tripping. The value of the capacitor selected for this dissertation is calculated using equation (3.9) – (3.10):

Line Impedance is:

$$Z_L = Pl.l \tag{3.9}$$

Where, Z_L = Impedance of the line, Pl = Resistivity of the line and l = Length of the line.

$$Z_L = 0.2733e^{-3} \times 25$$

$$= 6.8325\,\Omega$$

Stray Capacitance is:

$$C_{dL} = \frac{t_{dL}}{Z_L}, \tag{3.10}$$

$$= \frac{0.2s}{6.8325\Omega}$$

$= 29255.65\,\mu F$

Where, C_{dL} = the stray capacitance delay , t_{dL} = the time delay for the circuit breaker and Z_L = the load impedance of the line .

3.3.5 MV Structure Specification

The MV H-Pole structure assist in stringing the hare conductor of the outgoing feeder to the load areas. The structure chosen is shown in Figure 3.1.

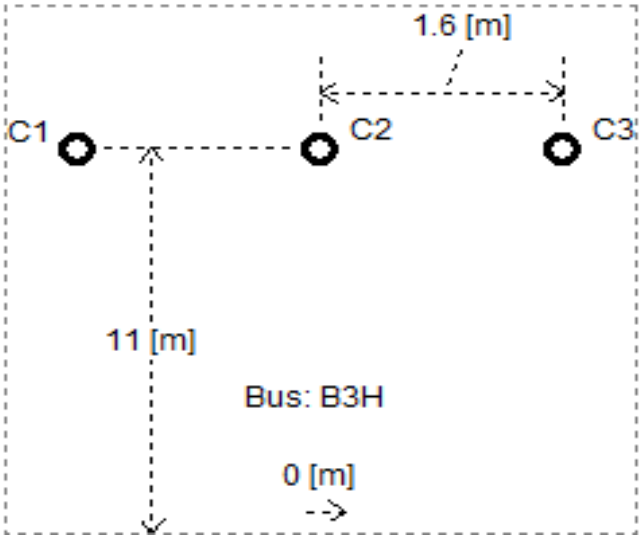

Figure 3.1: MV H-Pole Line Structure

The MV H-Pole structure selected as per SANS:754 AND SANS:457-3 for the conventional and controlled PSCAD simulation possess the characteristics shown in Table 3.4.

Table 3.4: MV H-Pole Line Structure Specification

Line Structure Characteristics	Specification	Applied
Pole Material	Wood (Creosote)	-
Impregnation treatment	Creosote	-
Bus Height above ground(Pole)	10 m	-
Horizontal spacing between phases	1.6 m	-
Relative X centre of bus centre on right of way	0 m	-
No. of Structures used	-	84
Curve Fitting Starting Frequency	0.5 *Hz*	-
Curve Fitting End Frequency	1.0e6 *Hz*	-
Maximum Fitting Error for Prop. Func	20	-
Cross arm	4.5 m	-
No. of cross arms	2	-
Modulus of Elasticity	11000 N / mm^2	-

3.3.6 Protection Relay Specification

The protection relay selected to provide protection against over current and earth faults for this dissertation is the Schneider electric Micom P145 relay. The Micom P145 relay possesses

the functionality required to protect the protection system coupled with it being reliable and economical viable. The Micom P145 relay model selected from the Cortec tables ordering schedule is 323A2BM0B38M. Each letter on the model number comprises of the options chosen [88]. The specification of the protection relay utilized is shown in Table 3.5.

Table 3.5: Protection Relay Specification

Relay Characteristics	**Specification**	**Applied**
Relay DC Input	110-250 *Vdc*	110 *Vdc*
Logic input/outputs	16	-
Communication Protocol	Modbus/DNP3	Modbus
Protection Functionality	OC/EF, SEF, REF	OC/EF
Mounting	Flash panel mount	-
Protection Time characteristics	IDMT/DT	DT
Nominal current (In)	1/5 *A*	1 *A*
Operating temperature range	-25 $^{\circ}C$ to +55 $^{\circ}C$	-5 $^{\circ}C$ to +40 $^{\circ}C$

3.3.7 Current Transformer

The current transformer(CT) applied in this study is for the purpose of both protection and measurement. The selected current transformer comprises of two cores of which one is allocated for the protection and the other for measurement. The protection core provides a current input to the protection relay while the measurement core assists in reading the level of current passing through the simulated model. The current transformer specifications applied is documented in Table 3.6.

Table 3.6: Current Transformer Specifications

CT Characteristics	**Specification**	**Applied**
Voltage	22 *kV*	11 *kV*
Primary Turns	1	-
Secondary turns	300	-
Secondary Resistance	0.5 Ω	-
Secondary Inductance	0.0008 H	-
Frequency	50 Hz	-
Area	0.0065 m^2	-
Remnant Flux	0.0 T	-
Flux density at Knee point	1.0 T	-
Eddy Current loss	0.1 *W*	-
Hysteresis loss coefficient	0.1 *W*	-
Burden Resistance	0.5 Ω	-
Burden inductance	0.0008 H	-
Core 1 Class	Protection (PX)	-
Core 2 Class	Measurement (Class 0.2)	-
Core 1 Ratio and Core 2 Ratio	800/400/200/1 *A* MR	400/1 *A*
BIL	150 *kV*	-
Isc	25 *kA*/ 3 Sec	-

3.4 Summary of PSCAD Power Circuit Components

Table 3.7: Summary of PSCAD Power Circuit Components

Specification	PSCAD Power circuit component description				
	Power Source	**Circuit Breaker**	**Breaker Arc**	**MV Line**	**Load**
Rated Voltage	-	17.5 *kV*		33 *kV*	
Frequency	50 *Hz*	50 *Hz*		50 *Hz*	50 *Hz*
Source Voltage	11 *kV*	11 *kV*		11 *kV*	11 *kV*
Source Currents	292 *A*	292 *A*		292 *A*	292 *A*
Rated Short circuit	-	31.5 *kA*		-	-
Rated Currents	-	4000 *A*		360 *A*	-
Name (Type)		Indoor Vacuum		Hare Aluminium Conductor	Residential
Power Supply	4 *MW*	4 *MW*			
Load	-	4 *MW*		-	4 *MW*
Pole Tripping	-	Single Pole		-	-
Distance	-	-		25 *km*	25 *km*
Breaker open resistance	-	1.e9 Ω		-	-
Breaker closed resistance	-	1e-9 Ω	1e-9 Ω	-	-
Rated lighting impulse within voltage (Up)	-	110 *kV*		-	-
Arc model	-	-	Mayr	-	-
Arc time constant	-	-	0.3 μS	-	-
Arc cooling Power	-	-	35 *kW*	-	-

3.5 Modelling Concept for Temperature Controller

The temperature measurement in a real time advanced controlled switching circuit breaker operates such that it has a temperature sensor that provides the function similar to a thermometer also known as a resistance temperature detector (RTD). The temperature sensor measures the hotness or coolness of the surrounding temperature using a variable resistor that changes the resistance indirectly proportional to the change in temperature. The sensor measures the temperature of the object on the principle that if the voltage difference between the transistor terminal and the emitter increases, then a signal is generated to increase the temperature.

The temperature of the circuit breaker changes with the environment the circuit breaker is within, which is a combination of the electrical heat energy produced through the electrical system together with the ambient temperature. The selected infrared radiation sensor for this dissertation is connected to the advanced controlled switching circuit where the temperature

increase or decrease is directly related to a millisecond delay or compensation of time to ascertain the circuit breaker tripping time during fault currents.

The temperature measurement on the controlled switching circuit breaker measures the temperature of the electrical system heat energy produced in relation to its operating current within the circuit and the ambient temperature relevant to the circuit breakers housed environment. The logical measurement of the electrical system temperature works on the principal of heat energy dissipation using equation (3.11). We have the relationship between Heat with Voltage and Current first:

$$H = I^2.R.t \tag{3.11}$$

Where, H = Heat Energy, I = Current, R = Resistance, t = Time of simulation.

The temperature from the heat energy generated in the circuit is calculated on the principal of 1 joule being equivalent to $5{,}271e^{-3}°C$ hence the above equation (3.11) for heat energy was modified to calculate the temperature generated using equation (3.12):

$$T = I^2.R.t.(5,271e^{-3}) \tag{3.12}$$

Where, T = Temperature, I = Current, R = Resistance and t = Time of simulation.

In a medium where two source temperatures are present, these temperatures do not have a linear relationship. The higher temperature in the medium dictates the overall temperature within the medium [89]. The logic circuitry using PSCAD incorporates the two temperatures and automatically defaults to the selection of the higher temperature.

The ambient temperature which is referred to the air space around the circuit relating to its environmental. This ambient temperature for the purpose of the simulation may be set by the user at various temperatures from $-5°C$ to $40°C$. Both temperatures are subsequently processed to depict the time delay in relation to the temperature.

The delay times will be calculated for each degree in the positive and negative directions of the ambient temperature range to provide the circuit breaker controller with continuous loop feedback on the pre-calculated timings inputs based on its existing temperature. The logic of the temperature in the simulation will mimic the real time application of an infrared temperature sensor.

In [6], the relationship between the time delay in opening and closing a circuit breaker for every increase in degrees Celsius was established. In a circuit breaker where the temperature ranged from $-40°C$ to $40°C$, the circuit breaker opening time was delayed for $30\ \mu s/°C$ when using a spring rewind circuit breaker at base temperature of $40°C$. The temperature logic at an ambient temperature of $-5°C$ to $40°C$ will be implemented as indicated in Table 3.8.

Table 3.8: Temperature Delay Logic

Vacuum - Spring Rewind - Temperature Delay					
Temperature (-5 $^{\circ}C$ to 17 $^{\circ}C$)			**Temperature (18 $^{\circ}C$ to 40 $^{\circ}C$)**		
Temperature ($^{\circ}C$)	**Opening Circuit Breaker Delay (*ms*)**	**Closing Circuit Breaker Delay (*ms*)**	**Temperature ($^{\circ}C$)**	**Opening Circuit Breaker Delay (*ms*)**	**Closing Circuit Breaker Delay (*ms*)**
-5	1.38	3.22	18	0.69	1.61
-4	1.35	3.15	19	0.66	1.54
-3	1.32	3.08	20	0.63	1.47
-2	1.29	3.01	21	0.6	1.4
-1	1.26	2.94	22	0.57	1.33
0	1.23	2.87	23	0.54	1.26
1	1.2	2.8	24	0.51	1.19
2	1.17	2.73	25	0.48	1.12
3	1.14	2.66	26	0.45	1.05
4	1.11	2.59	27	0.42	0.98
5	1.08	2.52	28	0.39	0.91
6	1.05	2.45	29	0.36	0.84
7	1.02	2.38	30	0.33	0.77
8	0.99	2.31	31	0.3	0.7
9	0.96	2.24	32	0.27	0.63
10	0.93	2.17	33	0.24	0.56
11	0.9	2.1	34	0.21	0.49
12	0.87	2.03	35	0.18	0.42
13	0.84	1.96	36	0.15	0.35
14	0.81	1.89	37	0.12	0.28
15	0.78	1.82	38	0.09	0.21
16	0.75	1.75	39	0.06	0.14
17	0.72	1.68	40	0.03	0.07

The temperature controller uses the Mayr model logic which determines the arc resistance using the arc voltage and arc current similar to the conventional measurement of contact resistance which uses the principle of ohms' law.

The electrical arc resistance is inversely proportional to the current flow as outlined above. It is also eminent that the thermal energy of the arc is increased with the increase in current of the arc hence we can conclude that the resistance of the arc is inversely proportional to the thermal energy of the arc [59, 60]. The heat intensity of the arc is determined by the thermal energy produced which is in relation to the amount of heat flux produced which in essence determines the impact of the circuit breaker.

3.6 Modelling Concept for Idle Time Controller

The idle time of a circuit breaker is difficult to quantify without the influence of the ambient temperature in the room. Research in [6] indicates that there is not sufficient research data available to quantify the effects of idle time on a circuit breaker. The data which is available represents the idle time of a spring operated circuit breaker. The spring circuit breaker data indicates delays during opening operation over a 65-day test period which does not provide sufficient sampling data logs to obtain an accurate idle time delay estimate. Extensive funding is required to carry out these idle time tests to produce more accurate statistics on idle time. This in essence limits the accuracy of our idle time logic controlled circuit when simulating using PSCAD. However, the data in set produced in [90] even with its sampling period limitation had proven to be consistent over a period of 50 days.

Research indicates that the general medium voltage line circuit breaker operates at an average of between 4 to 40 times a year [91]. If we abstract the average of this data, a MV line circuit breaker trips almost every 10 days which in effect validates the use of programming the logic for the idle circuitry over a period of 50 days rather than over an annual circle. The idle time delay over a 65-day period does not exceed $0.2\,ms$ hence the effects are minimal. However, when the controlled logic circuit is programmed to trip at the current zero crossing, the $0.2\,ms$ impacts the current zero tripping instant significantly [90]. The controlled logic idle time will process a delay of $3.1\,\mu s / day$ the circuit breaker is idle for the purpose of this dissertation. In essence for a period of 50 days, the idle time will be incorporated into the PSCAD simulated logic as per the Table 3.9.

Table 3.9: Circuit Breaker Idle Time Delay Logic

Vacuum - Spring Rewind - Idle Time Delay			
Idle Days (1 to 25)		Idle Days (26 to 50)	
Idle Days	Idle Time (us)	Idle Days	Idle Time (us)
1	3,1	26	80,6
2	6,2	27	83,7
3	9,3	28	86,8
4	12,4	29	89,9
5	15,5	30	93,0
6	18,6	31	96,1
7	21,7	32	99,2
8	24,8	33	102,3
9	27,9	34	105,4
10	31,0	35	108,5
11	34,1	36	111,6
12	37,2	37	114,7
13	40,3	38	117,8
14	43,4	39	120,9
15	46,5	40	124,0
16	49,6	41	127,1
17	52,7	42	130,2
18	55,8	43	133,3
19	58,9	44	136,4
20	62,0	45	139,5
21	65,1	46	142,6
22	68,2	47	145,7
23	71,3	48	148,8
24	74,4	49	151,9
25	77,5	50	155,0

3.7 Modelling Concept for Fault Current Logic Controller

Single pole circuit breaker tripping is applied to this dissertation hence the fault trips the faulted circuit breaker pole, wait for 3 *ms* and subsequently return the circuit breaker to its normal state if the fault is cleared successfully on that faulted phase. This technology prevents the remaining circuit breaker poles from completing opening therefore maintaining the power supply to the consumers. The fault current logic controller for this dissertation, therefore only measure the phase angle on the faulted phase rather than entire 3-phases simultaneously.

The fault phase angle and its related parameters are used as inputs to the fault current logic controller using the logic derived from equation (3.13) to determine the fault current time instant in relation to the system frequency [6].

$$T_{If} = I_F . [sin(\omega \cdot t + \alpha - \varphi) - sin(\alpha - \varphi) \cdot e^{(-t/\tau)}] \quad (3.13)$$

Where, T_{If} = Fault current logic instantaneous time, t = time, ω = 2πf; f = power system (fundamental) frequency, α = phase angle on phase voltage when fault initiated, I_F = fault current magnitude, L = source-to-fault inductance, R = source-to-fault resistance, $\tan(\varphi) = (\frac{\omega L}{R})$ and $\tau = \frac{L}{R}$; time constant of the asymmetrical transient component of fault current. The fault angle time instant signal that is processed using the logic from equation 3.13 in relation to the current waveform is subsequently sent as an input signal to the predicted current zero controller to provide a basis for its logical processing.

3.8 Predicted Current Zero Controller

This advanced controlled switching integrated logic uses the principals of summation and comparator logic to provide swift fault clearing times coupled with reduction in arcing effects and inrush currents [4]. The predicted controlled trip time is formulated using equation (3.14) which forms part of the advanced controlled switching logic:

$$T_{co} = \left[\left(T_{If}\right)\right) + \left(\Delta T_{temp} + \Delta T_{Idle} + T_{std}\right)]\left|\left[\left(T_{If}\right)\right) + \left(\Delta T_{temp} + \Delta T_{Idle} + T_{std}\right)]\right| + 0.01\right\rfloor \quad (3.14)$$

Where, T_{co} = Predicted current zero trip time, T_{If} = Fault current logic instantaneous time, ΔT_{temp} = Compensation time based on temperature times, ΔT_{Idle} = Compensation time based on idle time and T_{std} = Standard Vacuum breaker opening time. The predicted current zero controller module determines the future current zero trip time with the use of the fault current time as reference point coupled with the summation of the idle, temperature and standard time delays. The circuit breaker delays in conjunction with the fault time instant is processed to ascertain the trip time. The trip time results are rounded to the nearest 10^{th} of a millisecond to facilitate only current zero tripping.

The predicted current zero controlled logic developed is tested against phase-to-Earth faults with earth connection by synchronizing it to the trip commands of phase 1(Phase A) of the 3-phase $11\,kV$ indoor vacuum breaker using PSCAD simulation software. The remaining breaker poles operates at no more than half a cycle apart in a RYB/ABC sequence.

3.9 Single Line Diagram

The single line diagram representation in Figure 3.2 reflects the real time network configuration from the point of supply up to the load namely the 2-way ring main unit which

is the consumers point of power supply. This single line diagram configuration is adopted for analysis in this dissertation using both the vacuum circuit breaker for advanced controlled switching and conventional circuit breaker interruption.

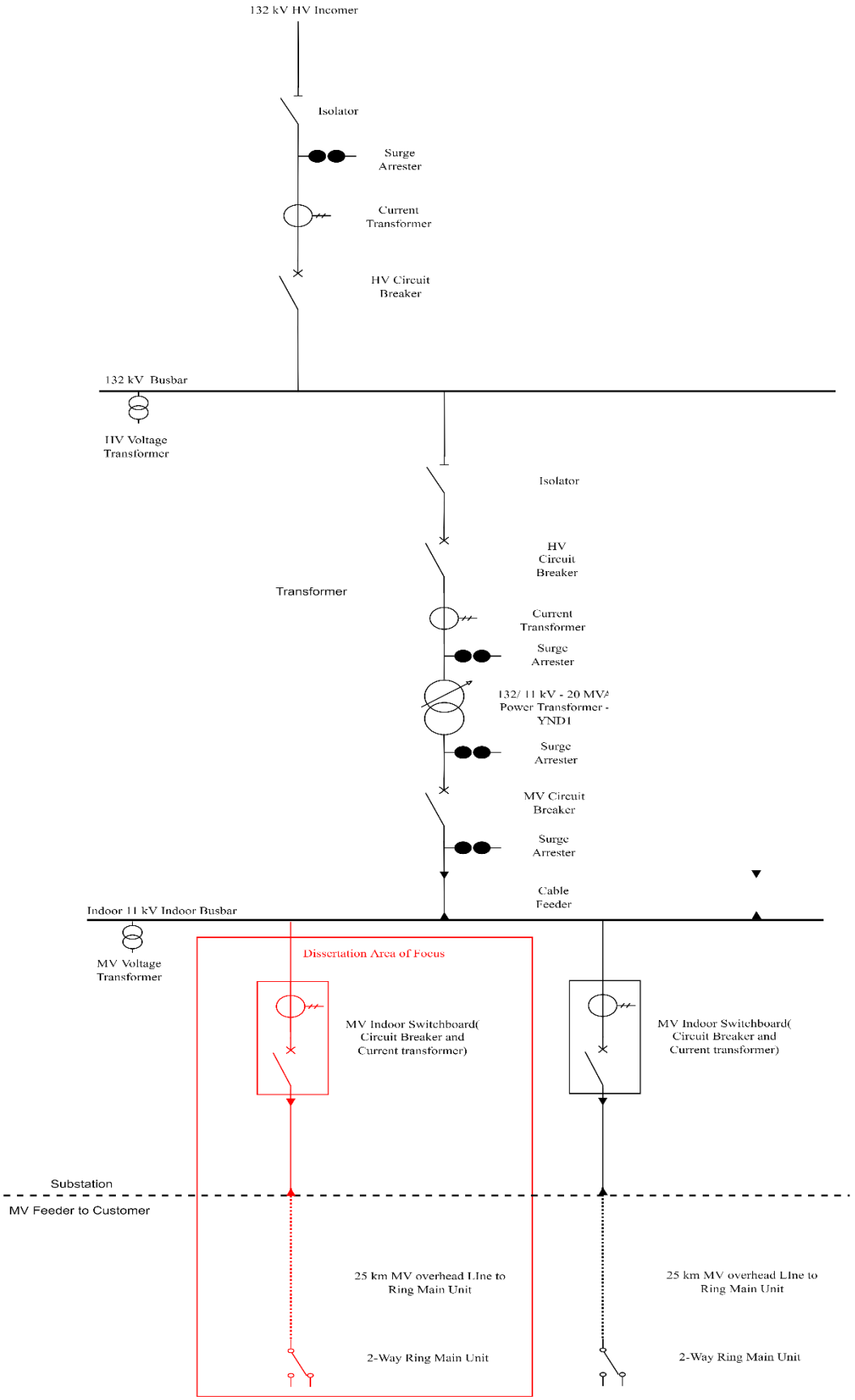

Figure 3.2 : Single Line Diagram of Simulated Network Model

3.10 Modelling Concept: Conventional PSCAD Model

3.10.1 Flow Block Representation

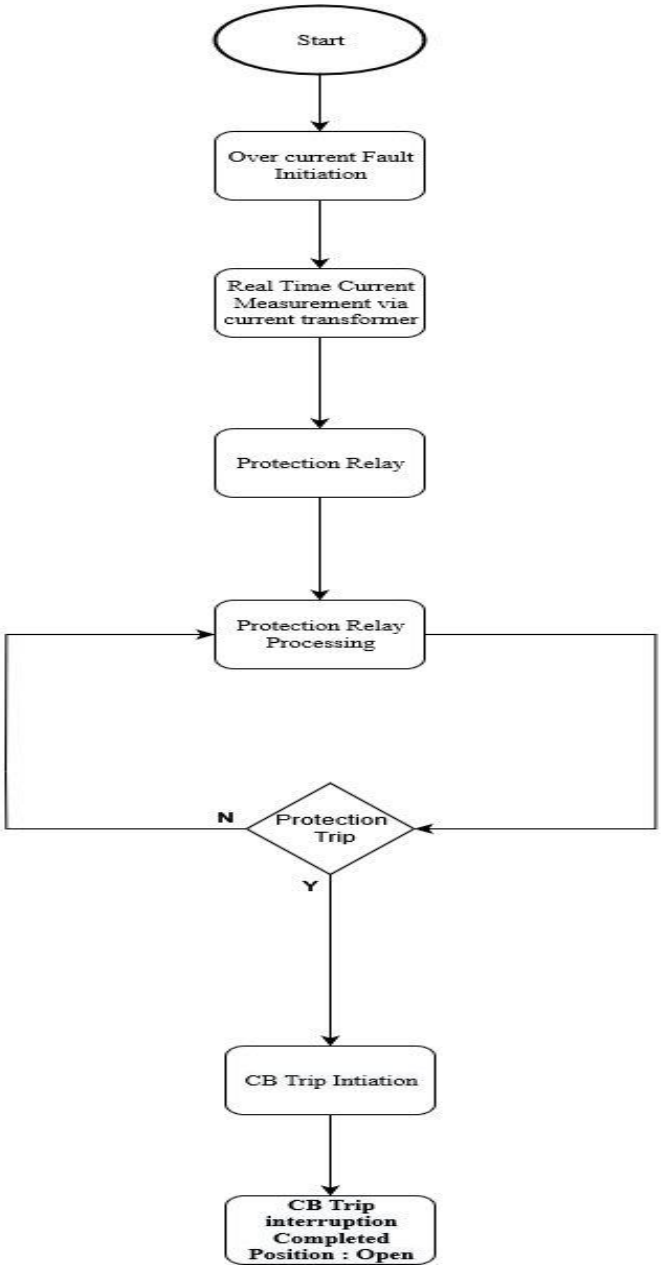

Figure 3.3 : Conventional Logically Flow Diagram

The conventional logically flow diagram in Figure 3.3 is a typical circuit breaker with overcurrent and earth fault protection. The start flow is followed by a fault initiation which is measured by the current transformer. The current transformer transmutes the fault current to its secondary side so its safety measurable by the protection relay. The protection relay picks up the fault and subsequently sends a trip signal to the circuit breaker trip coil to initiate a trip and interrupt the fault.

3.10.2 Input Output Signals and Controllers

The simulation software has two forms of inputs namely, the inputs signals which are derived from multiple output signals that are calculated during simulation or inputs that are inserted manually through controllers. The output signals are transposed through output channels in two forms namely the graph which is graphically representation such as waveform and a polymeter which is a digital metered reading. The input output signals and controllers used in the simulation are shown Table 3.10.

The control slider in Figure 3.4 is used to vary the circuit breaker standard operating time based on the manufacturers specification. This standard breaker time includes the arcing time.

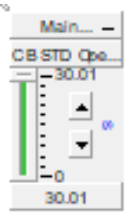

Figure 3.4 : Standard Breaker Operating time Control Slider

The switches in Figure 3.5 comprise of the fault current angle switch controllers which is used to alter the input fault current angle at 30°, 60° and 90°. This signal is subsequently sent as an input to the power circuit to change the fault current angle. This feature is to provide a comparative analysis at different fault current angles during simulations.

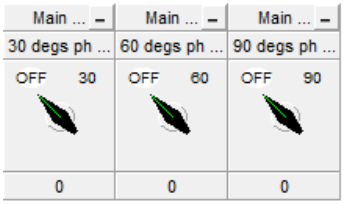

Figure 3.5 : Fault current angle switches

Table 3.10: Input/output Signals

Inputs/Output Signals		
Description of signal	**Prefix Code**	**SI Units**
Circuit Breaker Voltage (3-Phase)	VbrkX	kV
Source Input Current (3-Phase)	IbrkX	A
Circuit Breaker Current (Red Phase)	IbrkAX	A
Circuit Breaker Current (White Phase)	IbrkBX	A
Circuit Breaker Current (Blue Phase)	IbrkCX	A
Circuit Breaker Voltage (Red Phase)	EaX	kV
Circuit Breaker Current (3 – phase)	IspX	A
System Active Power	PsX	kW
System Reactive Power	QsX	$kVar$
Circuit Breaker Post Arc Active Power	BrkPsX	kW
Circuit Breaker Post Arc reactive Power	BrkQsX	$kVar$
System Current input to Current Source (3-phase)	IsX	A
Secondary Current input to RMS Meter	IsecAX	A
Circuit breaker Arc Active Power	ArcPX	kW
Circuit breaker Arc Reactive Power	ArcQX	$kVar$
Fault Current Phase Angle	PhAX	$^{\circ}$
Fault current time instant	FIinstX	s
Circuit Breaker Idle Time delay	IdleX	s
Source input current (3-phase)	IbrkAAX	A
Average System Temperature	TempTX	$^{\circ}C$
Resistance of Arc	RarcX	Ω
Average Temperature time delay	TempX	s
Total circuit breaker time delay	tdelayX	s
Circuit Breaker Trip time instant	TripTX	s
Fault current angle	PHSW	$^{\circ}$
Circuit Breaker Arc Voltage	VaX	kV
Restrike Voltage	ResX	kV

Simulated Output Graphs

The following graphs are simulated to display the results graphically in Chapter 4 which is used to measure the results produced during the current Interruption Phenomena:

- Circuit Breaker Arc Voltage
- Circuit Breaker Arc Current
- Arc Power (Active, Reactive)
- Post Arc Power
- Chopping Current
- Transient Recovery Voltage

- Restrike
- Arc Temperature

Simulated Output Polymeter's

The following Output Polymeter's are used as a system visual dashboard to confirm the status of the power system during simulations:

- Total circuit breaker time delay
- Circuit Breaker Trip time instant
- Fault Phase angle
- Fault Trip time

3.10.3 Power Circuit

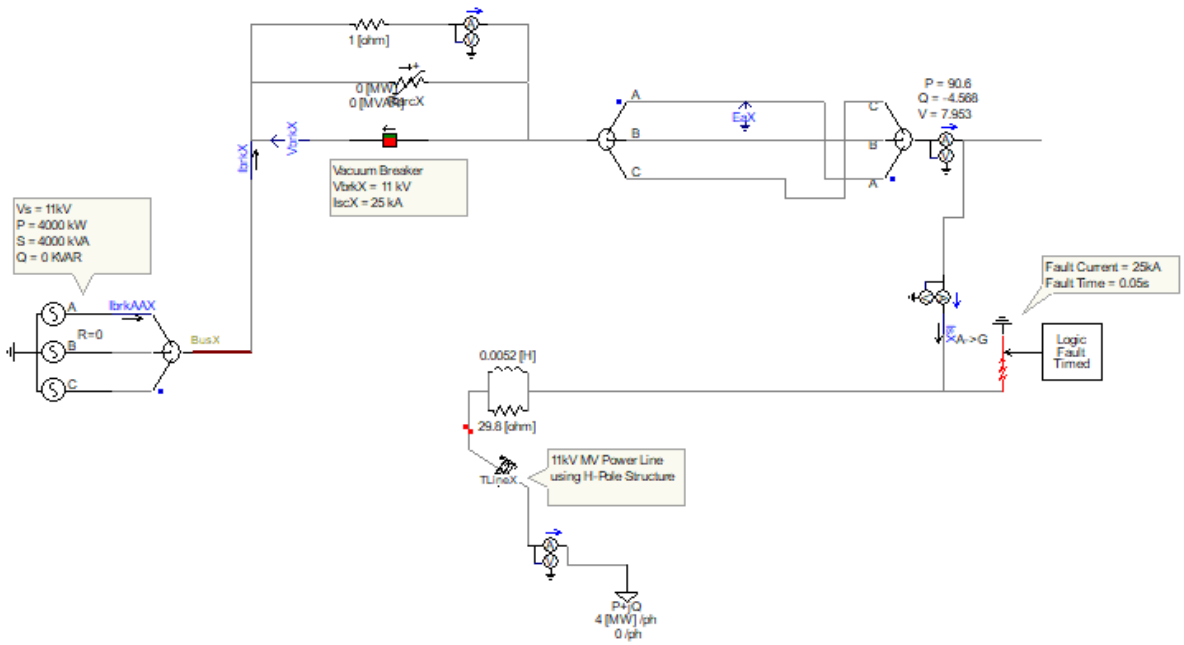

Figure 3.6 : Conventional Power Circuit Logic Diagram

The conventional PSCAD model was built using a 3-phase 50 *Hz* 11 *kV* power supply with a 4000 *kW* power capacity and a 11 *kV* vacuum circuit breaker that is protecting a MV feeder as shown in Figure 3.6. The 11 *kV* vacuum circuit breaker is connected to a 25 *km* overhead medium voltage power line using H-Pole structures which is subsequently connected to a load on the remote end with line surge protection. The power line electrical properties namely the capacitance of the line, inductance and resistance is represented by their subjective components on the model. To ensure that the electrical parameters are measured at the relevant positions on the simulated model in Figure 3.6, multi-meters are strategically positioned to measure the outputs of the model which subsequently feeds into the logic circuitry as shown

in Figure 3.7 to facilitate the circuit breaker protection. A resistor of $1\,\Omega$ is used in series to the multi meter that is parallel to the arc resistor to facilitate more accurate current measures as recommend in [92]. In parallel to the circuit breaker on the power circuit model is an arc resistor and a single line to 3-phase splitter converter on the model. This splitter assists in splitting the single line representation into a 3-phase system presentation in efforts to allow for measurement of the red phase parameters and the circuit is subsequently returned to a single line presentation the by using a 3-phase to single line splitter.

3.10.4 Conventional Breaker Time Delay Logic

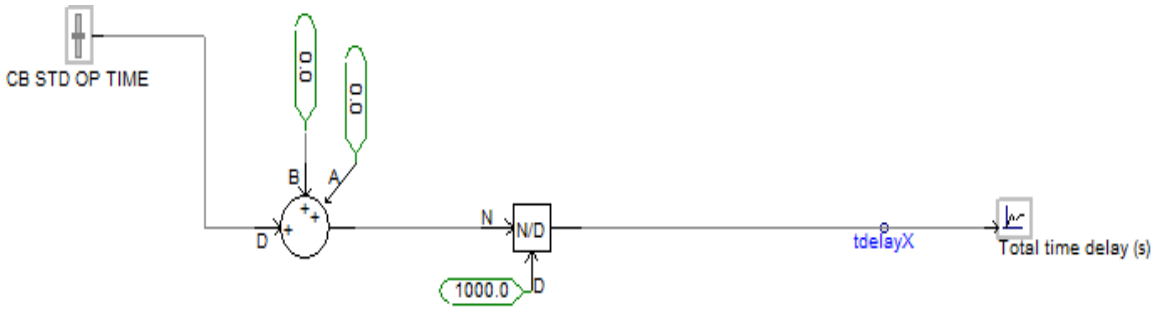

Figure 3.7 : Conventional Breaker Time Logic Diagram

The simulated circuit breaker model in PSCAD doesn't possess the capability of factoring the real time delays namely the arcing time delays and standard circuit breaker operating time delays. Hence the conventional breaker time delays attributed to the circuit breaker are summated using a conventional time delay circuit which operates using logic such that it processes the summated results through a logic divider that transposes the total delay time from millisecond to seconds. The total circuit breaker delays based on the circuit breaker manufacturer data are inputted from the logic delayed simulation circuit as a signal named *t-delay* to the sequencer module to facilitate a simulation closer to real time.

The outputs of the power circuit simulated model in Figure 3.7 are used as inputs to other parts of the circuit namely the protection relay circuit and the conventional time delay circuit and vice versa. The effective input output signal communication between modules assist the model to produce a calculated response thus out putting the results through the output channels. The conventional breaker time delay circuit is being used for both the conventional and controller circuit breaker simulation.

3.10.5 Restrike Measurement Module

Figure 3.8 : Restrike Module

The restrike module in Figure 3.8 is an added component which relies on the circuit breaker arc current to simulate the restrike occurrences if present, the frequency and phase angle between the current are variable on the module [93]. However, it is set in synchronization with the simulated power circuit to achieve its results. The results of the restrike is subsequently displaced by using an output channel to measure the analysis the restrike occurrences. The restrike component is being used for both the conventional and controller circuit breaker simulation.

3.10.6 Chopping Reignition Measurement Module

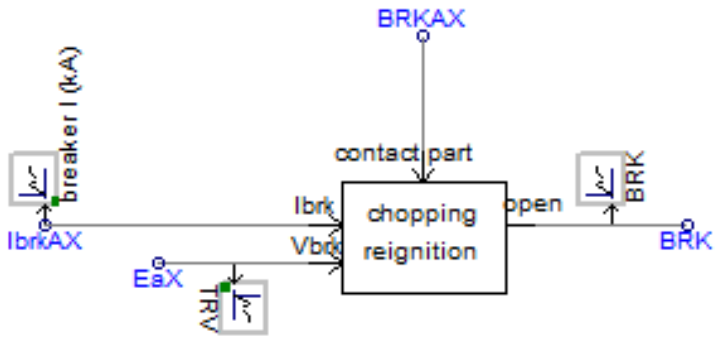

Figure 3.9 : Chopping Reignition Module

The chopping reignition module in Figure 3.9 is also is an added component which facilitates the chopping current analysis of the circuit breaker during closing of the circuit breaker when present [93]. It used the circuit breaker current and the transient recovery voltage as an input to the module. The output waveform is dependent on the angle of the fault current and is displayed using an output channel. The chopping reignition module has several parameters of the circuit breaker that may be set to simulate a close to real time chopping current. The selected parameters are shown in Table 3.11 below are set has per the circuit breaker manufacture data.

Table 3.11: Chopping Current Module Parameters

Parameter Description	SI Unit	Breaker Set Value
Current chopping level	kA	5 A
Rate of rise of dielectric strength	kA/s	1e5
Rate of rise of quenching capability	kA/s^2	1e5

3.10.7 Overcurrent Relay Protection Logic

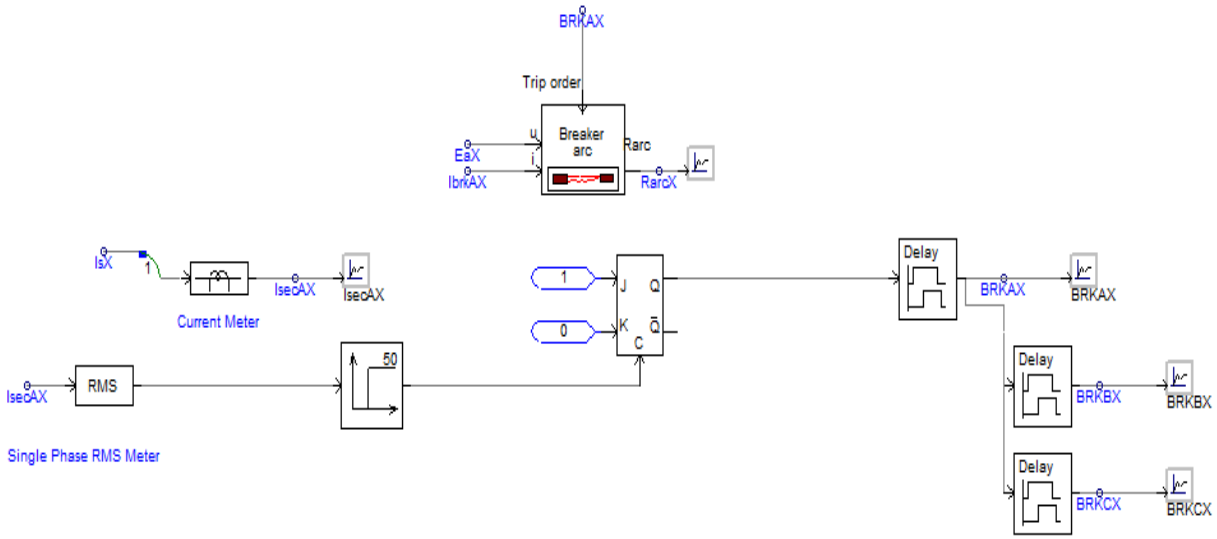

Figure 3.10 : Conventional Overcurrent Relay Protection Logic Diagram

The overcurrent protection relay as shown in Figure 3.10 is fed via a current meter module which operates as a current transformer that steps the current down on its secondary side to 1 *A*. The 1 *A* signal from the current meter module is an analogue signal which is converted to a digital signal using a route mean square (RMS) module thus making possible for the over current protection relay to receive the 1 *A* input and monitor the current on the system similar to the real time connections at substations. The overcurrent protection relay is equipped to operate using the single pole circuit breaker tripping, to pick up on over current between lines and also between line and earth. The phase-to-earth fault simulated on the power circuit model is achieved by a 3-phase fault module and the fault time duration that is timed by the conventional circuit breaker logic module as shown in Figure 3.10.

The protection relay logic circuit output trip signal is processed through a JK flip-flop module to ensure that the relay trip high signal is latched for a circuit breaker trip command when succumbed by a circuit breaker trip delay inputted by the conventional time delay logic circuit shown in Figure 3.10. In real time relays and on the simulated model, the trip command high output from an over current protection relay is issued for a short time duration and is then

reverted to a low if the circuit breaker trip signal is not received during this short trip duration and the trip signal from the protection relay is lost hence the use of a JK- flip flop to preserve the signal by latching it on the high signal command. The circuit breaker 3-pole tripping capability was achieved using a Binary delay module which was place on each of the three phases which allowed for a half cycle delay on tripping between circuit breaker poles. The circuit breaker arcing dynamics are simulated using the resistance of the Arc namely RarcX which is connected in parallel to the vacuum circuit breaker as shown in Figure 3.10. The variable resistive parameters are obtained using a Breaker arc module outputs which are calculated using the Mayr modelling algorithms that is reliant on the inputs of the system voltage and current together with the trip output of the circuit breaker.

3.11 Modeling Concept: Advanced Controlled Switching PSCAD Model

3.11.1 Flow Block Representation

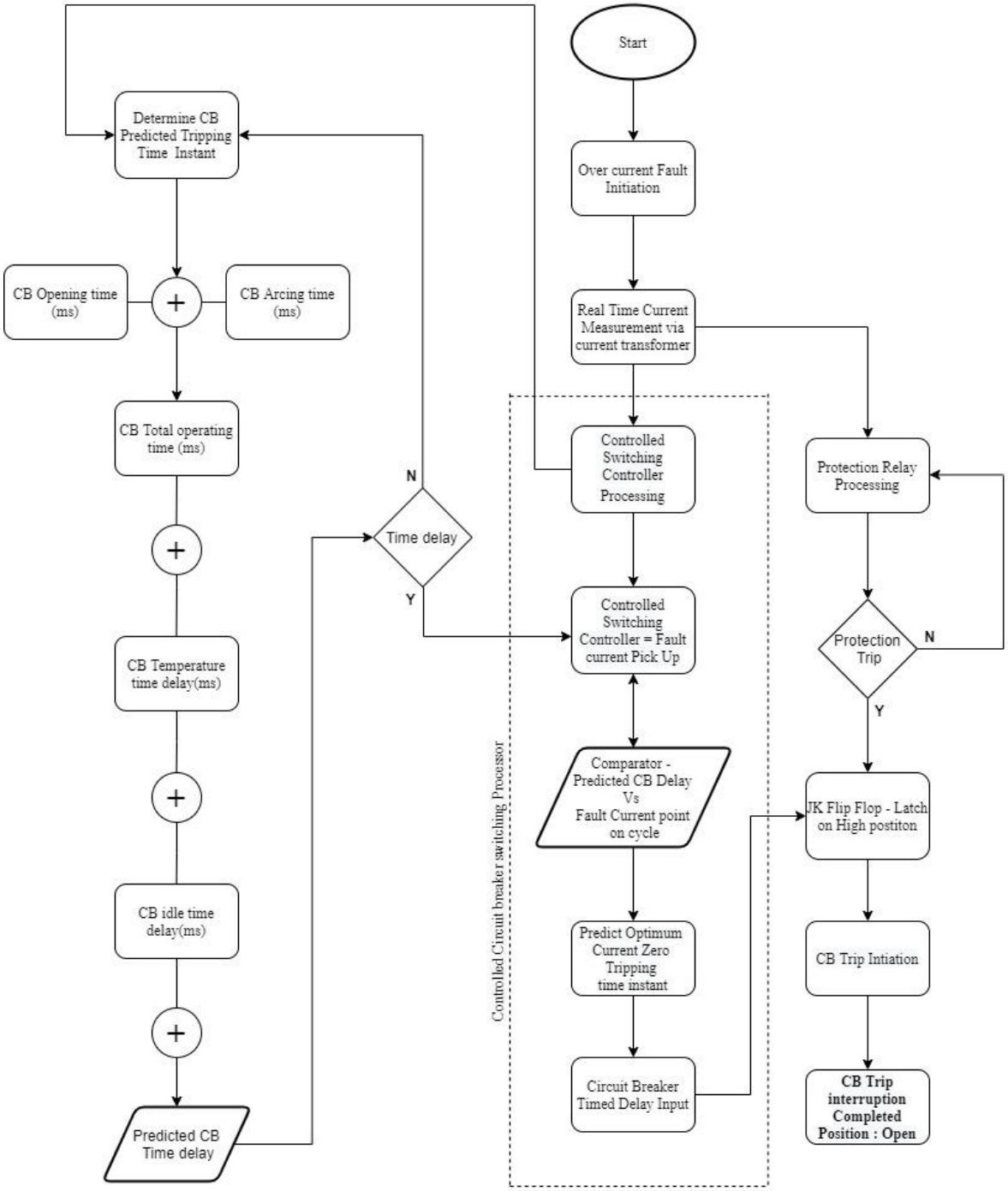

Figure 3.11 : Controlled Switching Logically Flow Diagram

The controlled switching logic in Figure 3.11 is initiated by a start. When a fault is initiated, the current transformer transmutes the fault current to an output secondary current that feeds as an input to the protection relay and controlled switching controller. When the fault signal is received at the protection relay, the protection relay outputs a trip signal to the JK flip flop to latch the signal on a high. Consequently, the trip signal to the circuit breaker initiator which processes the input awaits the trip signal from the controlled switching controller prior to sending a trip signal to the circuit breaker to interrupt the fault. The input received from the current transformer to the controlled switching controller determines the circuit breaker predicted time output by processing the various delays the circuit breaker inhabits. The delays are subsequently sent as an input to the controlled switching controller which processes the delay and sends it to the comparator where the delays are compared to the fault current time instant in relation to the system frequency to determine the conventional trip time. The conventional trip time output from the comparator is sent as an input to the predicted current zero-time processor where the total delay required to achieve the optimum current zero trip is predicted and subsequently send as an input to the circuit breaker trip time instant processor where the delay is initiated. Once the delay time has lapsed, a trip signal is sent to the circuit breaker initiator. The circuit breaker initiator processes the trip signal to the circuit breaker now that it received two trip signals which allows the circuit breaker to trip at current zero. In an event that the breaker failed to trip at current zero using the time delay by the controlled switching logic, the protection relay signal is then allowed to trip the break after the time delay has lapsed which is a failsafe logic embedded.

3.11.2 Input Output and Controller Signals

The secondary current and voltage output signals from the power circuit in Figure 3.6 are used as inputs to the protection relay, predicted current zero controller circuit, temperature and idle time logic time controller circuits. These inputs assist the relay and controllers to provide a calculated response to determine the ideal trip time of the circuit breaker.

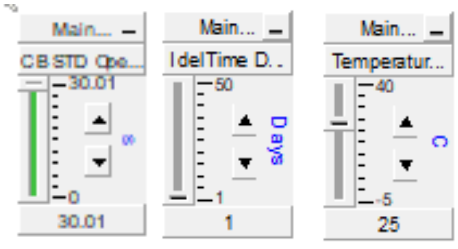

Figure 3.12 : Advanced Control Sliders Inputs

The advanced input control sliders in Figure 3.12 are used to vary the input parameters comprising of the standard breaker operating time, the circuit breaker idle time and the ambient temperature to provide a comparative simulation analyses for advanced controlled switching.

Simulated Output Graphs

The following graphs are simulated to display the results graphically in Chapter 4 which is used to measure the results produced during the current Interruption Phenomena:

- Circuit Breaker Arc Current
- Circuit Breaker Arc Voltage
- Arc Power (Active, Reactive)
- Post Arc Power (Active, Reactive)
- Chopping Current
- Transient Recovery Voltage
- Restrike
- Arc Temperature

Simulated Output Polymeter's

The following Output Polymeter's are used as a system visual dashboard to confirm the status of the power system during simulations:

- Average System Temperature
- Circuit Breaker Idle Time delay
- Total circuit breaker time delay
- Circuit Breaker Trip time instant
- Fault Phase angle

The Multimeter and current transformers in the power circuit coupled with the integrated input output signals position at various points on the simulated models allows for calculated outputs based on the input parameters. The outputs are sent via output channels to display the output graphs and the Polymeter's listed which provides the results in both graphical and metered form to allow integrating and detailed analyse which forms part of chapter 4.

3.11.3 Power Circuit

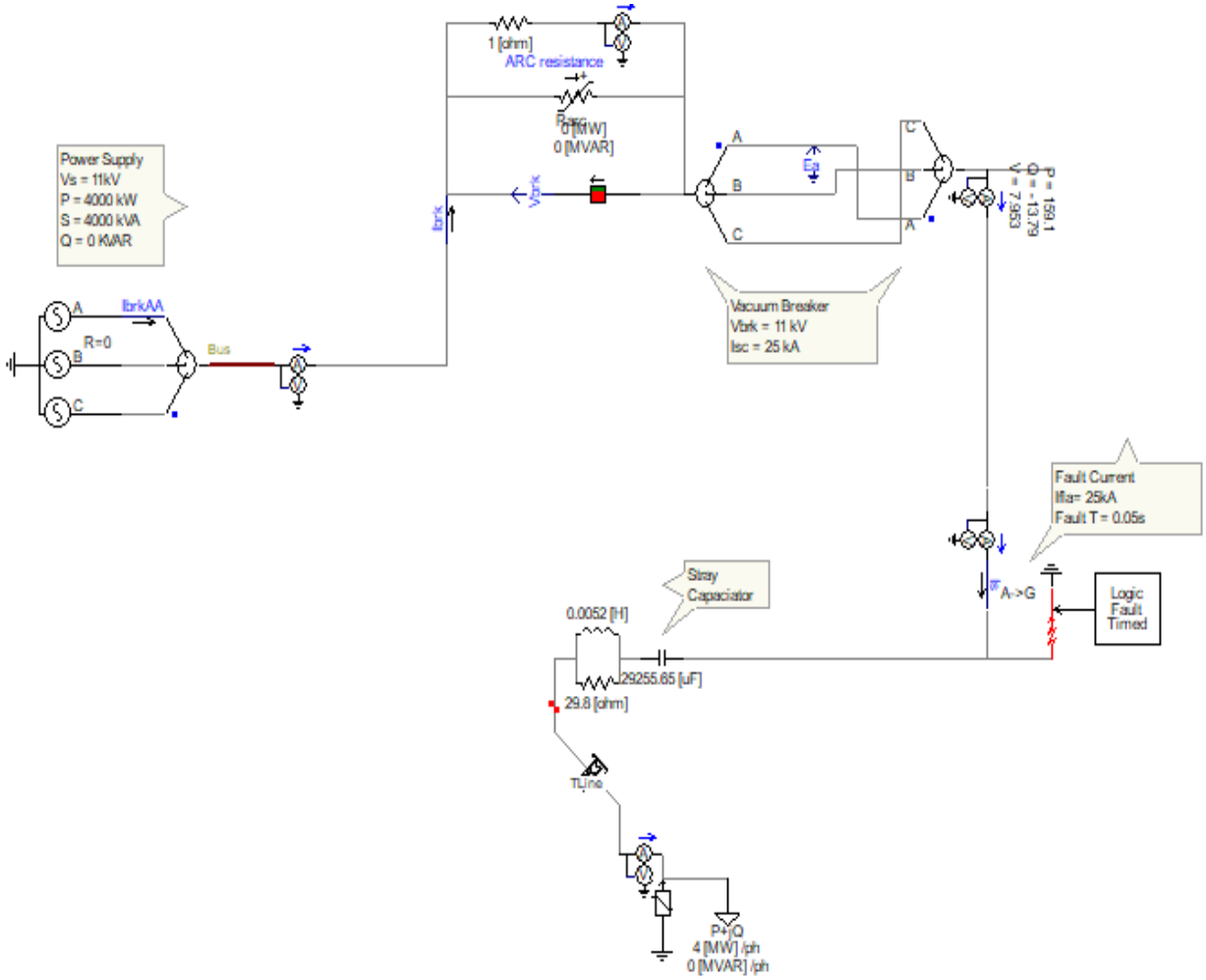

Figure 3.13: Advanced Controlled Switching Power Circuit

The advanced controlled switching circuit in Figure 3.13 is built using the same power circuit model circuitry and relay protection logic circuitry as per the conventional PSCAD model as shown in Figure 3.6. with the addition of a stray capacitor and multiple controlled logic black box models to provide the advanced controlled switching functionality as shown in Figure 3.14 to Figure 3.16. The input models that forms part of the advanced controlled switching logic is the fault current logic controller, idle time controller, temperature controller and predicted current zero-time controller.

3.11.4 Fault Time Instant Logic Controller Diagram

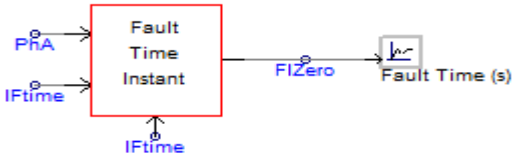

Figure 3.14: Fault Time Instant Black Box Model

The fault time instant logic controller represented by a black box model in Figure 3.14 consists of a Divider module(N/D) which converts the phased angle fault (PhA) into a fault time instant (FIZero) on the current cycle in relation to the frequency. The logic continuously processes time instants based on the position of the current phase angle per cycle in efforts to process possible fault instant times prior to the fault occurring. This effectively provides the controller with a data continuously therefore reducing the effects of delays in processing. The output from the divider modules are processed through an absolute value module to ensure the fault time output is always represented by a positive value. Negative outputs cause the trip breaker protection relay to malfunction thus failing to trip on command hence the absolute value module forms part of a protective measure to prevent tripping failure. The output fault time instant (FIZero) signal is subsequently processed as an input to the predicted current zero controller circuit.

3.11.5 Idle Time Logic Controller Diagram

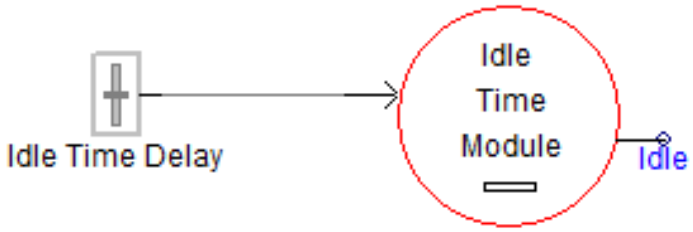

Figure 3.15: Idle Time Logic Controller Black Box Model

The ideal time logic controller represented by a black box model in Figure 3.15 has a manual controlled input slider which is where the idle time in days are inputted to the logic. The idle controller is limited to 50 days as per the research indicated in [6]. The idle time black box model operates such that the idle time is processed through a rate limiter which ensures that the logical output is limited to an increase or decrease of 1 unit per day. This effectively enables the logic processing output signal to the multiplier within the idle time black box to be processed in days rather than hours. The output signal from the multiplier in relation to the average per day as indicated in [91] produces an idle time from the idle time logic controller black box model that is subsequently processed through as an input signal to the predicted current zero controller circuit.

3.11.6 Temperature Delay Time Controller Logic Controller Diagram

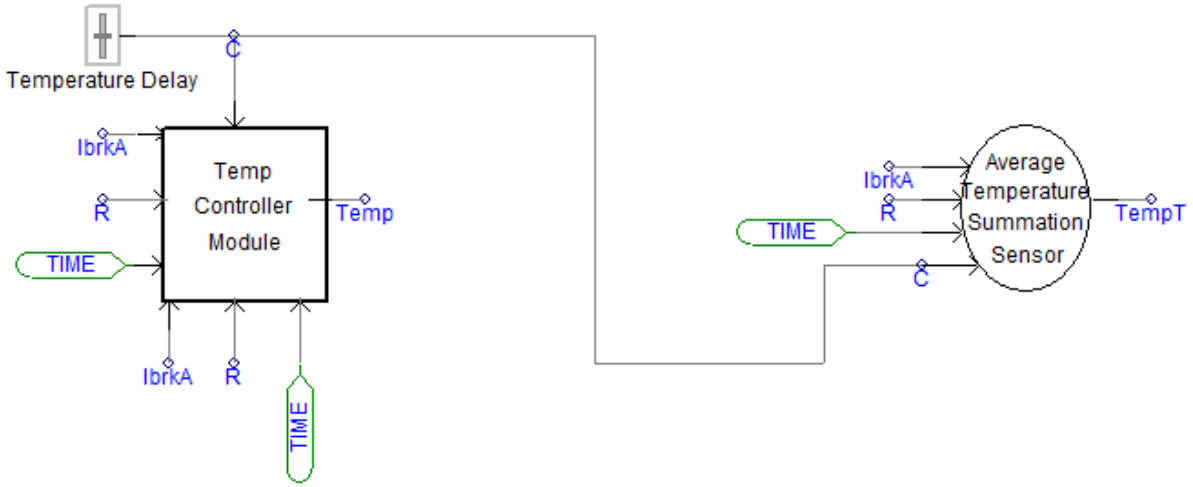

Figure 3.16: Temperature Delay Time Logic Controller Diagram

The temperature logic controller is represented by a black box model shown in Figure 3.16 which is formed with the integration of two temperature sub modules of which both operate with the manual input for the ambient temperature from the manual slider that is controlled by the user. The manual temperature is limited to a range of -5 $^{\circ}C$ to 40 $^{\circ}C$ as this is in line with the circuit breaker withstand temperatures outlined by the circuit breaker manufacturer. The output temperature signal from the slider is processed through the rate limiter within the temperature controller model to ensures that the logically output is limited to a change in temperature by increments of 1 $^{\circ}C$.

The 2nd part of the model namely the average temperature uses logic to calculate the temperature within the electrical system based on the systems electrical heat energy produced from the operating current during the simulation. This is achieved by the input circuit breaker current of the system being processed through a divider module which is used to convert from kilo amps to amps in efforts to convert to the international system of units. The signal is subsequently processed through a square module and several multiplier modules within the average temperature summation sensor model. The multiplier modules have been designed to produce processing logic that is in line with the research logic in [94]. The system resistance is represented by the input R to the 1st batch of multipliers modules and the output is subsequently processed through the 2nd batch of multiplier modules within the temperature summation sensor model with an input time that represents the time duration of the simulation during circuit breaker interruption. The temperature outputs of both logic processors are processed to output the average temperature of the system. This average temperature is subsequently processed to

obtain a time delay relevant to the average temperature of the system which is finally processed through the predicted current zero controller circuit.

3.11.7 Summation Module Controller

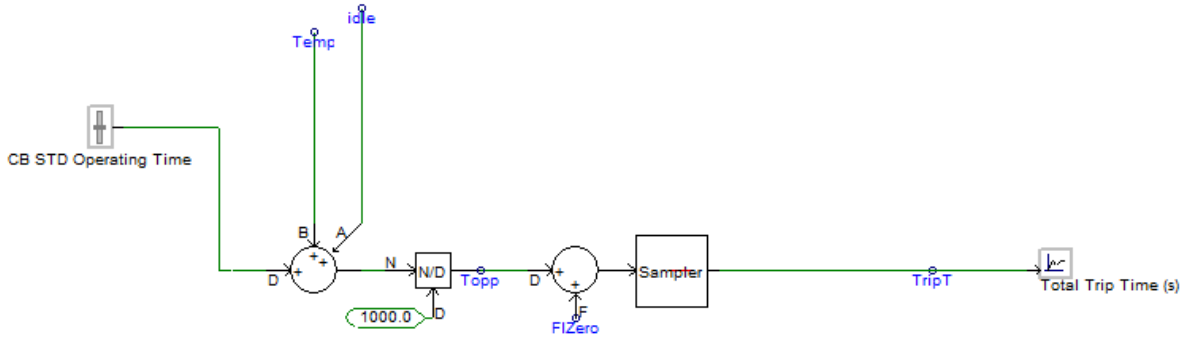

Figure 3.17: Predicted Current Zero Controller Switching Logic Diagram

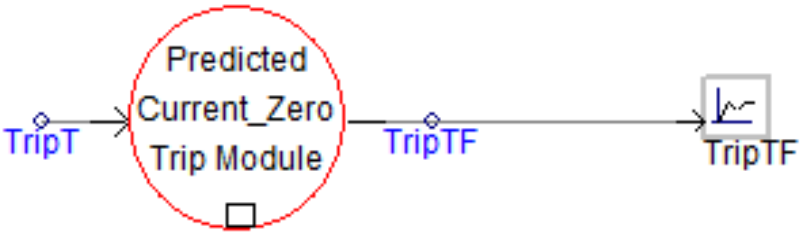

Figure 3.18: Predicted Current Zero Module

The summation module controller comprised of the predicted current zero controller and the predicted current zero model. The output results from the idle(idle), temperature(Temp) and fault current instant (FIInst) zero logic controllers are summated together with the standard circuit breaker time in the predicted current zero controller in Figure 3.17. to produce an inputs to the predicted current zero controller switching circuit shown in Figure 3.18. Each of the above logic controllers have a sider input to them which can vary its parameters for integrative analyses as shown in Figure 3.17 to 3.18. The total delay time is processed through a divider module to covert the output results from milliseconds to seconds. The time delay signal (tdelay) in seconds is subsequently processed through a sampler module to capture the instantaneous time in order to prevent continuous processing delays which hampers the protection relay from operating timeously. The signal that is processed through a predicted current zero module as shown in Figure 3.18 adds the shortfall time to the total delay time calculated to achieve the current zero tripping instant. The time delay (tdelay) is subsequently sent as a delayed input to the overcurrent protection relay logic circuit. The combination of the black box models in this section effectively forms the advanced controlled switching circuitry.

3.11.8 Overcurrent Protection Relay Logic

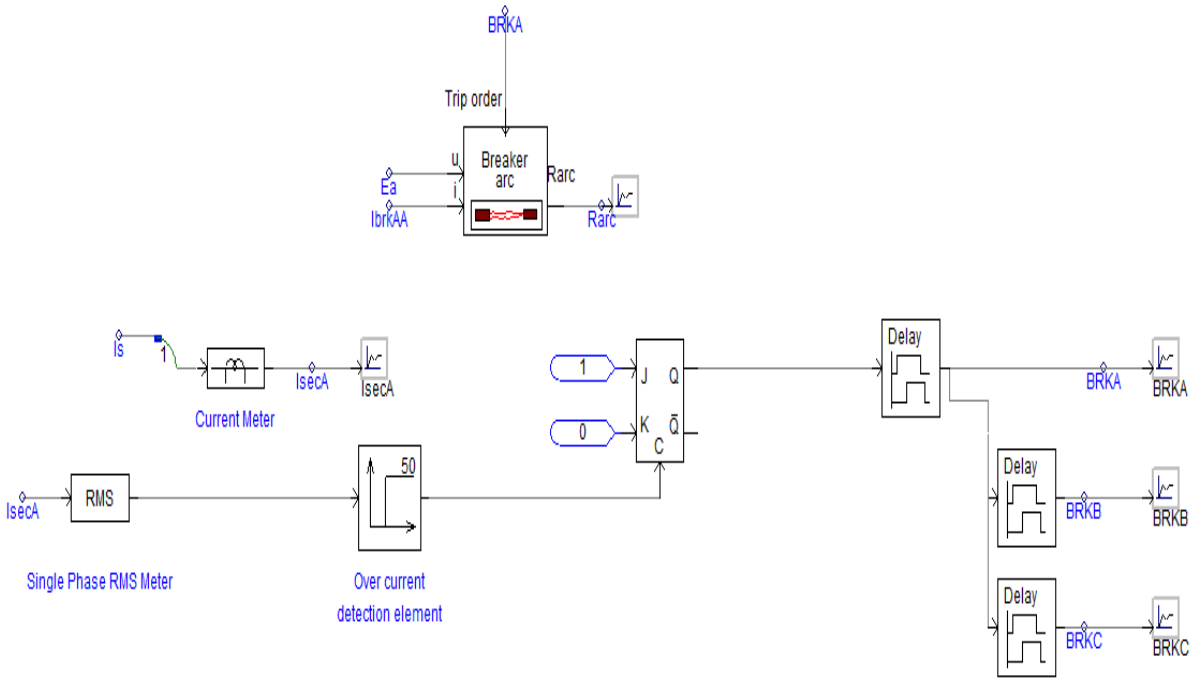

Figure 3.19: Overcurrent Protection Relay Logic

The controlled overcurrent protection relay logic in Figure 3.19 works on the same principals as the conventional overcurrent protection relay shown in Figure 3.10 with the exception that the input (tdelay) to the delay binary module on the phase A is from the predicted current zero controller switching logic. The time delay signal (tdelay) for the tripping of phase A at current zero is followed by the tripping of the remaining un-faulted phases namely B and C at half cycle apart.

Chapter 4

Analysis and Results

4.1 Introduction

The modelling of the circuit breaker was achieved using the EMTP in order analyse the arcing phenomenon. In addition, the PSCAD software is utilised to perform the simulation and testing of the controlled circuit breaker for fault interruption. Black box models were built to represent several components in this design in an effort to provide an advanced switching controller (ACS). Several of the controllers are built from black box models that provided measurements capabilities that did not feature as a standard in the EMTP software. These black box models have integrated logical circuits which have been constructed to provide the required results that was subsequently compared to the predicted controlled trip time equation to verify the consistency of the results.

4.2 Simulation Methodology

Advanced controlled switching integrated logic was created within the EMTP. This program uses the principals of summation and comparator logic to provide swift fault clearing times coupled with reduction in arcing effects and inrush currents [95]. The model comprises of several black box models. One of the black box models developed, is the predicted controlled trip time logic module which extrapolates the fault time instant results using the logic derived from equation (3.6). These fault time results are obtained from equation (3.8) and are used as the input variables into equation (3.7) to obtain the overall predicted current zero trip time that was derived to form part of the advanced controlled switching logic. The predicted current zero controller is the core black box module which determines the future current zero trip time considering the fault current time as a reference point. This summation black box model which summates the idle, temperature and standard time delays as shown in Figures 3.19 and 3.20. The circuit breaker delays in conjunction with the fault time instant is processed to ascertain the earliest current zero trip time. The trip time results use the logic to facilitate only current zero tripping. The predicted current zero controlled logic was implemented on a Phase-to-Earth faults with earth connection by synchronizing it to the trip commands of phase A of the 3-phase 11 kV indoor vacuum breaker using EMTP. The remaining breaker poles operate at no more than half a cycle apart in a RYB/ABC sequence.

The circuit breaker interruption phenomena result's from both the advanced controlled switching and conventional fault interruption were compared and analysed using the EMTP to obtain the thermal rise and energy results. The thermal and energy results were transposed into the Arrhenius equation (2.23) to measure the rate of change in relation to the circuit breaker lifespan, with reference to the temperature and energy of the arc [76, 77]. The comparison of these results provided the indication of the effectiveness of the predicted controlled trip logic equation. The remaining results from the advanced controlled switching then allowed the comparison of results from simulated advanced controlled switching to the conventional switching to ascertain the impact using the advanced controlled switching over conventional circuit breaker switching for fault interruption.

4.3 Power Circuit Analysis

The power circuit in the conventional and the advanced controlled switching logic, provides the source of analysis in this chapter for all results in this dissertation. The supply voltage of 11 kV is simulated for the circuit at 50 Hz . The instantaneous short circuit fault current of 25 kA was injected into the circuit at several fault angles of 30°, 60° and 90° in efforts to analyse the impact on the output results. The simulated fault angle range was limited in this dissertation due to the substantial data variables which will not invariably differ from the final output results. Each fault current angle selected varied the time instant of the fault. It was established that in all simulated models, the selected fault currents produced trip times as indicated in Table 4.1. where the current lags the voltage.

Table 4.1: Fault Current Interruption Time

Fault Current Simulated Interruption Time	
Short Circuit Fault Current Angle	**Current Interruption Trip Time Instant**
30°	0.0187 s
60°	0.0084 s
90°	0.0273 s

The interruption time of the vacuum circuit breaker via the overcurrent protection relay resulted in an instantaneous trip at the instant of trip signal input. The PSCAD software did not factor in any mechanical delays of the circuit breaker when simulating the power circuit for the conventional and advanced controlled switching circuits, this deviates from the results obtained in real time. The deviation was picked up when it was compared with typical circuit breaker trip time outlined by the circuit breaker manufacturers specification. These delays were

integrated into the design using the slider controller that was subsequently incorporated into the power circuit to ensure the simulated results are aligned to the real-time results. A mechanical delay of 35.05 ms was inserted comprising of the standard circuit breaker time of 25 ms and an arcing time of 10.05 ms. A slider controller allows for varying the circuit breaker delays in accordance with the circuit breaker manufactures data.

4.4 Analysis and Results

The abbreviation SN denotes "Simulation Number". The simulations SN1 to SN3 as implemented for conventional switching and subsequently compared to the simulations SN1 to SN3 for the advanced controlled switching, is used to benchmark improvements when advanced controlled switching is applied. Thereafter, the results of SN1 to SN3 of the advanced controlled were compared to SN4 to SN6 to analyse the impact on the circuit breaker when idle time and temperature varied.

Table 4.2: Conventional Breaker Standard Electrical Input Parameters

Conventional Breaker Inputs			
Simulation No. (SN)	**Fault angle (°)**	**Idle Time (days)**	**Temperature (°C)**
SN 1	30	N/A	N/A
SN 2	60	N/A	N/A
SN 3	90	N/A	N/A

The conventional model was analysed based on varying the fault angle to measure the impact on the circuit breaker results and subsequently use it as a baseline comparison to the advanced controlled switching results. The inputs in Table 4.2 were used for the simulation and calculations for the conventional analysis.

Table 4.3: Advanced Controlled Breaker Electrical Input Parameters

Advanced Controlled Breaker Inputs				
Simulation No. (SN)	**Fault Angle (°)**	**Idle time (days)**	**Temperature (°C)**	**Breaker Standard Operating (ms)**
SN 1	30	1	23	35.05
SN 2	60	1	23	35.05
SN 3	90	1	23	35.05
SN 4	30	1	25	35.05
SN 5	60	25	23	35.05
SN 6	90	50	-5	35.05

The inputs in Table 4.3 was used for the advanced controlled switching simulations. The advanced controlled simulated analysis is based on varying the fault angle, idle time and temperature of the circuit breaker with a constant input voltage of 11 *kV* and a constant fault current of 25 *kV* to measure the impact on the vacuum circuit breaker results for advanced controlled switching interruption. The detailed comparison of the results is outlined in this section to guide on the overall outcome of the advanced controlled switching technology in comparison to the conventional vacuum circuit breaker for fault interruption. The high level comparison of the conventional to the advanced controlled switching results is relevant to the power of the arc, temperature of the arc and arc energy for all simulations are summarized in Appendix C.

4.4.1 Interruption Time

The interruption time for the conventional and advanced controlled switching simulation SN1 to SN3 was implemented by varying the fault current angle, with an additional variation of idle time and temperature being implemented for advanced controlled switching, for simulation SN4 to SN6. The instantaneous time for fault interruption of the conventional and advanced controlled switching was completed using the standard protection relay operation time and circuit breaker opening time. The interruption output results for the simulations are shown in Figure 4.1 to 4.6, where IspX represents the conventional switching graph and Isp represents the advanced controlled switching

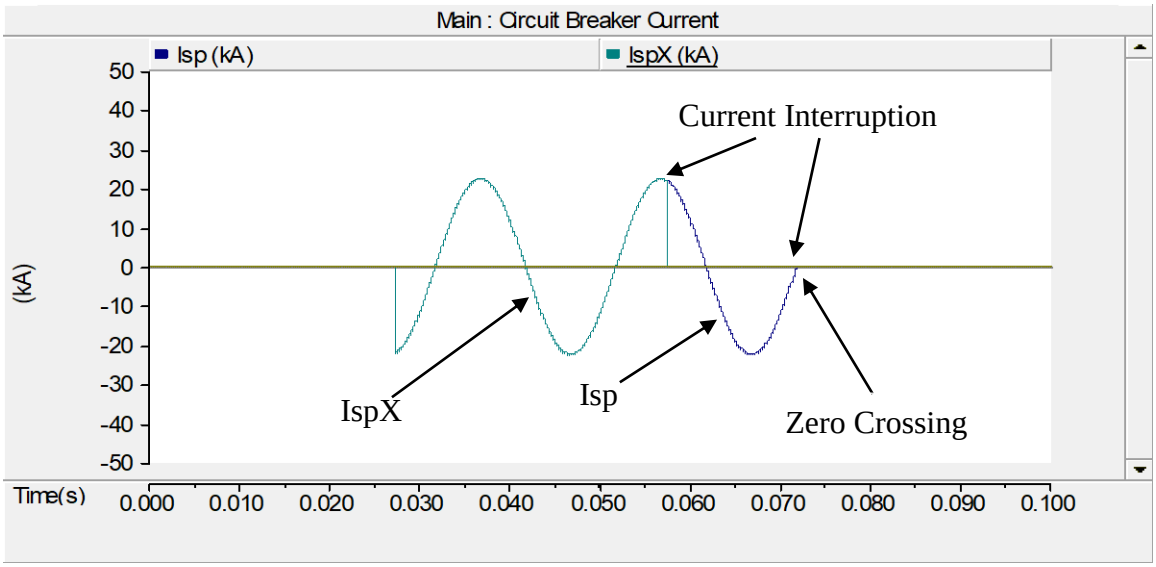

Figure 4.1: SN1 Controlled Switching Vs Conventional Interruption time

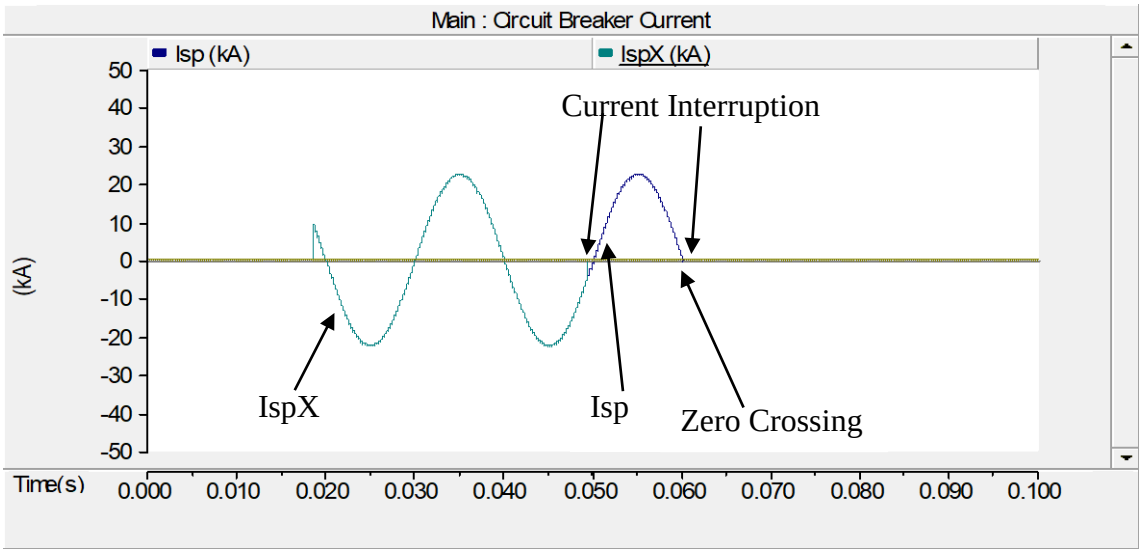

Figure 4.2: SN2 Controlled Switching Vs Conventional Interruption time

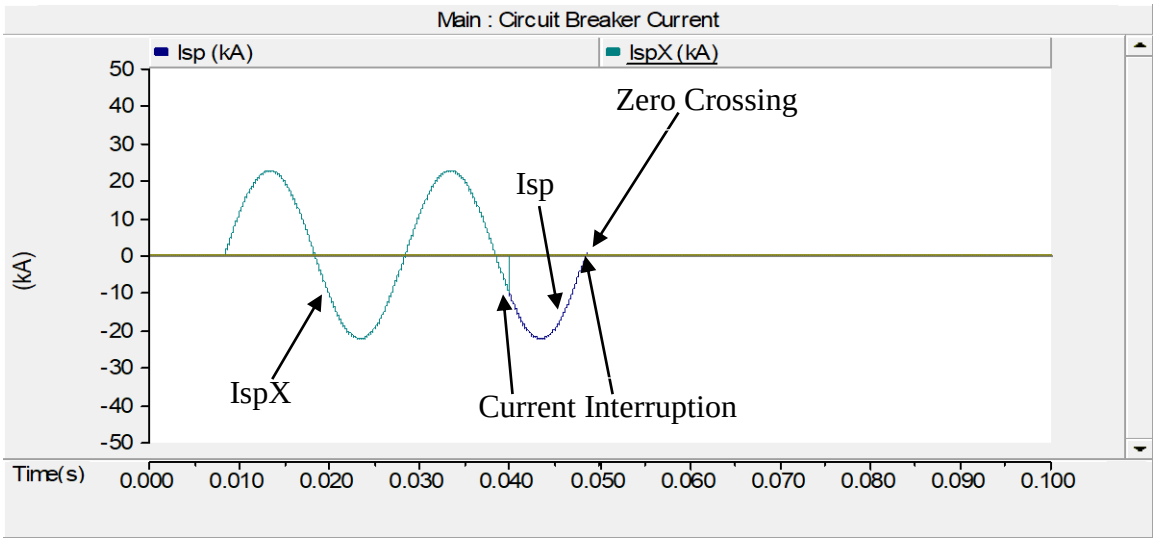

Figure 4.3: SN3 Controlled Switching Vs Conventional Interruption Time

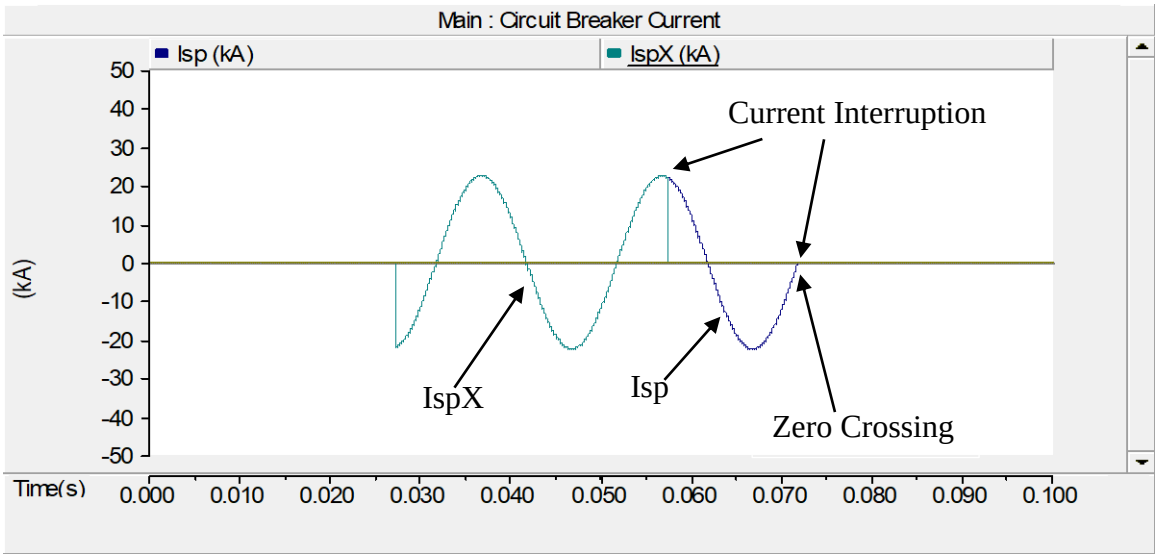

Figure 4.4: SN4 Controlled Switching Vs Conventional Interruption Time

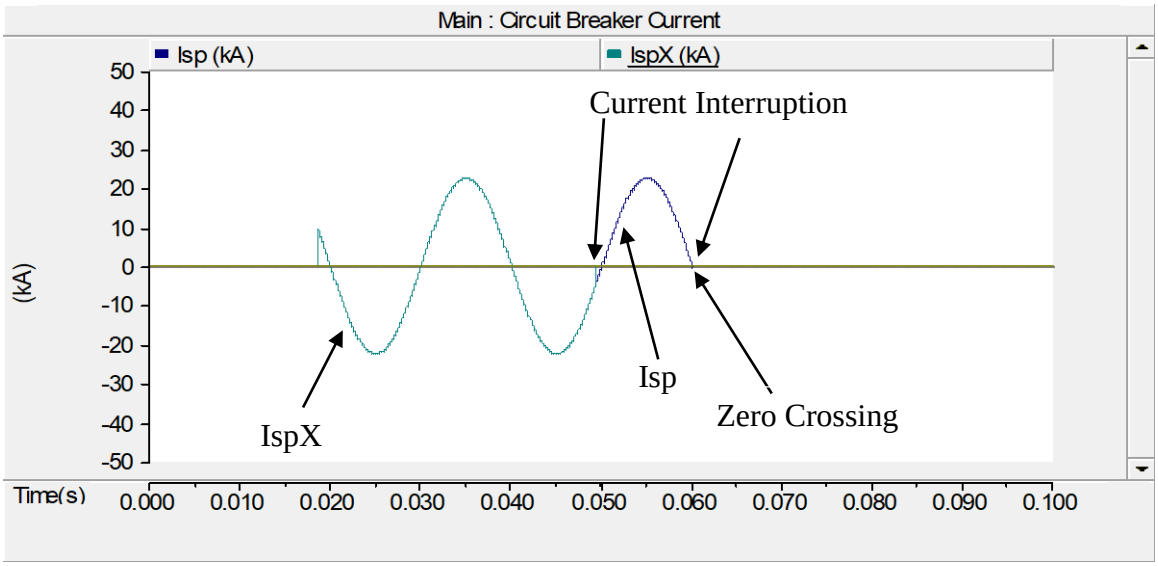

Figure 4.5: SN5 Controlled Switching Vs Conventional Interruption Time

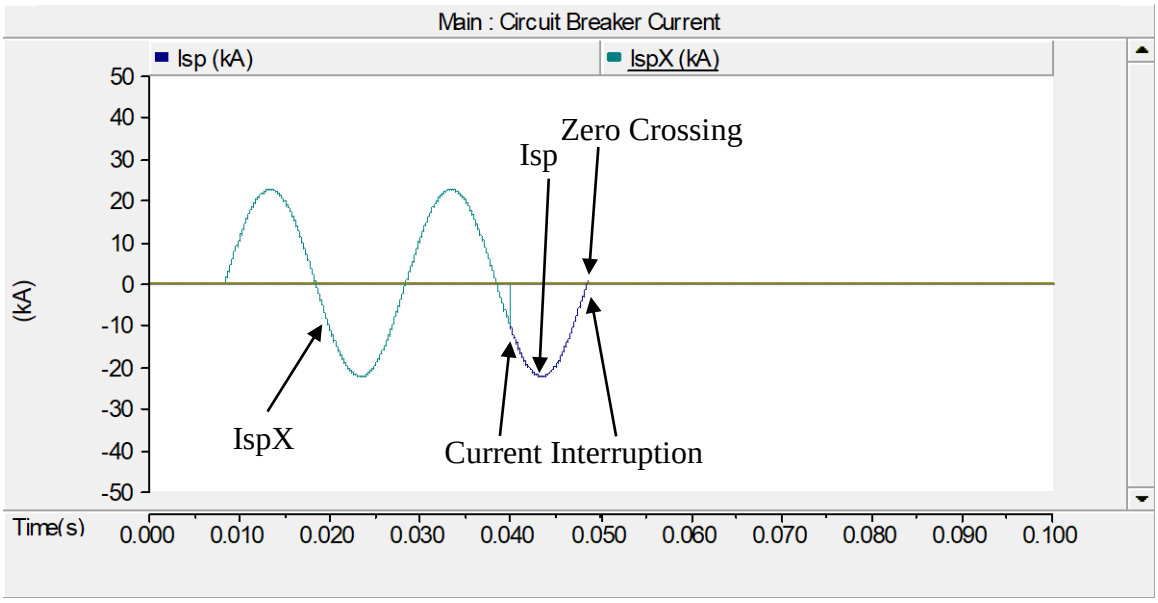

Figure 4.6: SN6 Controlled Switching Vs Conventional Interruption Time

4.4.1.1 Conventional Switching Case

The interruption time instant results changes as the fault phase angle is varied for each simulation as shown in Figure 4.7. These results as documented in Table 4.4 indicate that the fault phase angle is a catalyst for the instantaneous trip time when conventional switching is independently applied.

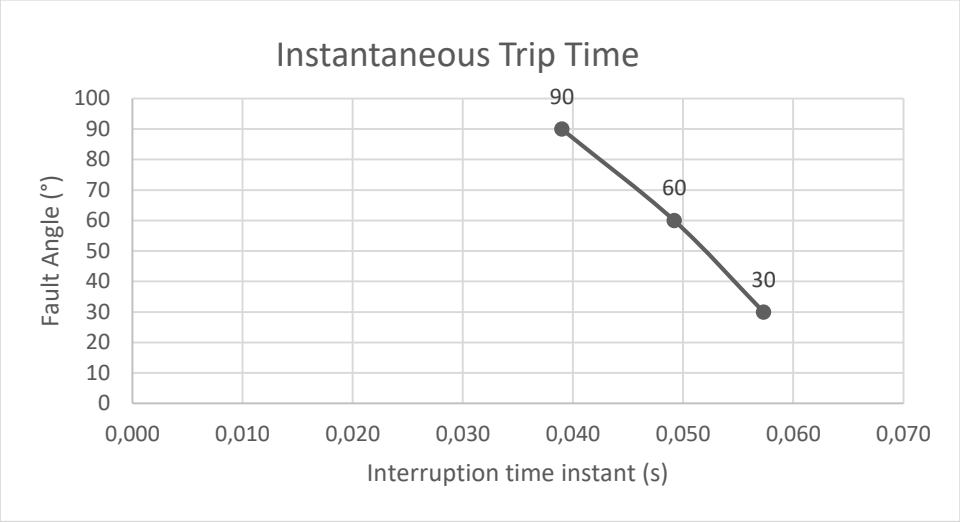

Figure 4.7: Instantaneous Simulation Graphs

Table 4.4: Conventional Switching Instantaneous Trip Time Results

Conventional Switching Trip Time Results		
Simulation No. (SN)	**Fault angle (°)**	**Current Interruption Time (*s*)**
SN 1	30	0.057
SN 2	60	0.049
SN 3	90	0.039

4.4.1.2 Advanced Controlled Switching Case

The calculated and simulated results was analysed in this advanced controlled switching case for interruption time. The fault current equation (3.13) had limitations as it does not take into account the reduction from the implementation of idle time and temperature controlled time logic. Hence the equation (3.14) was derived which accounts for the predicted operating time. This was based on the input variables namely compensation time based on fault current, temperature, idle time and standard breaker operating time. The fault current instantaneous time results (T_{If}) taken from equation (3.13) as shown in Appendix A for all simulations are used as an input to equation (3.14) to determine future current zero times. The detailed future current zero calculated results using equation (3.14) shown in Appendix B are compared to the actual simulated results to ascertain the accuracy of the results. A summary of the findings is found in Table 4.5.

Table 4.5: Advanced Controlled Switching Trip Times Summary – Calculated vs Simulated

Advanced Controlled Interruption Time Results – Calculated vs Simulated							
Simulation No. (SN)	**Fault angle (°)**	**CB Temp Time Delay (s)**	**CB Idle time delay (s)**	**Calculated Current Interruption Time (s)**	**Simulated Current Interruption Time (s)**	**Current Interruption Difference (s)**	**Figure No.**
SN 1	30	0.00054	0.000031	0.071	0.071	0.000	4.1
SN 2	60	0.00054	0.000031	0.060	0.060	0.000	4.2
SN 3	90	0.00054	0.000031	0.049	0.048	0.001	4.3
SN 4	30	0.00048	0.000031	0.070	0.071	0.001	4.4
SN 5	60	0.00054	0.000077	0.059	0.060	0.001	4.5
SN 6	90	0.00138	0.000155	0.049	0.049	0.000	4.6

In Table 4.5 , the interruption time calculated vs simulated variance is zero amongst SN1, SN2 and SN6 while for SN3, SN4 and SN5 the variance is -1 ms. The input standard circuit breaker operating time was 35.05 ms for all simulations.The deviation of 1 ms for SN3 to SN5 in real time is within a 1% tolerance while the remaining results have a 0% deviation. This effectively confirms that the equation (3.14) is in line with the controlled implemented logic for fault interruption. The energy, power and temperature parameters produced based on the trip time results for advanced controlled switching will be discussed in the remaining parts of this chapter.

Its visibly noted that the change in fault angle impacts the current interruption time in both calculated and simulated results as shown in SN1, SN2 and SN3 which yield the same results. However, when the same fault angles are applied with a change in the input parameters relevant to the circuit breakers environment, for SN4, SN5 and SN6, the current interruption time only deviates by 1 ms for SN3 and SN5 in the simulated results which is considered negligible. In essence, it's found that the current interruption time was highly impacted for the simulations where the fault angle was changed as shown in Figure 4.8.

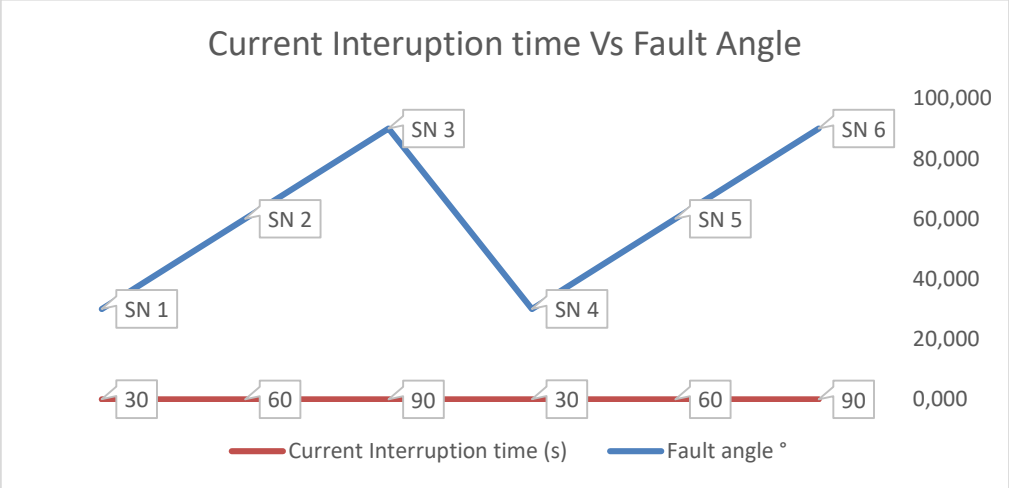

Figure 4.8: Advanced Controlled Switching Current Interruption Time vs Fault Current

The results of current interruptions at fault angle 30°, 60° and 90° for the simulations SN1 to SN6 for the simulations in the Figures 4.1 to 4.6 above produced the current interruption time at zero yet the input parameters relevant to its environment was changed. This effectively confirms that the advanced controlled switching logic functions compensates for circuit breaker interruption trips at current zero times, irrespective of the circuit breaker environment namely the variable input delays such as temperature and idle to provide a current zero interruption time.

4.4.1.3 Case Comparison

The advanced controlled circuit breaker interruption time deviates from the conventional circuit breaker at current interruption. The advanced controlled switching interruption time as shown in Figure 4.1 to 4.6 all achieve current zero interruption. The conventional circuit breaker reflects tripping at current peak for SN1 and SN4, and near current zero tripping for the remaining simulations. The advanced controlled switching current interruption throughout the simulations SN1 to SN6 in Figure 4.1 to 4.6 reflect a delay by three quarters of a cycle for a 30° fault current angle, half a cycle for a 60° and less than half a cycle for 90° when compared to the conventional circuit breaker. It's also noted that current interruption at current zero crossing for all simulations are prevalent for advanced controlled switching while fault current interruption for the conventional circuit breaker switching occurs at any instant. The fault trip angles between simulations have proven to have an impact on the current interruption angle and current interruption trip time for non-controlled switching. However, for the controlled circuit breaker, the current interruption time is the only parameter impacted due to the fault trip angle with all the simulated interruptions occurring at current zero [6]. The advanced controlled

circuit breaker simulation in SN1 to SN6 all trip later than the conventional circuit breakers due to the incorporation of the time delays to achieve the nearest current zero tripping.

4.4.2 Arc Voltage and Arc Fault Current

The Arc Voltage and Arc fault current for the conventional and advanced controlled switching simulation SN1 to SN3 was completed by varying the fault current angle, with an additional variation of idle time and temperature being implemented for advanced controlled switching, for simulation SN4 to SN6. The Arc Voltage and Arc fault current output simulation results for the simulations are jointly shown where VaX the arc voltage and IspX the arc current, represents the conventional graphs while Va the arc voltage and Isp the arc current, represents the advanced controlled switching graph results in Figure 4.9 to 4.14.

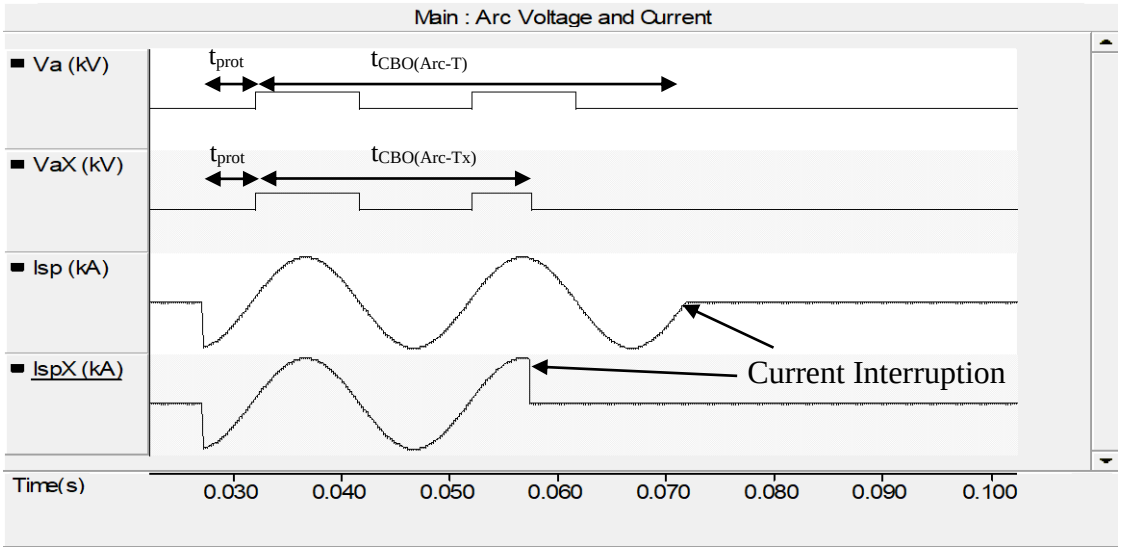

Figure 4.9: SN1 Controlled Switching Vs Conventional Arc Voltage and Current

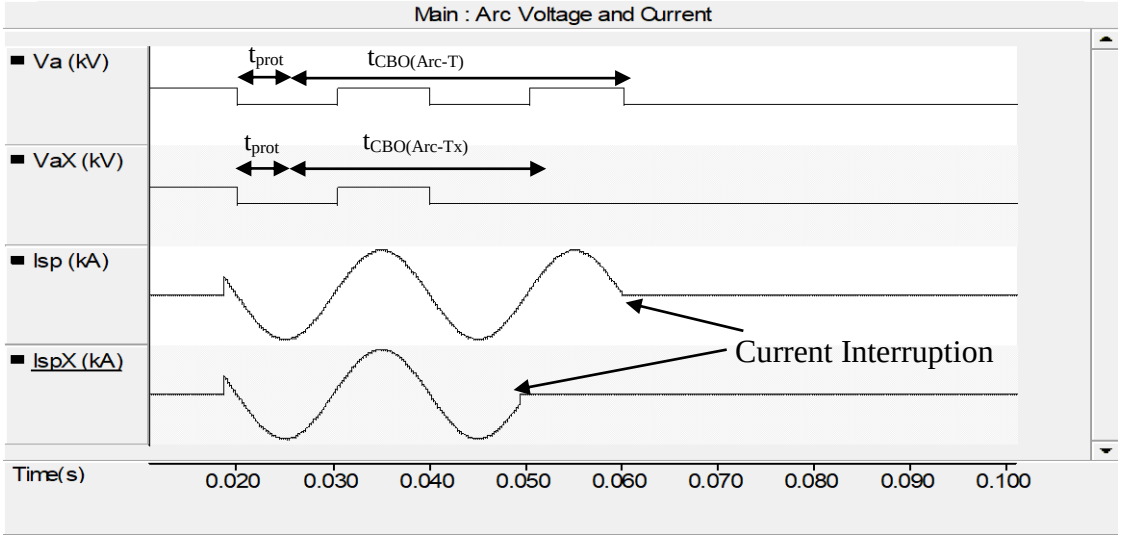

Figure 4.10: SN2 Controlled Switching Vs Conventional Arc Voltage and Current

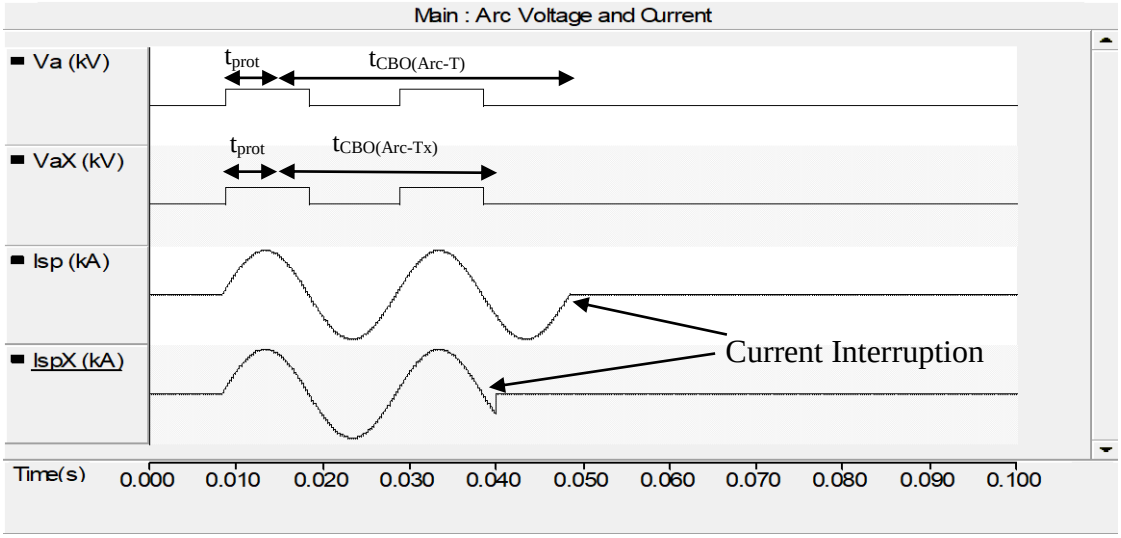

Figure 4.11 : SN3 Controlled Switching Vs Conventional Arc Voltage and Current

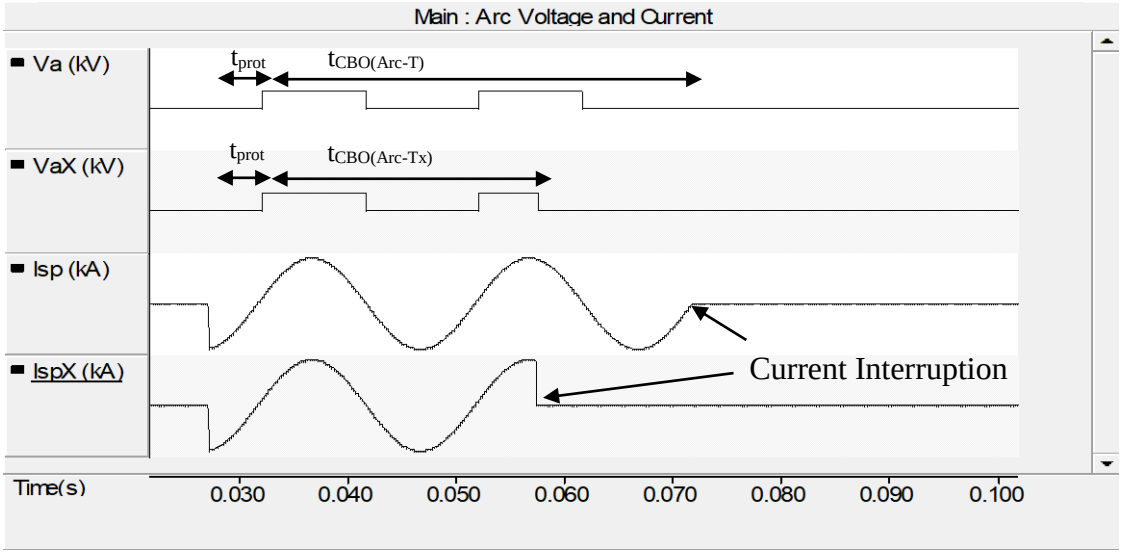

Figure 4.12: SN4 Controlled Switching Vs Conventional Arc Voltage and Current

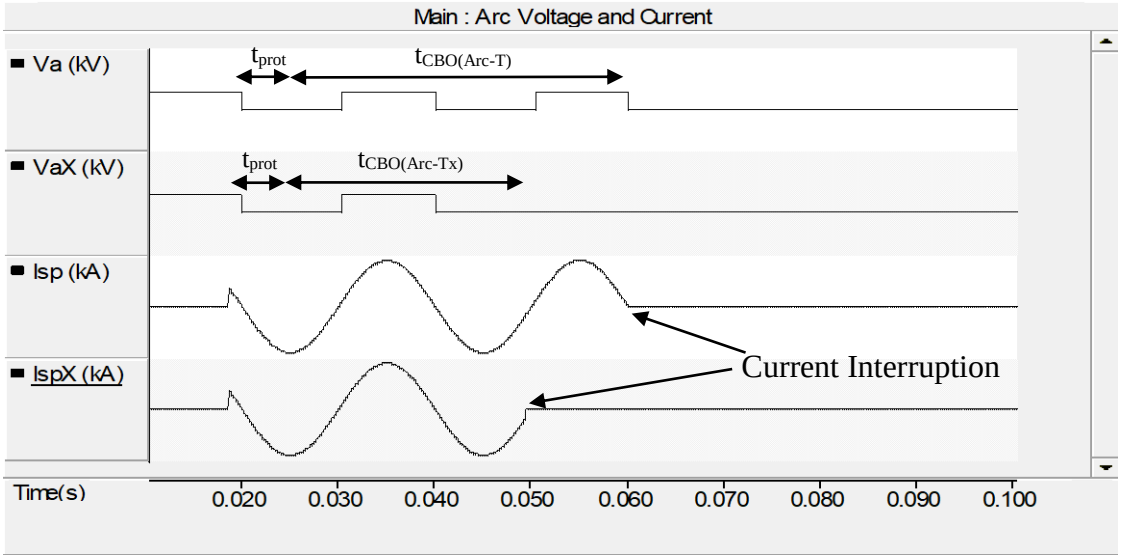

Figure 4.13: SN5 Controlled Switching Vs Conventional Arc Voltage and Current

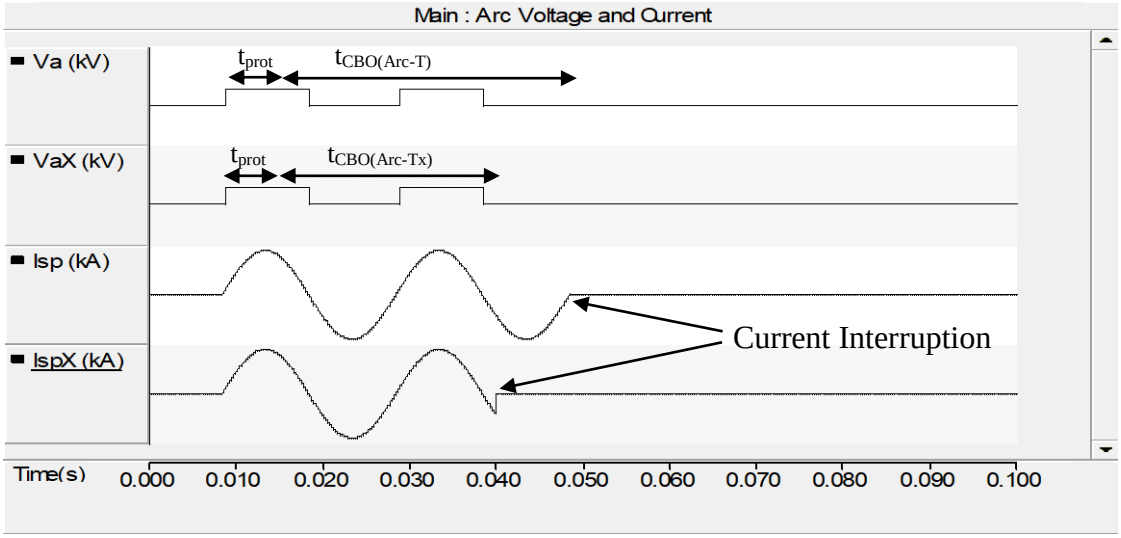

Figure 4.14: SN6 Controlled Switching Vs Conventional Arc Voltage and Current

The combined simulation output of Arc voltage and current are represented together in Figure 4.9 to 4.14 above.

4.4.2.1 Conventional Switching Case

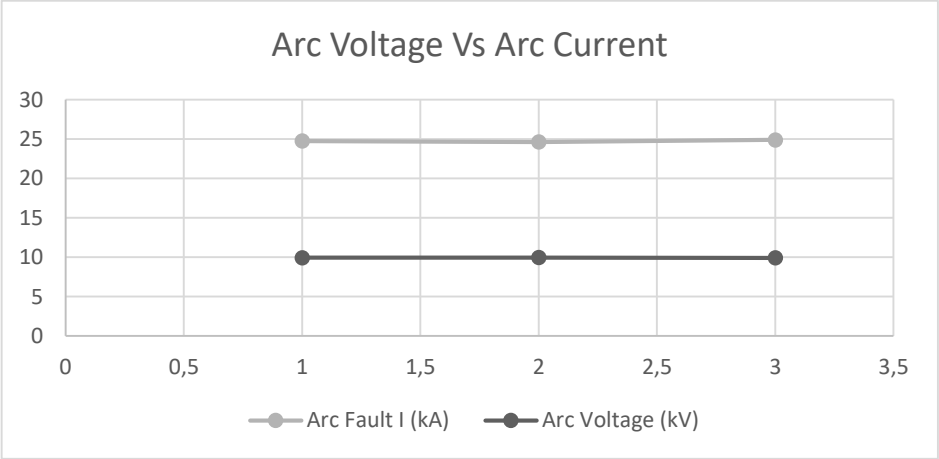

Figure 4.15: Calculated Output Arc Voltage Vs Current

Table 4.6: Conventional Circuit Breaker Output results for Arc Current and Voltage

Simulated Output Results				
Simulation No. (SN)	**Simulated Arc Fault I (kA)**	**Arc Voltage (kV)**	**Arc Quenching ($A/\mu s$)**	**Figure No.**
SN 1	24.76	9.95	2.476	4.9
SN 2	24.64	9.97	2.464	4.10
SN 3	24.89	9.93	2.489	4.11

The plotting of the simulated results on Figure 4.9 to 4.14 indicate a negligible change in arc voltage and current with the change in fault phase angle. The negligible change in the circuit breaker arc fault current and arc voltage may not have any impact on the system power for one tripping event. However, the accumulative change is what impacts the lifespan of the circuit breaker and the interconnected power system.

Arc Current

The calculated Arc fault current for SN1 to SN3 is $24.58\,kA$. These calculated results from conventional calculation using equation (3.5) and (3.8) vary by $0.06\,kA$ to $0.31\,kA$ when compared to the simulated arc fault current results shown in Table 4.6. The difference in the calculated arc fault current to the simulated arc fault current in Table 4.6 is less than 1% for SN1 to SN3 . The deviation is due to the calculated method that had not taken into account the standard circuit breaker delays namely circuit breaker opening times and arcing time. The simulated results have accounted for the standard circuit breaker delays with the assistance of the breaker time logic circuit in Figure 3.7. The observation during simulation indicated that the circuit breaker arc current is lower than the bolted fault current of $25\,kV$ injected to the simulation. This is due to the impedance properties the arc fault retains [96]. In Figure 4.9 to 4.11 the current interruption occurs prior to current zero with the time for protection operation indicated as t_{prot} while the actual circuit breaker opening is represented by t_{CBO} which is effectively the arcing time.. The vacuum circuit breaker arc quenching capability for these simulations was calculated using equation (2.15). The results were in the range of $2.47\,A/\mu s$ for all simulations which proved to be in the range of the circuit breaker high frequency current quenching capacity of $600\,A/\mu s$ therefore the conventional circuit breaker is suited for normal operation. However, the effects of the phenomena after point of interruption needs to be investigated.

Arc Voltage

The circuit breaker arc voltage is chopped during the simulation of the circuit breaker interruption reflecting a square wave due to the cut in power frequency during the circuit breaker opening time as shown in Figure 4.9 to 4.11. The simulated arc voltage when compared to the calculated arc voltage for SN1 to SN3 was 1% higher which is negligible. The transient voltage post circuit breaker current interruption is analysed in the latter part of this chapter. It is visible that the fault phase angle had negligible impact on the arc fault current and arc voltage peak values between the simulations. However, the 1st peak arc voltage and current cycle occurs

at different times as the phase angle is changed in the simulations as shown in Figure 4.9 to Figure 4.11. The fault phase angle was found to change the time of which the arc current peaks which effectively impacted the current interruption process of the arc [4]. In an everyday power system, faults can occur at any phase angle instant hence all the fault current parameters need to be accounted for, while maintaining a regulated trip time.

4.4.2.2 Advanced Controlled Switching Case

Table 4.7: Advanced Controlled Switching Arc Voltage and Current Outputs

Advanced Controlled Arc Voltage and Current Output					
Simulation No. (SN)	**Simulated Arc Fault I (kA)**	**Simulated Vs Calculated Arc Current Difference (%)**	**Arc Voltage (kV)**	**Arc Quenching ($A/\mu s$)**	**Figure No.**
SN 1	22.25	9	8.82	2.225	4.9
SN 2	22.11	10	8.74	2.211	4.10
SN 3	22.45	9	8.93	2.245	4.11
SN 4	22.34	9	8.82	2.234	4.12
SN 5	22.11	10	8.89	2.211	4.13
SN 6	22.28	9	8.95	2.228	4.14

Arc Fault Current

In Figure 4.9 to 4.14, the circuit breaker current arcing duration represented by t_{CBO} varies with the fault current angle. However, the magnitude of the fault current is relatively constant at an average of $22\,kA$ with a negligible deviation between the simulations SN1 to SN6. It is also noted that the changes between simulations SN3 to SN6 relevant to the environment of the circuit breaker has no significant impact on the circuit breaker arc fault current results due to the advanced controlled switching technology using logic to ensure current zero interruption is achieved irrespective of the delays attributed to the input parameters relative to the circuit breakers environment. The vacuum breaker arc quenching capability for these simulations was calculated using equation (2.15). The results shown in Table 4.7 were in the range of 2.2 $A/\mu s$ for all simulations which proved to be in the range of the circuit breaker high frequency current quenching capacity of 600 $A/\mu s$.

In each simulation, the graphs in Figure 4.9 to 4.14 indicate that the arc current and voltage peaks are synchronised during the breaker opening operation. The breaker interruption occurs when the arc current is extinguished at the current zero crossing as logically programmed by the advanced controlled switching circuit breaker. The calculated Arc fault current for SN1 to

SN6 is 24.57 kA.When comparing the calculated results to the simulated arc fault current in Table 4.7, its shown that the arc fault current deviates from the simulated arc fault current by approximately 2 kA between simulations. The deviation of an average of 9 % is due to the calculated fault using equation (3.8) which does not factor in the advanced controlled switching technologies, this logical input parameters is relevant to the breakers environment.

Arc Voltage

The results for the breaker arc voltage for SN1 to SN6 in Figure 4.9 to 4.14 above have no significant change with the change in fault current angle or change in input parameters relevant to its environment hence its relatively constant between simulations. The arc voltage is an average of 2000 V less than the supply voltage for breaker interruption and is found to be extinguished at current interruption. The lower arc voltage is due to its inverse nature to that of current emanating from 1st principles.

Arc Current Vs Arc Voltage

The overall findings reflect a negligible impact on the arc fault current and arc voltage peak values between the simulations. Its further noticed that the varying in fault phase angles from SN1 to SN3 had a sinusoidal time shift relevant to the supply frequency with trip times varying but occurring all at current zero. When the inputs relevant to the environmental conditions changed for each various fault angle in SN3 to SN6, the interruption still occurred at current zero due to the advanced controlled switching logic. The fault phase angle changes the time at which the arc current peaks thus impacting the current interruption process of the arc yet still achieving current zero interruption [4].

4.4.2.3 Case Comparison

Table 4.8: Conventional Arc Voltage and Current Output Results

Conventional Vs Advanced Controlled Output Results							
Simulation No. (SN)	**Figure No.**	**Conventional Arc Fault I (kA)**	**ACS Arc Fault I (kA)**	**Arc I Difference (%)**	**Conventional Arc V (kV)**	**(ACS) Arc V (kV)**	**Arc V Difference (%)**
SN 1	4.81	24.76	22.25	8.25	9.95	8.82	11.36
SN 2	4.82	24.64	22.11	10.27	9.97	8.74	12.34
SN 3	4.83	24.89	22.45	9.80	9.93	8.93	10.07
SN 4	4.84	n/a	22.34	8.22	n/a	8.82	11.36
SN 5	4.85	n/a	22.11	10.27	n/a	8.89	10.83
SN 6	4.86	n/a	22.28	10.49	n/a	8.95	9.87

Arc Current

In Table 4.8, the conventional vs controlled circuit breaker arc voltage and fault current for SN1 to SN6 commences at the same time. This is for its related fault current and fault angle which is as per the expected outcome shown in Figure 4.9 to 4.14. However, the magnitude of the arc voltage and fault is what differs between all simulations when comparing the conventional to the controlled circuit breaker. The simulated output arc fault current for SN1, SN2 and SN3 is found to have decreased by an average of 9% when advanced controlled switching was implemented.

When the arc fault current results of SN4 to SN6 for advanced controlled are compared to the conventional results of SN1 to SN3, the arc current output produced had also decreased by an average of 9% in the advanced controlled switching. The major influence on the arc fault current output is the ability of the advanced controlled switching of the circuit breaker to interrupt at current zero. The arc quenching capabilities specification required of the conventionally operated circuit breaker is found to be 9% higher in Table 4.6 when compared to the advanced controlled results in Table 4.7 and is proportional to the arc fault current produced. The within stand fault current capabilities for both advanced controlled switching and conventional circuit breaker switching are below the withstand capabilities of $600\ A/\mu s$ of the selected circuit breaker.

Arc Voltage

In Table 4.8 , the simulated output circuit breaker arc voltage for SN1 is found to have decreased by 11% while the percentage decrease for SN2 is 12% and for SN3 10% when advanced controlled switching was implemented. A significant improvement is present in reduction of circuit breaker arc voltage when current zero tripping is implemented. When the arc fault voltage of SN1 is compared to SN4 where the parameters relevant to the environmental conditions have changed, the arc fault voltage remains relatively the same within a 0.5% tolerance. Effectively the environmental input parameters changes on the circuit breaker had a negligible impact on the arc voltage output. The advanced controlled switching implementation at standard environmental conditions had reduced the arc voltage by an average of 11% and when the environmental parameters changed, the arc voltage still maintained an average reduction of 11% when compared to conventional circuit breaker arc voltage. The regulation of the arc voltage between simulations within a tolerance range of 1% for advanced controlled switching, increases the circuit breakers resistance within the contact's arc gap therefore

increasing its ability to trip swiftly while reducing the heat losses produced from high arc voltages [50]. Overall the advanced controlled switching circuit breaker produced lower circuit breaker arc voltage and current results when compared to a conventional circuit breaker.

4.4.3 Current Chopping

The chopping current of the circuit breaker for the conventional and advanced controlled switching simulation SN1 to SN3 was completed by varying the fault current angle, with an additional variation of idle time and temperature being implemented for advanced controlled switching, for simulation SN4 to SN6. The simulated results are shown in Figure 4.16 to 4.21. IflaX represents the conventional graphs while Ifla represents the advanced controlled switching graph results. The magnitude of the results for Ifla is smaller hence it's not visible on the Figure 4.16 to 4.21. Hence, for the advanced switching analysis, a closer scaled graph was completed to display the output chopping current Ifla as shown in Figure 4.22 to 4.27.

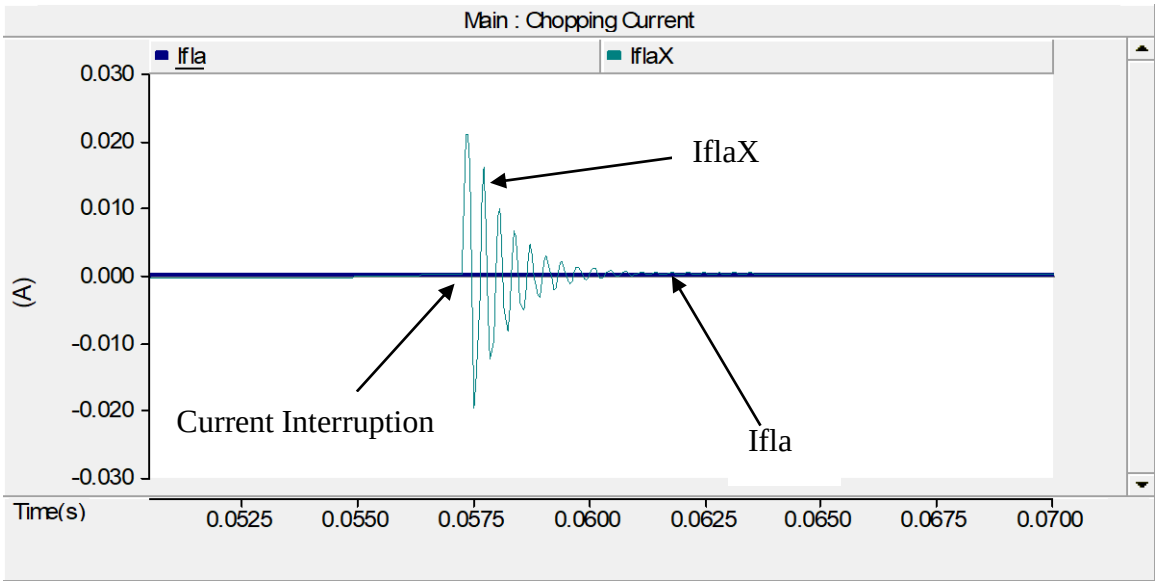

Figure 4.16: SN1 Controlled Switching Vs Conventional Chopping Current

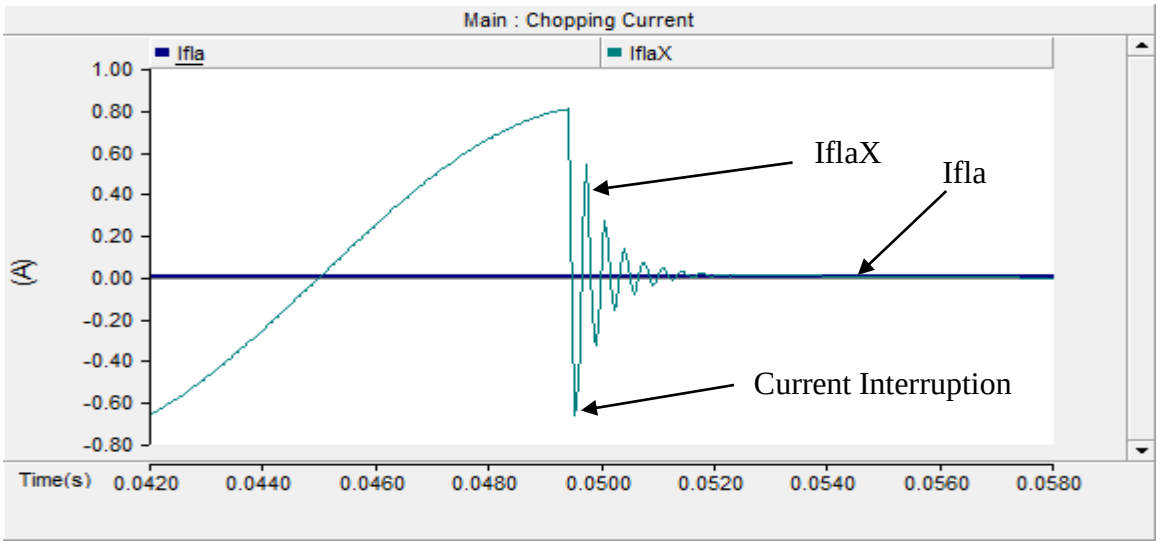

Figure 4.17: SN2 Controlled Switching Vs Conventional Chopping Current

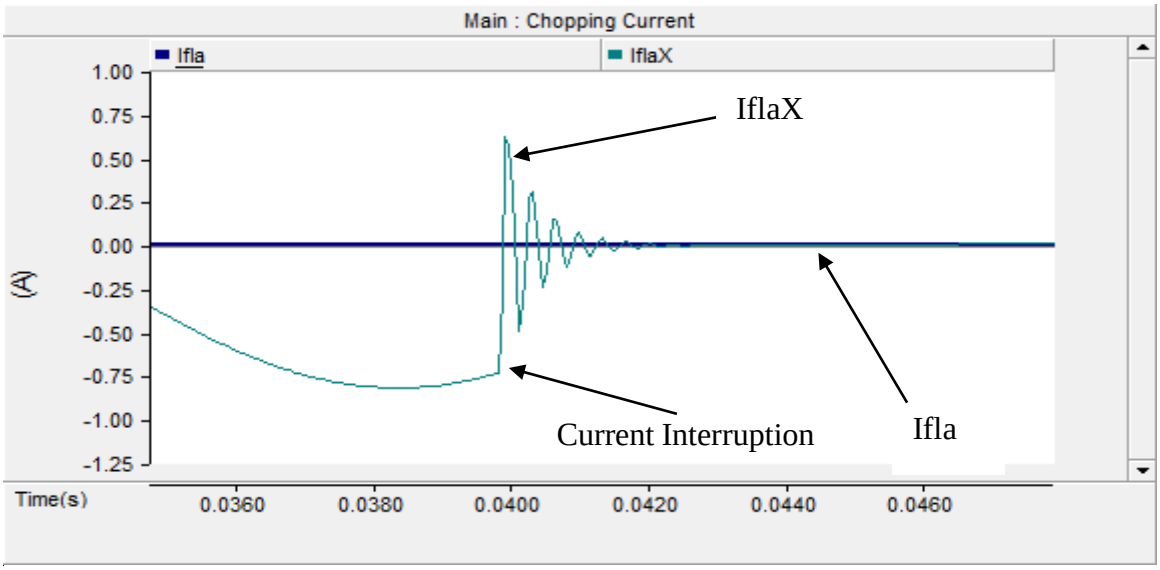

Figure 4.18: SN3 Controlled Switching Vs Conventional Chopping Current

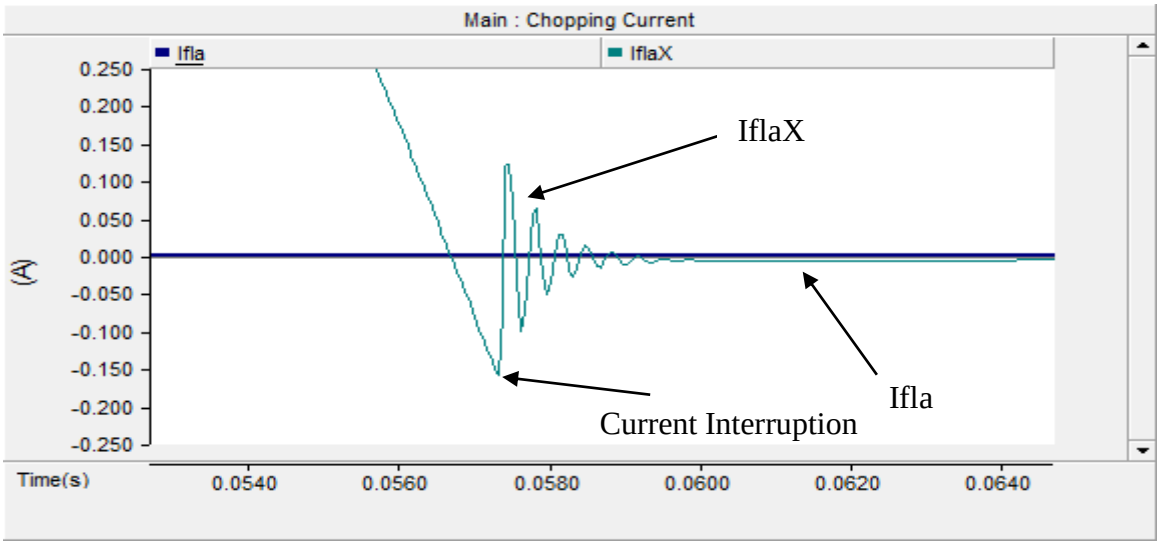

Figure 4.19: SN4 Controlled Switching Vs Conventional Chopping Current

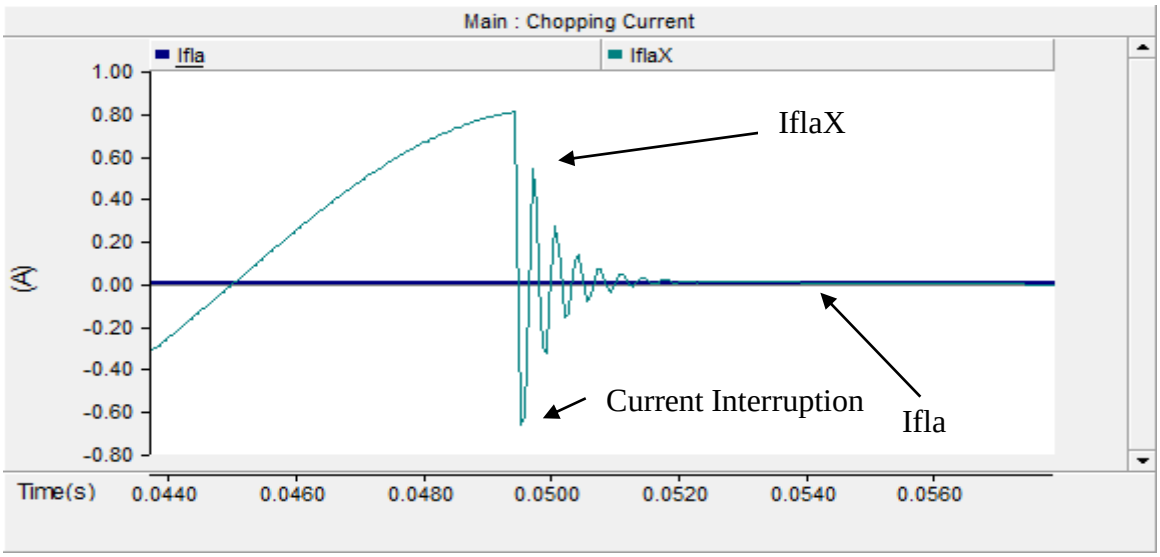

Figure 4.20: SN5 Controlled Switching Vs Conventional Chopping Current

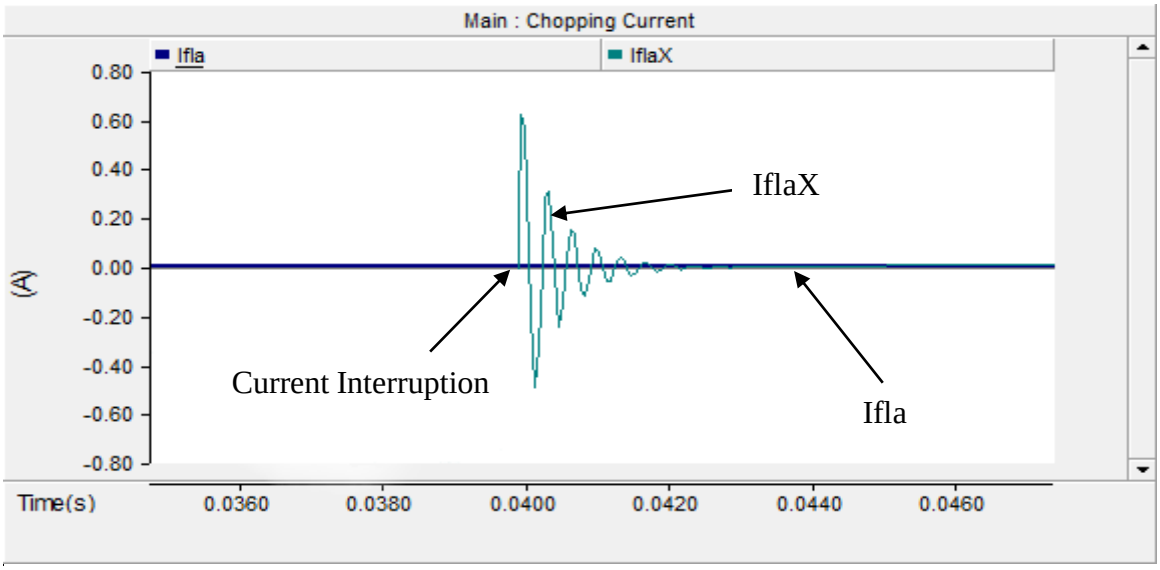

Figure 4.21: SN6 Controlled Switching Vs Conventional Chopping Current

4.4.3.1 Conventional Switching Case

Table 4.9: Conventional Breaker Current Chopping Output Results

Conventional Current Chopping Output Results					
Simulation No.	**Start (A)**	**End (A)**	**Duration (S)**	**Peak (kA)**	**Figure No.**
SN 1	-0.15	0.15	0.002	0.15	4.16
SN 2	-0.6	0.5	0.0034	0.5	4.17
SN 3	-0.65	0.6	0.0024	0.6	4.18

The chopping current is present throughout each simulation completed. However, the values are within the limits of the withstand nominal operation for a rated circuit breaker of 5 *A*. This is due to the circuit breaker not being connected directly to a power transformer hence a lower chopping current is expected as shown in Figure 4.16 to 4.21 [30]. The power transformer produces magnetizing currents that the chopping current arises from when interrupted prior to current zero. The other contributing factor to the lower current chopping is the remaining interconnected power system components that add impedance to the power system. In addition, the system is loaded whereas chopping occurs mainly on unloaded power systems [96]. The results in Table 4.9 are compared for each simulation to ascertain the impact when the fault angle is changed. The fault current reflected in SN1 to SN3 shows that the durations of the chopping current increases marginally when tripped near current zero. The chopping current is found to also vary by 0.5 *A* between SN1 and the remaining simulations SN2 and SN3. This is due to the chopping current having a higher magnitude current when tripped near current zero rather than at current zero. The general trend in all simulations shows the chopping current, starting to build up from a negative current towards a peak positive current but remain within the circuit breaker withstand limits.

4.4.3.2 Advanced Controlled Switching Case

The chopping current formed prior to the point of complete circuit breaker interruption is not visible when simulated on an ampere unit scale but only is visible on a nano ampere scale as shown in Figure 4.22 to 4.27 due to the smaller magnitude of the chopping current. The circuit is not connected to a transformer hence a small chopping current is expected similar to the conventional simulation. The results in Table 4.10 which are compared for each simulation to ascertain the impact when the fault angle is changed and its environmental conditions. The findings are that the fault current angle reflected on Figure 4.22 to 4.24 for SN1 to SN3 show that the fault angle affects the magnitude and duration of the fault current. It's also reflects in Figure 4.22 to 4.24 for SN1 to SN3 that when the fault angle increases by 30°, the magnitude

of the chopping current between simulations increases by $0.03\,nA$ at a constant duration of $1\,S$. When the input relevant to the environmental conditions change in SN4 to SN6, it reflects a small chopping current change by approximately $0{,}05\,nA$ on average which depicts that the advanced controlled switching technologies does regulates the chopping current in any environment to keep chopping currents low but it's considered susceptible to the fault current angle only. The overall impact of the chopping current is considered negligible. The chopping current produced is a catalyst to the production of transient recovery voltage.

Table 4.10: Advanced Controlled Current Chopping Output Results

Advanced Controlled Current Chopping Output Results				
Simulation No	**Start (nA)**	**End (nA)**	**Peak (nA)**	**Figure No.**
SN 1	-0.055	-0.03	-0.03	4.22
SN 2	0.01	0.075	0.065	4.23
SN 3	-0.085	0.01	0.01	4.24
SN 4	-0.05	-0.03	-0.02	4.25
SN 5	0.01	0.07	0.07	4.26
SN 6	-0.085	0.01	0.095	4.27

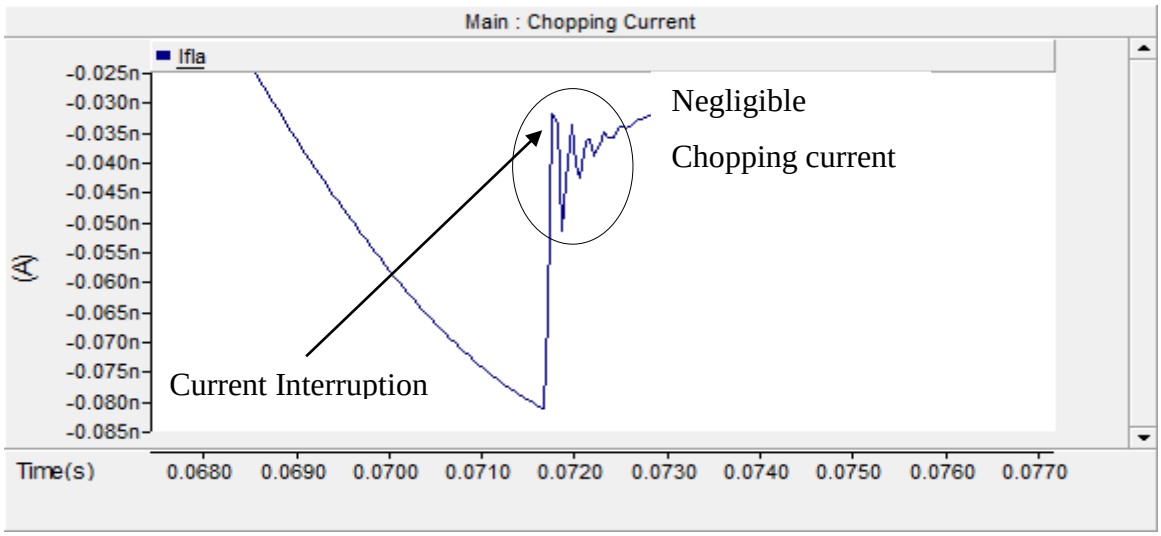

Figure 4.22: SN1 Controlled Switching Chopping Current

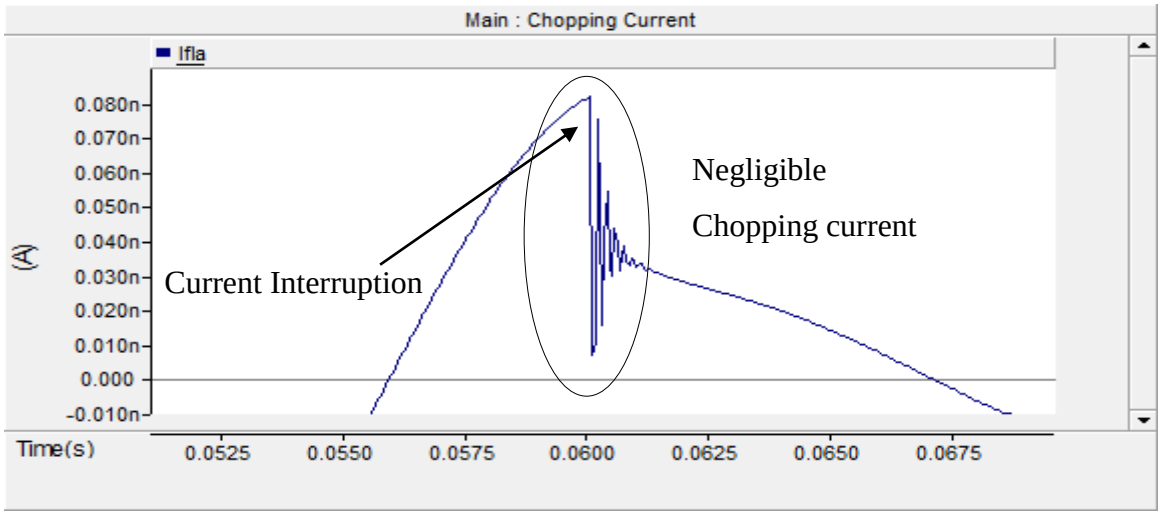

Figure 4.23: SN2 Controlled Switching Chopping Current

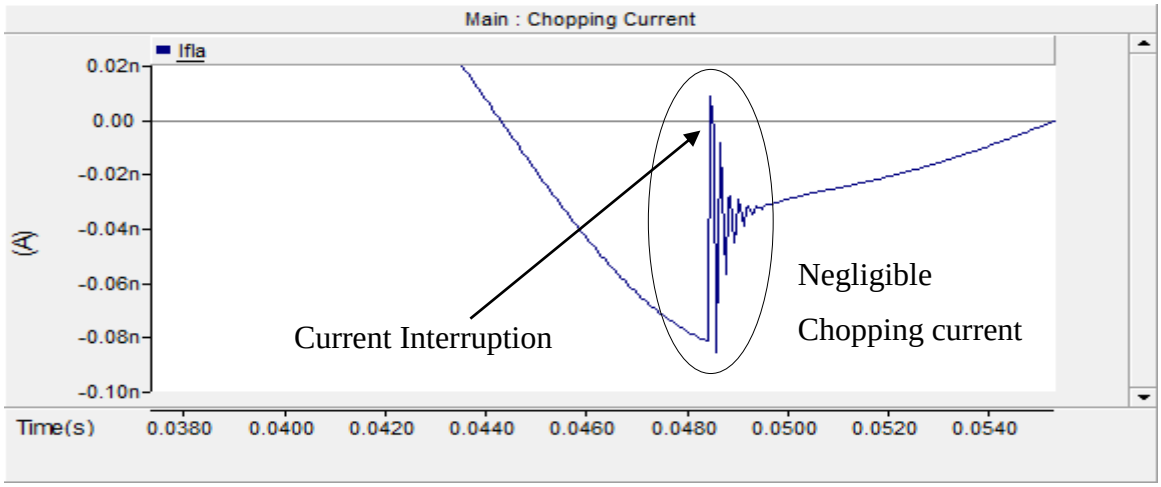

Figure 4.24: SN3 Controlled Switching Chopping Current

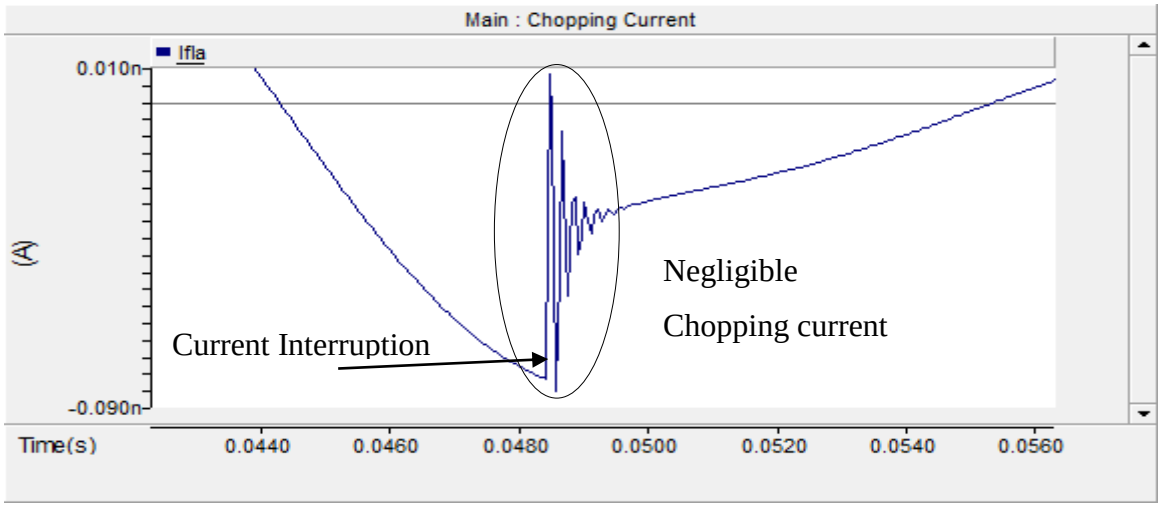

Figure 4.25: SN4 Controlled Switching Chopping Current

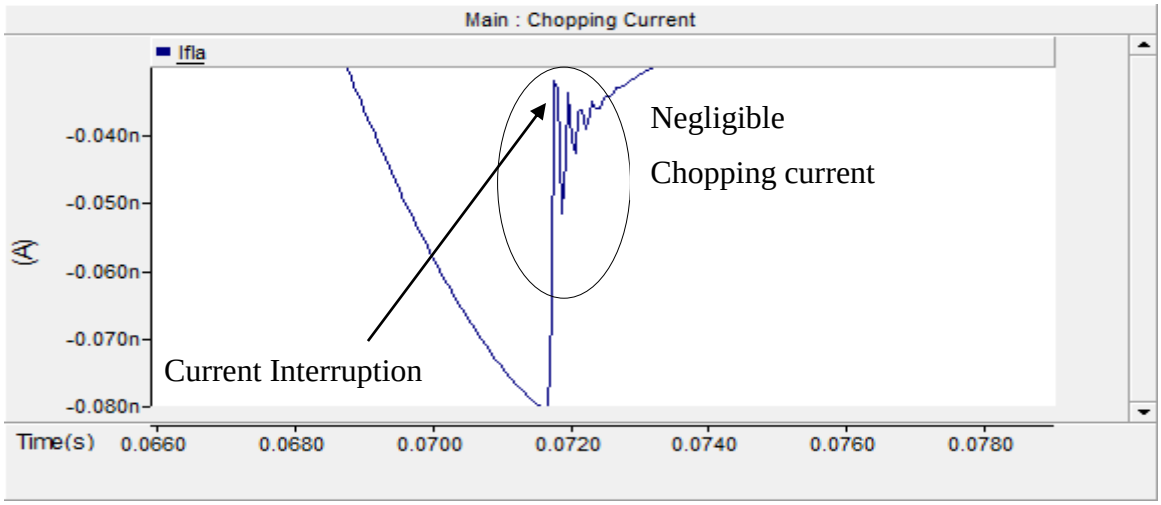

Figure 4.26: SN5 Controlled Switching Chopping Current

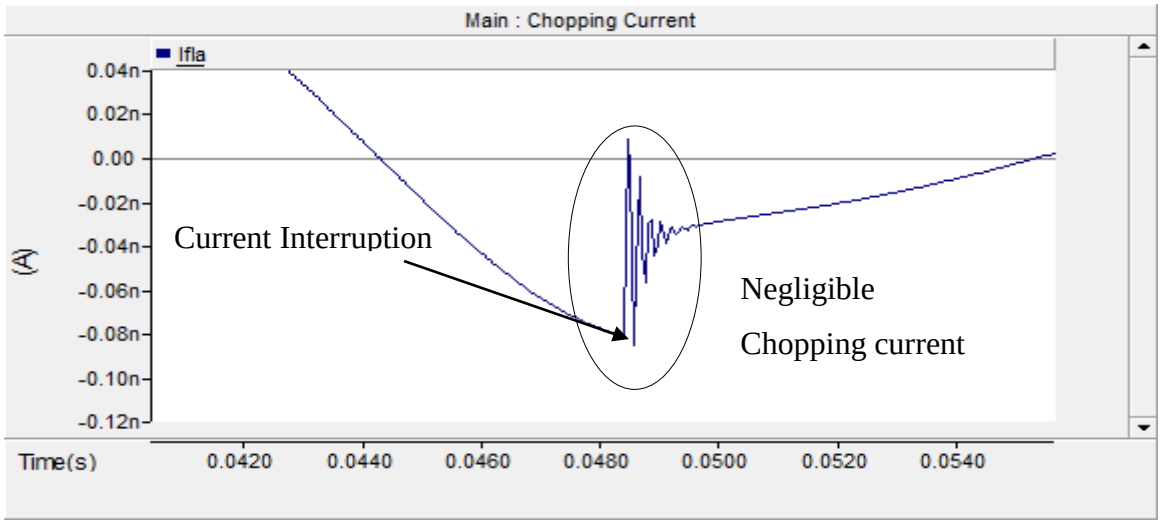

Figure 4.27: SN6 Controlled Switching Chopping Current

4.4.3.3 Case Comparison

The chopping current for SN1 to SN6 in Figure 4.16 to 4.21 are only visible for the conventional circuit breaker results and is found to increase as the fault phase angle increases which is noticeable as SN1 produces a chopping current at 0.15 A while SN2 and SN3 produces 0.5 A and 0.6 A respectively. This is also present for advanced controlled switching where SN1 produces a peak chopping current of -0.03 nA while SN2 and SN3 produces 0.065 nA and 0.01 nA respectively. The change in the chopping current for advanced controlled switching is present when the fault angle changes but negligible.

The controlled circuit breaker chopping current is much smaller than the conventional chopping current results for SN1 to SN3 with values not exceeding 0.065 nA. The chopping current is not visible hence represented as 0 A when compared to the conventional circuit breaker chopping

current results in Figure 4.16 to 4.21. The yields from Table 4.10 for advanced controlled switching chopping current indicates an average of over 1000 % decrease in chopping current when using advanced controlled switching. In SN4 to SN6, when the input parameters relevant to the environment changes for advanced controlled switching in Table 4.10 are compared to conventional circuit breaker chopping currents in SN1 to SN3 in Table 4.9, the decrease in chopping currents are below $0.07\,nA$ with an average of over 1000 % decrease.

The duration of the chopping current for conventional switching fluctuates as the fault angle changes, the duration for SN1 is at 0.002 *s*, SN2 at 0.0034 *s* and SN3 is at 0.0024 *s*. When advanced controlled switching is implemented for SN1 to SN6, the duration of the chopping current is kept constant at 1 *ms* with the chopping current duration being shorter than all the simulated results produced for the conventional circuit breaker. Effectively, the chopping current values when advanced controlled switching is implemented reduces the duration and magnitude of the chopping current irrespective of the environmental conditions change and still maintains a constant chopping current duration.

4.4.4 Transient Recovery Voltage

The transient recovery voltage of the circuit breaker for the conventional and advanced controlled switching simulation SN1 to SN3 was completed by varying the fault current angle, with an additional variation of idle time and temperature being implemented for advanced controlled switching, for simulation SN4 to SN6. The simulated results are shown in Figure 4.28 to 4.33. EaX represents the conventional graphs of the transient recovery voltage while Ea represents the advanced controlled switching graph results.

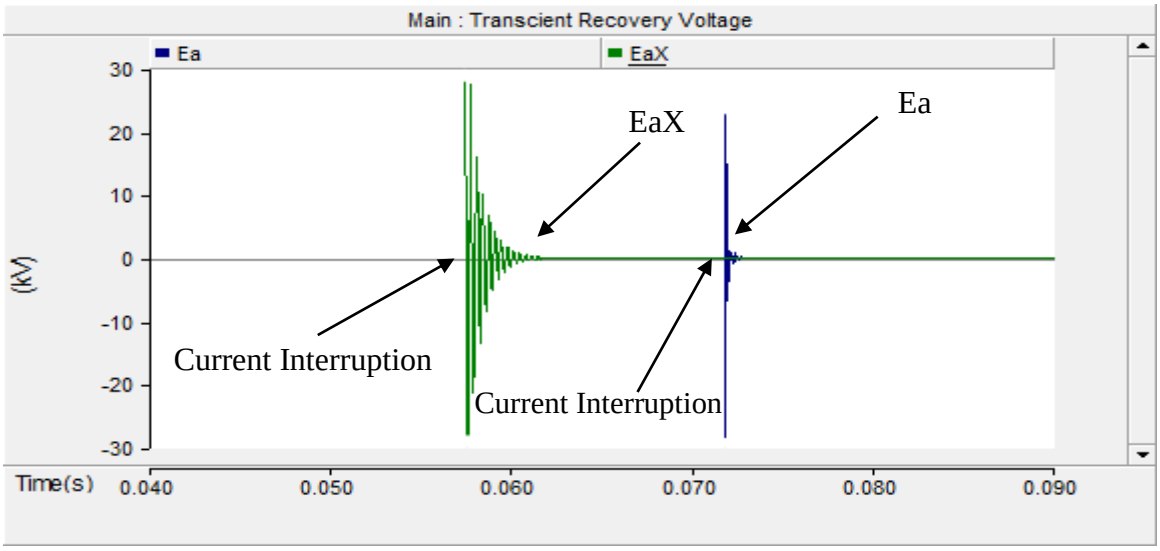

Figure 4.28: SN1 Controlled Switching Vs Conventional Transient Recovery Voltage

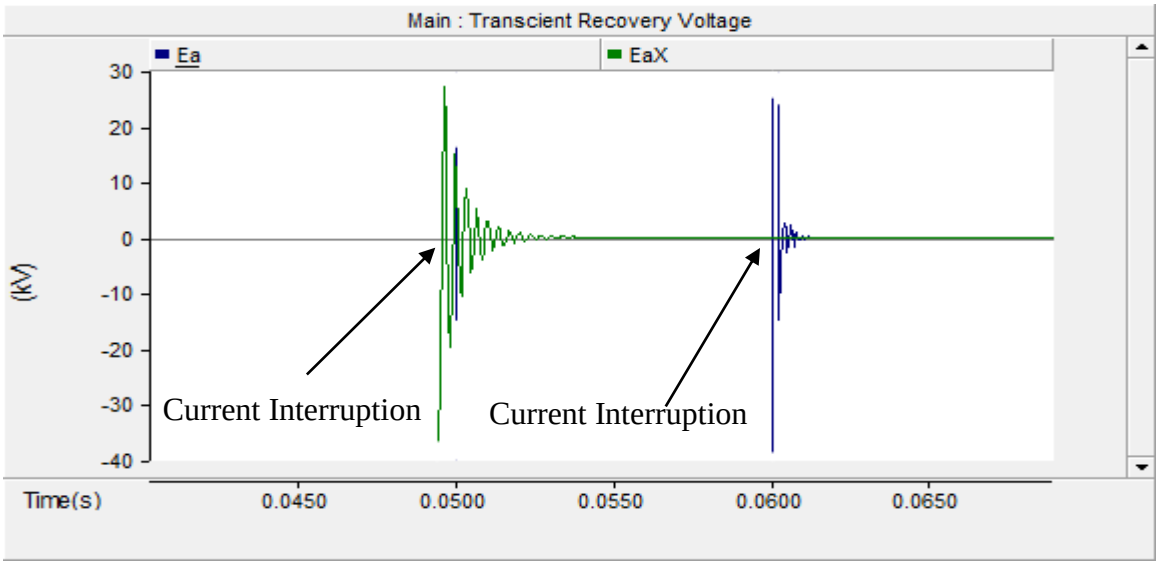

Figure 4.29: SN2 Controlled Switching Vs Conventional Transient Recovery Voltage

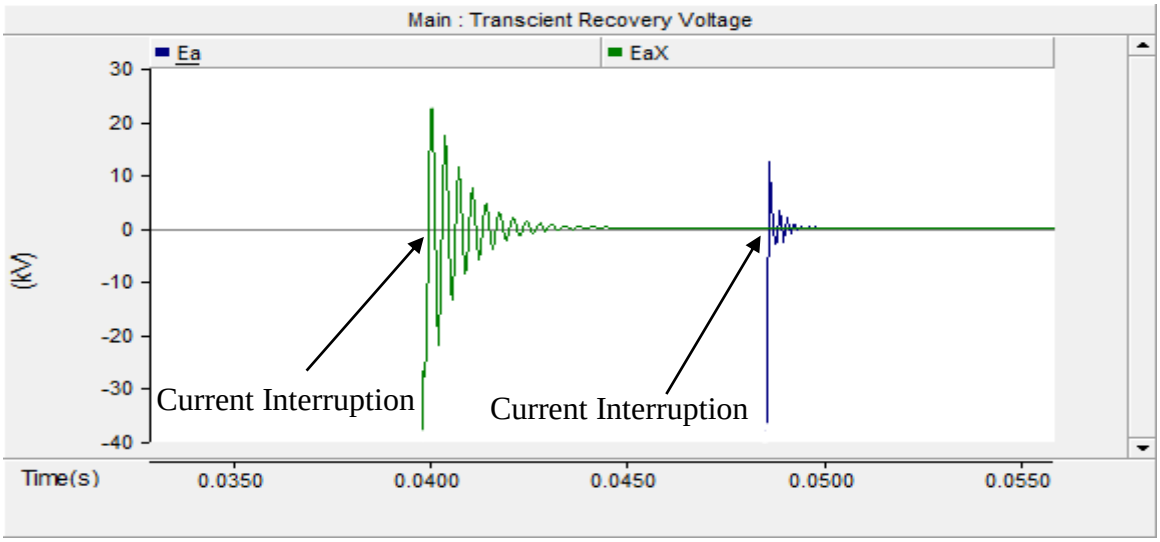

Figure 4.30: SN3 Controlled Switching Vs Conventional Transient Recovery Voltage

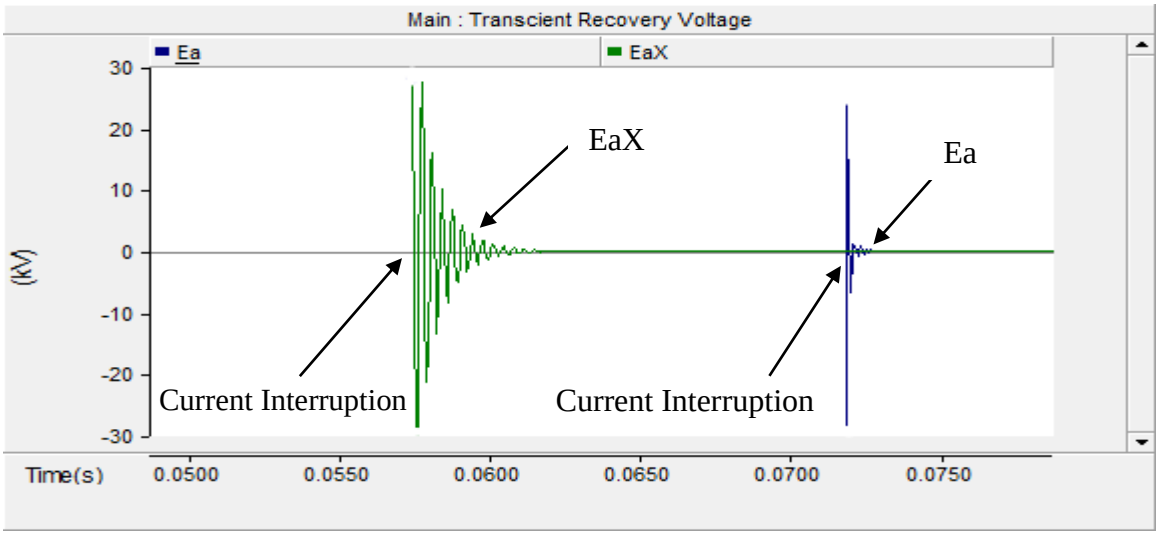

Figure 4.31: SN4 Controlled Switching Vs Conventional Transient Recovery Voltage

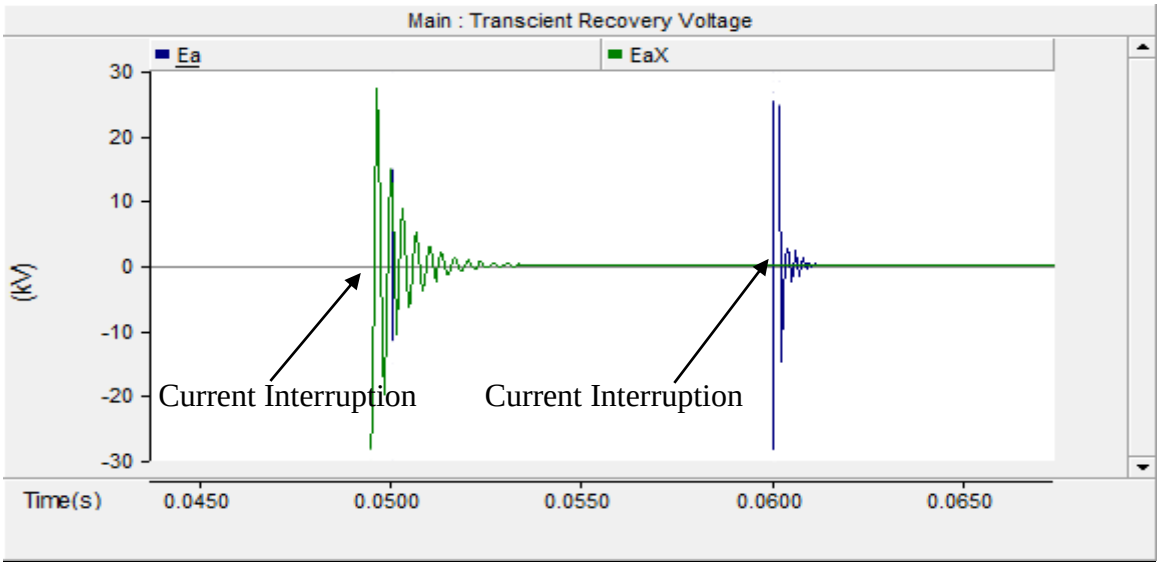

Figure 4.32: SN5 Controlled Switching Vs Conventional Transient Recovery Voltage

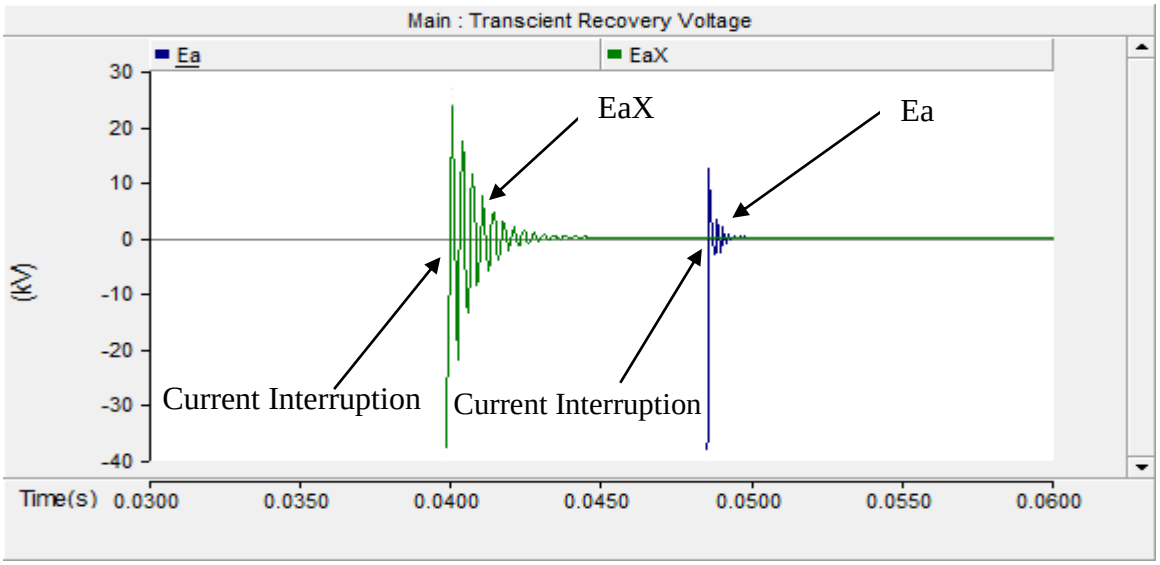

Figure 4.33: SN6 Controlled Switching Vs Conventional Transient Recovery Voltage

4.4.4.1 Conventional Switching Case

Figure 4.28 to 4.30 show an increase in transient recovery voltage after the 1st quarter of each cycle for EaX. The current interruption did not occur at current zero which effectively resulted in the magnitude of transient recovery voltage produced in Table 4.11. Subsequent to the current interruption, the arc voltage is returned to its sinusoidal waveform with a power frequency immediately after fault interruption in a form of transient recovery voltage as represented in simulations Figure 4.28 to 4.30. Hence, the formation from a square wave arc voltage to a sinusoidal waveform as shown in Figure 4.9 to 4.11. In the simulated results, it is found that the transient voltage appears for 3 *ms* at SN1 while for SN2 and SN3 the duration is 4 *ms* [38]. The peak of the transient recovery differs marginally between simulations with SN1 having the

lowest TRV that's proportional with its shortest transient duration. The reasons attributed to the difference in transient voltage in SN2 and SN3 is due to the circuit breaker current interruption angle which differs from SN1. The magnitude of the transient recovery voltage which gave rise to a higher rate of rise of recovery voltage is attributed to rapid reduction in current and fault trip angle [97]. The standard circuit breaker under conventional operation is complaint with IEEE C37.04-199 standard for SN1 to SN3 where the peak voltage did not exceed 30 kV . The calculated rate of rise of recovery voltage (RRRV) is below 0.43 $kV/\mu s$ with the largest being on SN2 at 5.35e-5 $kV/\mu s$ as indicated in Table 4.11.

Table 4.11: Conventional Breaker Transient Recovery Voltage Results

Conventional Switching TRV Output Results (No Stray Capacitor)					
Simulation No. (SN)	**Arc Voltage (kV)**	**Duration (s)**	**TRV (kV)**	**RRRV ($kV/\mu s$)**	**Figure No.**
SN 1	9.95	0.003	29.95	5.19E-04	4.28
SN 2	9.97	0.004	29.75	5.35E-04	4.29
SN 3	9.93	0.004	23.37	4.67E-04	4.30

4.4.4.2 Advanced Controlled Switching Case

The TRV is found to be lower than the nominal TRV values with a lower chopping current [38]. The transient recovery voltage commences after current interruption as shown in Figure 4.28 to 4.33. The simulation results SN1 to SN6 in Table 4.12 produced the same duration of 1 *ms* for the Transient recovery voltage with the Transient recovery peak voltage itself varying marginally between simulations as indicated in Figure 4.28 to 4.33.

Table 4.12: Controlled Switching TRV Output Results

Controlled Switching TRV Output Results				
Simulation No. (SN)	**Arc Voltage (kV)**	**TRV (kV)**	**RRRV ($kV/\mu s$)**	**Figure No.**
SN 1	8.96	23.53	4.71E-04	4.28
SN 2	8.96	22.23	4.45E-04	4.29
SN 3	8.97	13.73	2.75E-04	4.30
SN 4	8.88	23.55	4.71E-04	4.31
SN 5	8.93	22.36	4.47E-04	4.32
SN 6	8.92	13.76	2.75E-04	4.33

The largest difference of 9.8 kV was found between SN1 and SN3 The variance in the transient recovery voltage peak was impacted by the fault angle. In SN1 and SN4 which have the same fault tripping angles, the transient recovery voltage is reported to be relatively similar at 23.53 kV and 22.35 kV respectively. This is also prevalent for SN2 and SN5 plus SN3 and SN6. Also, similar results were produced in the simulations with the same fault trip angle but with different

environmental conditions namely the idle and temperature. This proved the working of the controlled switching logic adapts to any environment to produce the similar results with exception of the fault angle change. The controlled switching is found to overall produce transients that are acceptable to the circuit breakers and withstand capabilities.

The overall impact of the transient is measured against the duration together with the transient recovery voltage to determine the rate of rise of recovery. The rate of rise of recovery voltage is higher for SN1 and SN4 at a fault angle of 30° in comparison to the remaining fault angles namely 60° and 90° simulated results, this proves that the rate of rise of recovery voltage and transient recovery voltage are impacted by the chopping current produced and the fault current trip angle. The Rate of rise of recovery voltage is also found to be higher when the transient recovery voltage is higher which are the expected results [98].The rate of rise of recovery voltage calculated is found to be lower than the circuit breaker dielectric withstand strength of $0.43\,kV/us$. Effectively, in the simulations SN1 to SN6, the lower transient recovery voltages due to current zero tripping had given way to a lower rate of rise of recovery voltage requirements for the circuit breaker.

4.4.4.3 Case Comparison

The comparative transient recovery voltage waveforms which have a similar profile in Figure 4.28 to 4.33 reflects the advanced controlled switching transient recovery voltage lagging the conventional transient recovery voltage due to the reduced chopping currents which is a result of the delay imposed by the advanced controlled switching logic to achieve current zero tripping. In Table 4.13, the duration of the transient recovery voltage on conventional switching for SN1 is 0.003 *s* and is subsequently increased to 0.004 *s* for SN2 and SN3 as the fault current angle is changed.

Table 4.13: Controlled Vs Conventional Transient Recovery Voltage Output Results

Simulation No. (SN)	Figure No.	Advanced Controlled Output Results			Conventional Output Results			
		Arc Voltage (kV)	TRV (kV)	RRRV ($kV/\mu s$)	Arc Voltage (kV)	Period (S)	TRV (kV)	RRRV ($kV/\mu s$)
SN 1	4.28	8.82	23.53	4.71E-04	9.95	0.003	29.95	5.19E-04
SN 2	4.29	8.74	22.23	4.45E-04	9.97	0.004	29.75	5.35E-04
SN 3	4.30	8.93	13.73	2.75E-04	9.93	0.004	23.37	4.67E-04
SN 4	4.31	8.82	23.55	4.71E-04	n/a	n/a	n/a	n/a
SN 5	4.32	8.89	22.36	4.47E-04	n/a	n/a	n/a	n/a
SN 6	4.33	8.95	13.76	2.75E-04	n/a	n/a	n/a	n/a

However, when the advanced controlled switching is implemented, the duration of the transient recovery voltage remains constant at 0.001 *s* for SN1 to SN6. The magnitude of the transient recovery voltage for advanced controlled switching is decreased by an average of 29% for SN1 to SN6 with SN3 and SN6 having the largest decrease when compared to conventional circuit breaker interruption. This is due to the near current zero interruption for conventional circuit breaker switching rather than current zero interruption.

The magnitude of the transient recovery voltage changes on the conventional switching only for SN1 to SN3 are not more than 22% when the fault current angle changes. This change is also present when advanced controlled switching only is implemented and compared between SN1 to SN6 at the same fault angle. In essence, this depicts that 2nd to the current zero tripping using advanced controlled logic, the fault angle also has an influence on the transient recovery voltage magnitude. The rate of rise of recovery voltage for the conventional circuit breaker increased by an average 10% when compared to the advanced controlled switching results. The rate of rise of recovery voltage is proportional to the transient recovery voltage itself. Effectively, the circuit breaker probability of gaining restrike voltage is reduced when the rate of rise of recovery voltage is reduced thus an improvement by an average of 11% is favourable when using advanced controlled switching. It is also observed that TRV peak decreases and time to peak increases with advanced controlled switching. This also causes the RRRV requirements to change accordingly in order to provide swift circuit breaker trip times. Overall, the TRV is much lower as a result of current zero interruption for advanced controlled tripping when compared to the conventional as expected [38].

4.4.5 Re-ignition

Re-ignition is not evident in the simulations as the transient recovery voltage did not exceed the circuit breaker dielectric strength of $0.43\,kV/\mu s$ [38].

4.4.6 Restrikes

The restrikes of the circuit breaker for the conventional and advanced controlled switching simulation SN1 to SN3 was completed by varying the fault current angle, with an additional variation of idle time and temperature being implemented for advanced controlled switching, for simulation SN4 to SN6. The restrikes for the conventional and advanced controlled switching circuit breaker operations for all simulations are shown in Figure 4.34 to 4.39. ResX

represents the conventional graphs while Res represents the advanced controlled switching graph results.

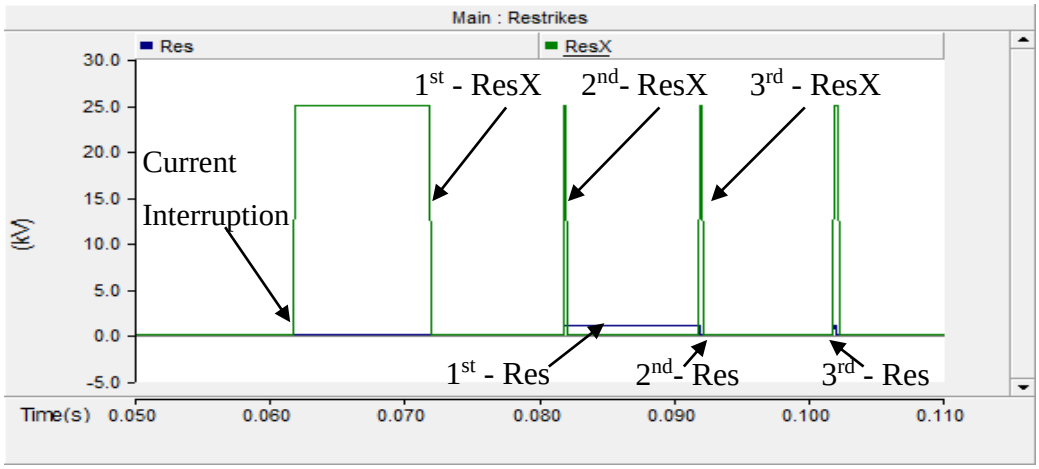

Figure 4.34: SN1 Controlled Switching Vs Conventional Restrike

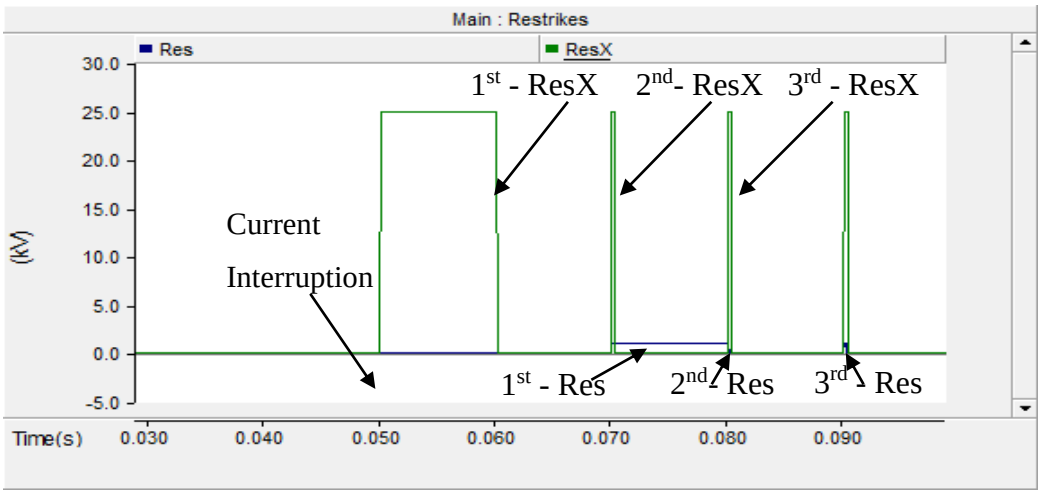

Figure 4.35: SN2 Controlled Switching Vs Conventional Restrike

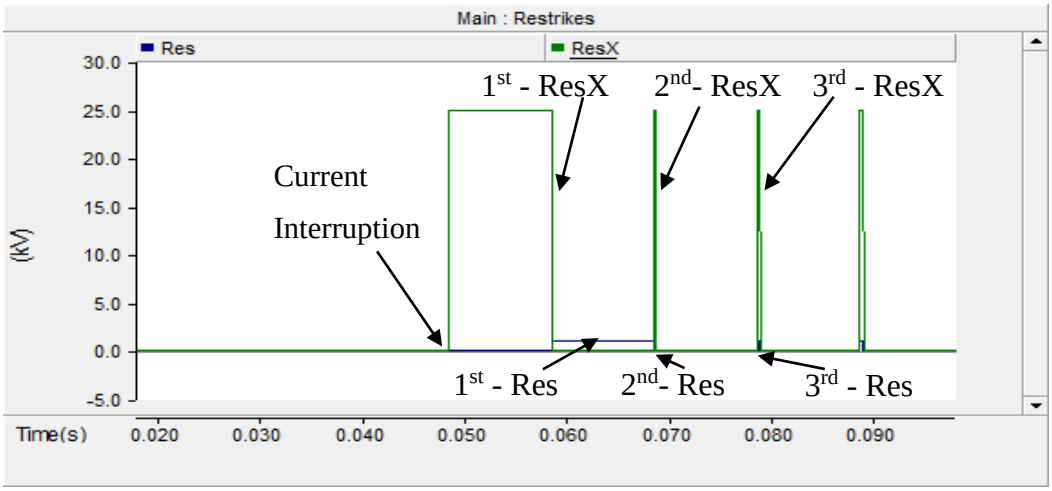

Figure 4.36: SN3 Controlled Switching Vs Conventional Restrike

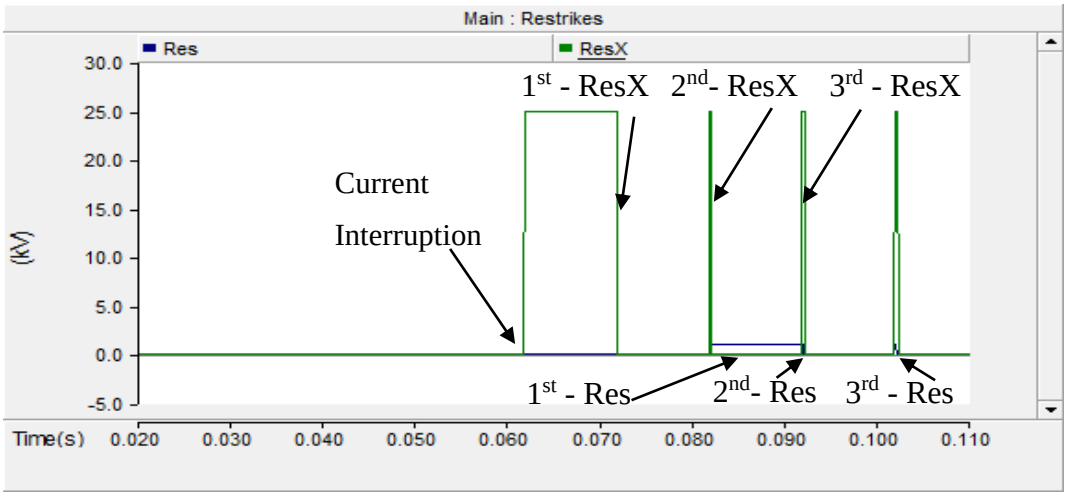

Figure 4.37: SN4 Controlled Switching Vs Conventional Restrike

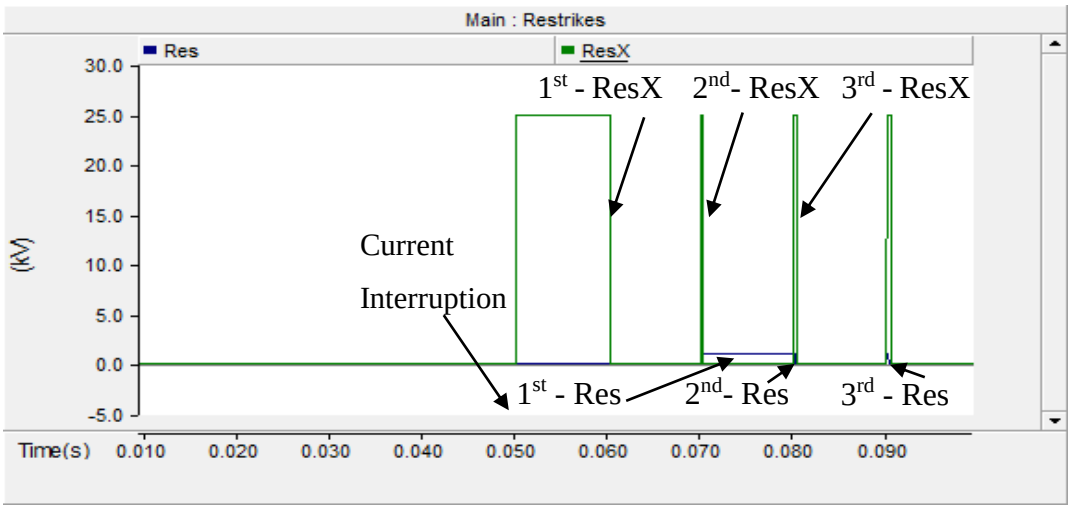

Figure 4.38: SN5 Controlled Switching Vs Conventional Restrike

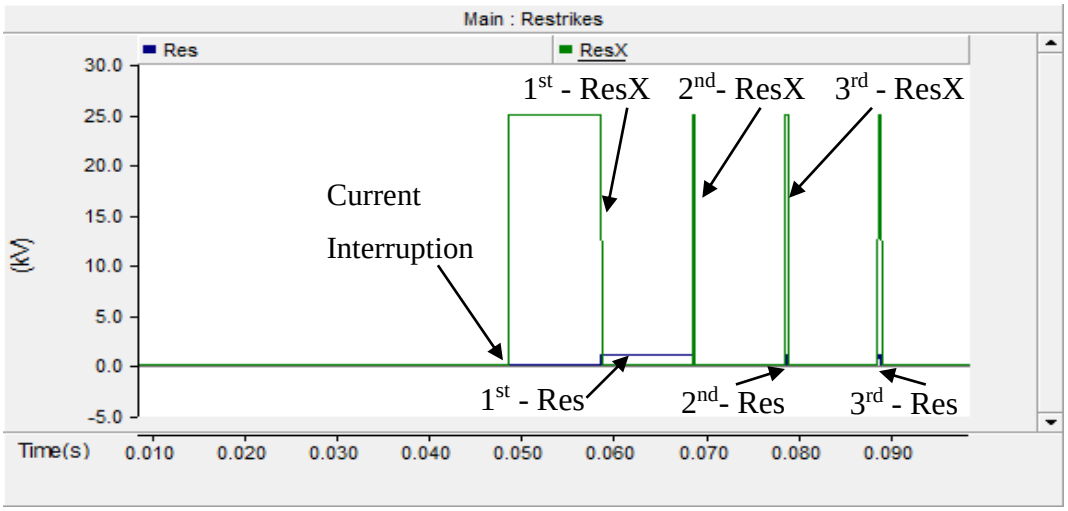

Figure 4.39: SN6 Controlled Switching Vs Conventional Restrike

4.4.6.1 Conventional Switching Case

In the simulated results for restrikes without a stay capacitor, the restrike occurrence for all simulation have a trend of occurring at least 0.25 cycle after current interruption, as indicated in Figure 4.34 to 4.36 [99]. The energy stored from the electrical field of stray capacitance was constant at 0 *J*.

The number of restrikes in SN1 to SN3 have no consistency due to the tripping occurring at various trip angle hence the current trip angle is posed to be one of the catalyst to the number of restrikes during circuit breaker interruption [99]. When the fault current angle was varied through each simulation, it was found to the have no impact on the magnitude of the restrikes. However, it does impact the time instant of the 1st restrike occurring. A total of 4 restrike instants are identified from Figure 4.34 to 4.36. However, for the purpose of this dissertation, only 3 of the restrike instants are being analysed. The restrike energy produced W_{osc} in Table 4.14 for SN1 to SN3 is within a 0.1% tolerance of each other therefore its it established that variation in the fault current and current trip parameter's marginally varies with the restrike energy produced. Restrike is abbreviated with Res in the tables below.

Table 4.14: Conventional Breaker Restrike Results with No Stray Capacitance

Restrike Results Output (Simulation with No Stray Capacitance)								
Simulation No. (SN)	**Load I (A)**	**Peak Ignition (kV)**	**Res Energy Produced (J)**	**Res Energy (J)**	**1st Time Res (s)**	**2nd Res Time (s)**	**3rd Res Time (s)**	**Figure No.**
SN 1	323	24.89	27125.54	27125.54	0.06	0.08	0.093	4.34
SN 2	323	24.99	27125.54	27125.54	0.05	0.07	0.08	4.35
SN 3	324	24.79	27293.76	27293.76	0.05	0.07	0.08	4.36

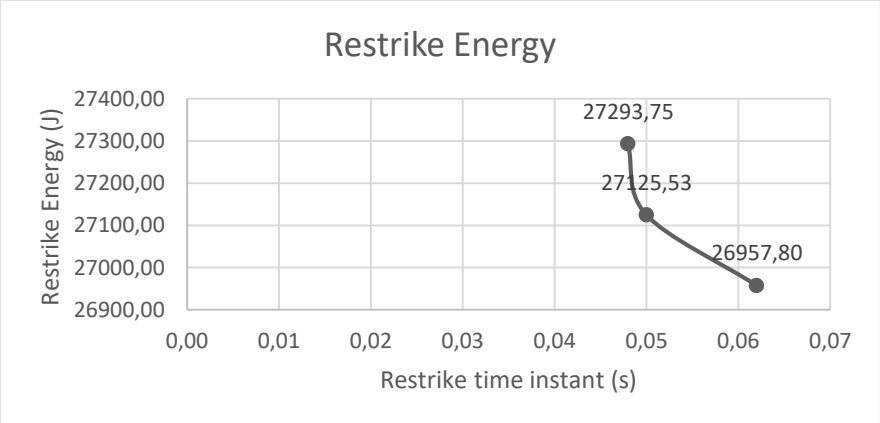

Figure 4.40: Restrike Energy Vs Time

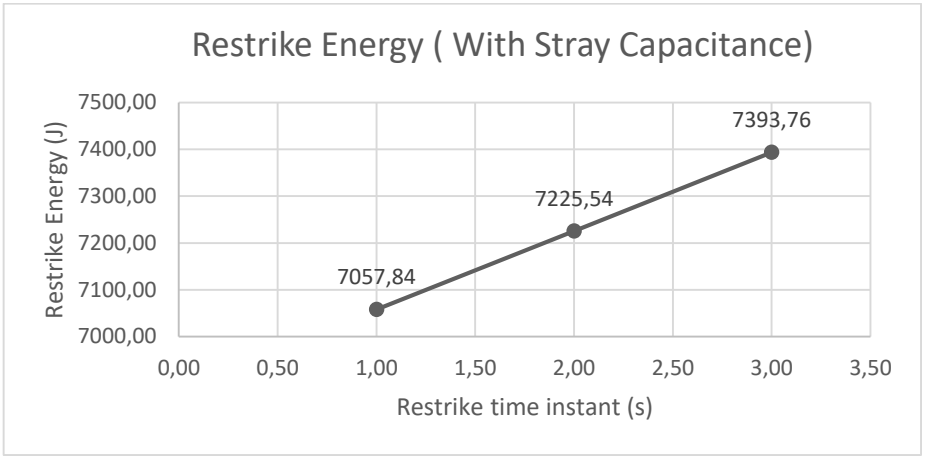

Figure 4.41: Restrike Energy Vs Time (With stray Capacitor)

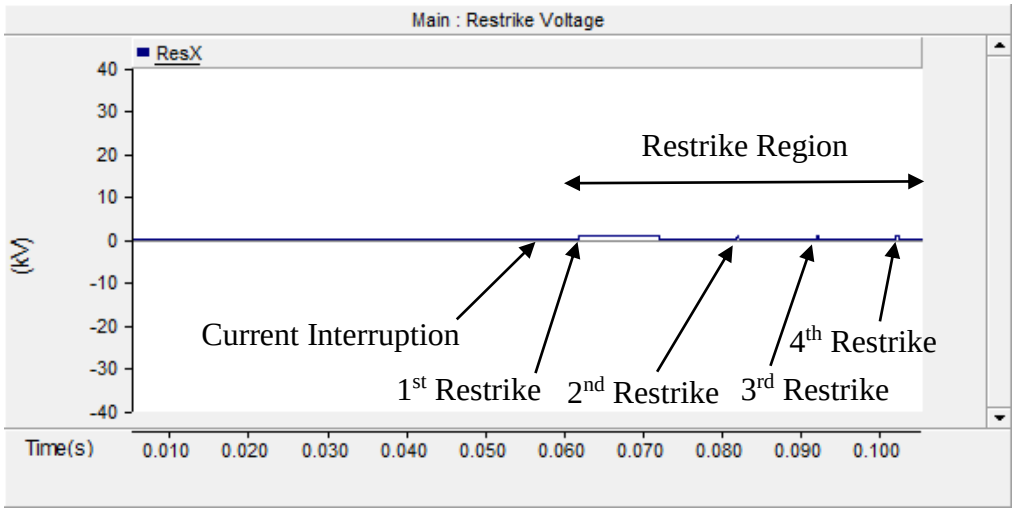

Figure 4.42: SN1 Restrikes with Stray Capacitor

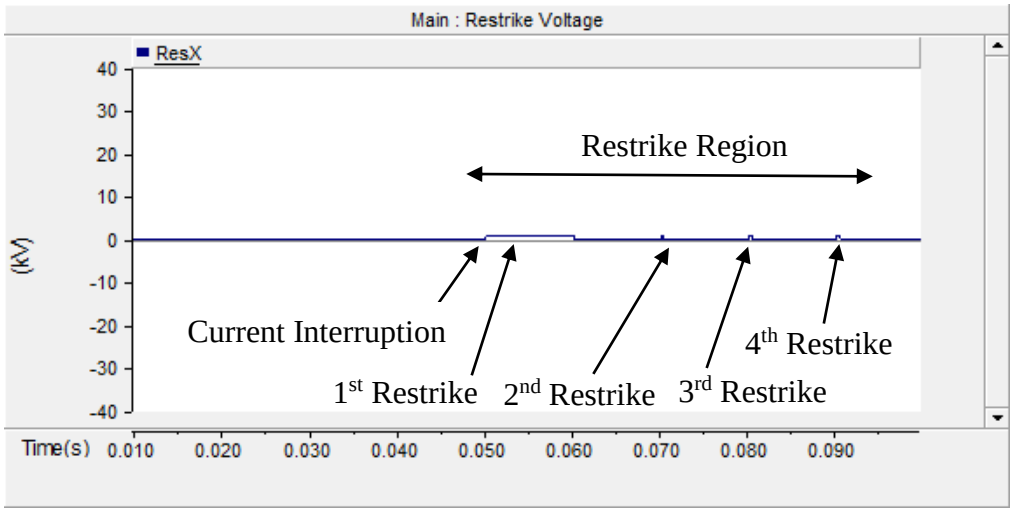

Figure 4.43: SN2 Restrikes with Stray Capacitor

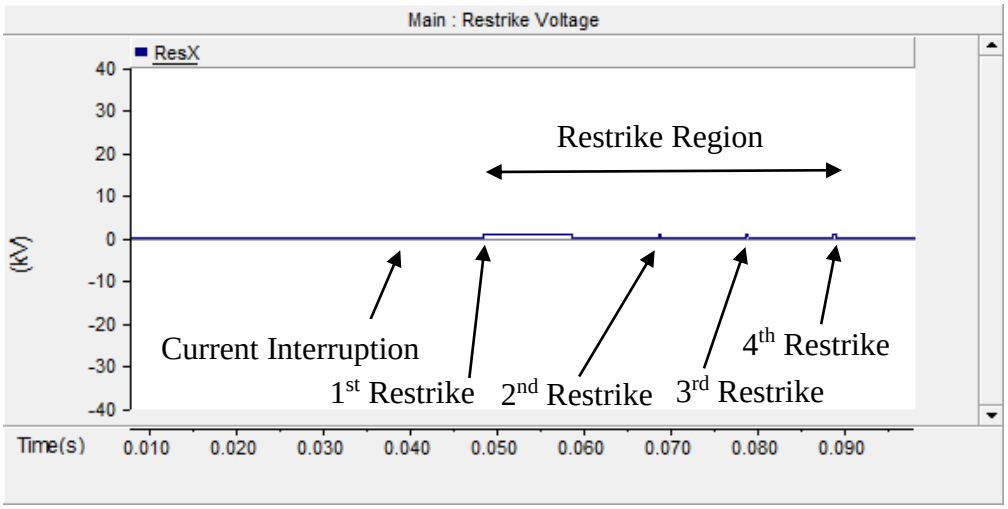

Figure 4.44: SN3 Restrikes with Stray Capacitor

Table 4.15: Conventional Breaker Restrike Results with Stray Capacitance

Conventional Switching Restrike Results (Simulation with Stray Capacitance)							
Simulation No. (SN)	**Load Current (A)**	**Res Energy Produced (J)**	**Res Energy (J)**	**1st Res Time (S)**	**2nd Res Time (S)**	**3rd Res Time (S)**	**Figure No.**
SN 1	323	27125.5	7225.54	0.06	0.08	0.09	4.42
SN 2	323	27125.5	7225.54	0.05	0.07	0.08	4.43
SN 3	324	27293.8	7393.76	0.05	0.07	0.08	4.44

During the simulations for restrikes with the stray capacitor, it was found that the magnitude of the restrike are reduced significantly with a stray capacitance which is charged to the limit of the transient recovery voltage that effectively limits the restrikes via a charged resistor that accelerates the gap breakdown. The results produced shows an average reduction of approximately 7000 *J* across all simulations while the number of restrikes and the time instant of the restrike occurring remained the same due to the same current trip angle. The energy stored from the electrical field of stray capacitance was constant at 19900 *J* and the peak ignition voltage was constant 1 *kV* for all simulations. The restrike energy is a component which forms part of the overall dynamism arc energy. The stray capacitance has reduced the restrikes as shown in Figure 4.42 to 4.44 therefore allowing for a more isolated analysis of the arc energy itself which is analysed in totality under Arc dynamism. The model without stray capacitor has been adopted for conventional circuit breaker simulations for the remaining simulations in this dissertation in an effort to display a real time standard conventional breaker output while all the advanced controlled switching simulations include a stray capacitor.

4.4.6.2 Advanced Controlled Switching Case

The restrike occurrence for all simulation have the same trend of occurring half a cycle after current interruption [99]. The fault current angle was found to impact the 1st restrike instant at which the restrike occurs as the fault angles are changed from SN1 to SN3 and subsequently SN4 to SN6 as indicated in Table 4.16. However, the restrike magnitude, restrike duration (T_{Res}) and number of restrike instants was not affected by the change in fault angle.

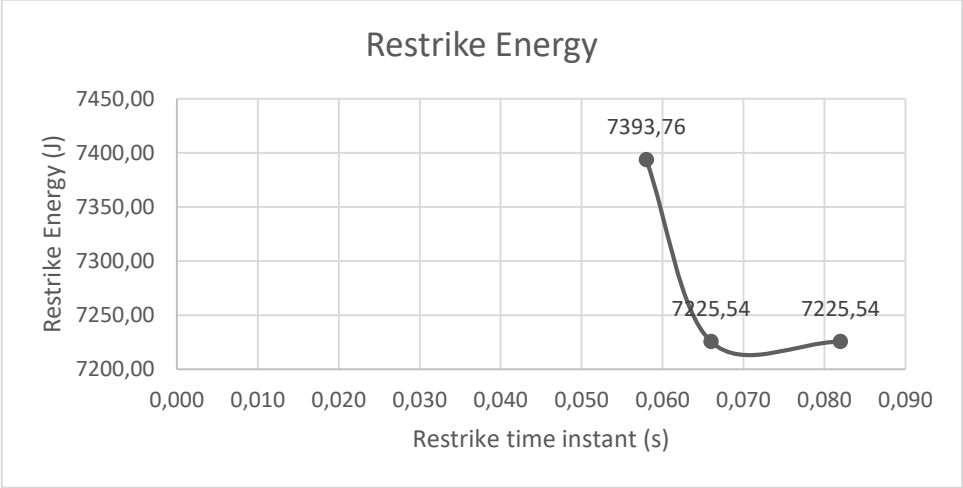

Figure 4.45: Controlled Switching Restrike Energy Vs Time Instant

Table 4.16: Controlled Switching Restrike Output Results

Controlled Switching Restrike Results (Simulation with Stray Capacitance)							
Simulation No. (SN)	**Load Current (A)**	**Res Energy Produced (J)**	**Res Energy (J)**	**1st Res Time (S)**	**2nd Res Time (S)**	**3rd Res Time (S)**	**Figure No.**
SN 1	323	27125.54	7225.54	0.082	0.101	0.113	4.34
SN 2	323	27125.54	7225.54	0.066	0.080	0.09	4.35
SN 3	324	27293.76	7393.76	0.058	0.078	0.09	4.36
SN 4	324	27293.76	7393.76	0.082	0.101	0.105	4.37
SN 5	324	27293.76	7393.76	0.066	0.080	0.09	4.38
SN 6	324	27293.76	7393.76	0.058	0.078	0.09	4.39

In SN4 to SN6, when the input parameters relevant to the environmental conditions changed, the restrike magnitude, restrike duration (T_{Res}) and the number of restrike instants had not changed. The constant tripping at near current zero generally produces higher restrikes. However, due to the inclusion of the stray capacitor and the advanced controlled switching ability to achieve tripping at current zero, this limits the restrike magnitude for all simulations

to 1 *kV* and producing not more than 3 restrike instants which is consistence throughout SN1 to SN6 as shown in Figure 4.34 to 4.39.

The restrike magnitudes in SN1 to SN6 are noted to be similar with no reportable change exceeding 1% variance between simulations as shown in Table 4.16. The duration between the 1st and 2nd restrike is 1 cycle apart while the distance between the 2nd, and 3rd restrike is half a cycle apart for all simulations which is effectively expected in relation to this phenomena [99].

The restrike energy produced (W_L) at approximately 27000 *J* in Table 4.16 are marginally the same for all simulations as this is dependent on the load current. The stray capacitor (W_c) used in the power circuit has the capacity to absorb 19000 *J* hence the restrike energy (W_{osc}) is regulated at approximately average of 7300 *J* for SN1 to SN6 in Table 4.16. Its concluded that the stray capacitance with current zero interruption limits the magnitude of restrikes, duration of restrikes and the probability of restrikes continually occurring therefore limiting the energy produced by the restrikes.

4.4.6.3 Case Comparison

The 1st restrikes instant for conventional switching lags the 1st restrikes produced for the advanced controlled switching for SN1 to SN6 in Figure 4.34 to 4.39, the 1st restrikes delay is proportional to the delay trip time imposed by the advanced controlled switching logic. The number of restrikes are four for the conventional circuit breaker switching and three for the advanced controlled switching at the same fault current angle. This is a decrease in one restrike occurrence when advanced controlled switching is implemented. In this dissertation, the results of the 1st three restrikes is only analysed as indicated in Table 4.17 and Table 4.18.

Table 4.17: Conventional Restrike Output Results

Conventional Simulation Results (without Stray Capacitance)								
Simulation No. (SN)	**Figure No.**	**Peak Ignition (kV)**	**Res Energy Produced (J)**	**Absorbed Energy (J)**	**Res Energy (J)**	**1st Res Time (s)**	**2nd Res Time (s)**	**3rd Res Time (s)**
SN 1	4.99	24.89	27125.5	0.00	27125.54	0.06	0.08	0.09
SN 2	4.100	24.99	27125.5	0.00	27125.54	0.05	0.07	0.08
SN 3	4.101	24.79	27293.8	0.00	27293.76	0.05	0.07	0.08

Table 4.18: Controlled Restrike Output Results

Advanced Controlled Switching Results (With Stray Capacitance)							
Simulation No. (SN)	**Figure No.**	**Res Energy Produced (J)**	**Absorbed Energy (J)**	**Res Energy (J)**	**1st Res Time (S)**	**2nd Res Time (S)**	**3rd Res Time (S)**
SN 1	4.99	27125.54	7225.54	19900	0.082	0.101	0.11
SN 2	4.100	27125.54	7225.54	19900	0.066	0.080	0.09
SN 3	4.101	27293.76	7393.76	19900	0.058	0.078	0.09
SN 4	4.102	27293.76	7393.76	19900	0.082	0.101	0.11
SN 5	4.103	27293.76	7393.76	19900	0.066	0.080	0.09
SN 6	4.104	27293.76	7393.76	19900	0.058	0.078	0.09

In each simulation for both conventional and advanced controlled switching, the 2nd strike occurs 1 cycle after the 1st restrike and the 3rd restrike occurs and half cycle after the 1st restrike. The major deviation of results when advanced controlled switching is implemented is the magnitude of the restrike voltage which is represented by peak ignition in Table 4.18. The Peak ignition is decreased by up to 250% when advanced controlled switching is implemented for SN1 to SN6. This decrease is due to the stray capacitance implemented and standard gap separation and not the advanced controlled switching logic [37]. In Table 4.17, its due to the absence of a stray capacitor in the conventional circuit breaker that the capacitive energy (W_C) absorbed is 0 J of arc energy. However, when the advanced controlled switching logic for SN1 to SN6 is implemented, the capacitive energy absorbed is 19000 J. The chopping energy (W_L) produced is relatively the same for both conventional and advanced controlled switching since the energy in dependent on the load of the system. It's also noted for both conventional and advanced controlled switching that in SN1 to SN2 where the load is 323 A on the system, the chopping energy is 27125.54 J and when the load current increases to 324 A on the system for SN2 to SN6, the chopping energy increases by 1% to 27293.76 J which is a negligible change. The overall energy of the restrike produced (W_{osc}) on conventional switching for SN1 to SN3 is equal to the chopping energy (W_L) produced, due to no capacitor present to absorb the energy. In SN1 to SN6 for advanced controlled switching when the stray capacitor is introduced, the restrike produced (W_{osc}) is reduced by 19000 J to an average amount of 7337.7 J therefore reducing the restrike voltage produced hence providing a reduced impact on the circuit breaker even when the environmental input parameters have changed. It's important to note that for advanced controlled switching without a stray capacitor, it effectively increases the restrike energy. Hence, the controlled logic with a stray capacitor is implemented to provide effective results for a reduced restrike energy.

4.4.7 Dynamism of Arc

The Dynamism of the Arc within the circuit breaker for the conventional and advanced controlled switching simulation SN1 to SN3 was completed by varying the fault current angle, with an additional variation of idle time and temperature being implemented for advanced controlled switching, for simulation SN4 to SN6.The dynamics of the arc for the conventional and advanced controlled switching circuit breaker are shown in Figure 4.46 to 4.51. ArcPX represent the active power while ArcQx represents the reactive power for the conventional graphs results. ArcP represent the active power while ArcQ represents the reactive power for the advanced controlled switching graph results.

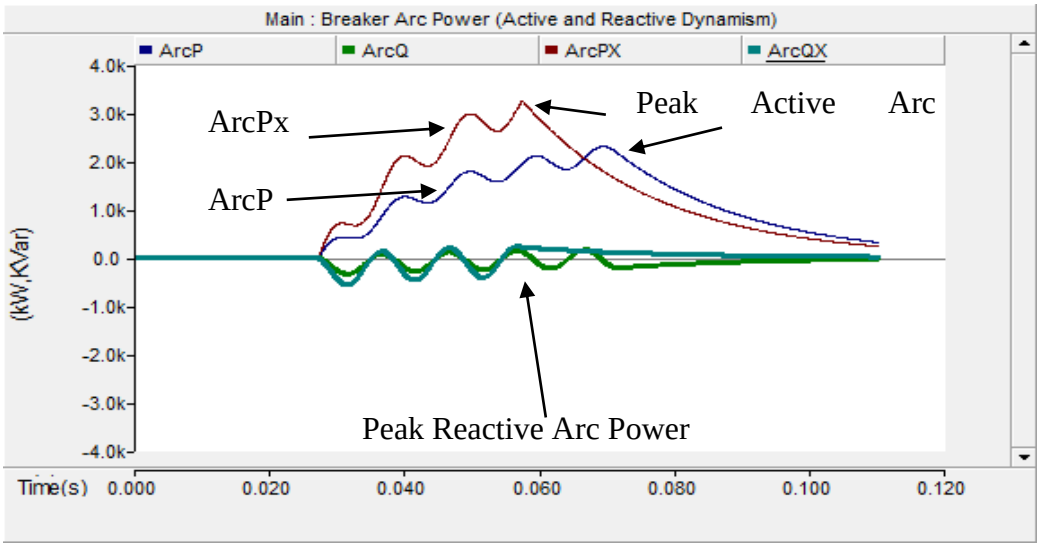

Figure 4.46: SN1 Controlled Switching Vs Conventional Arc Power

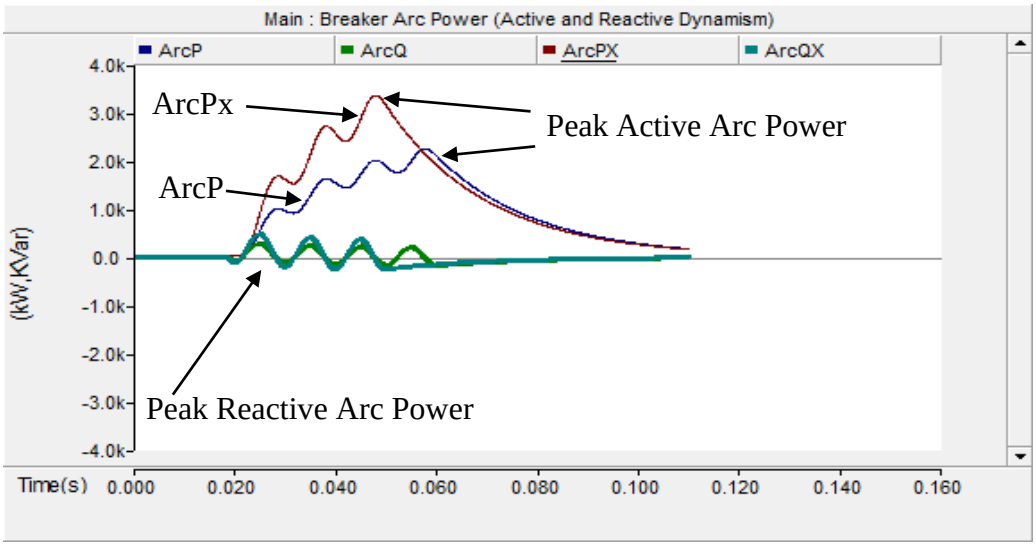

Figure 4.47: SN2 Controlled Switching Vs Conventional Arc Power

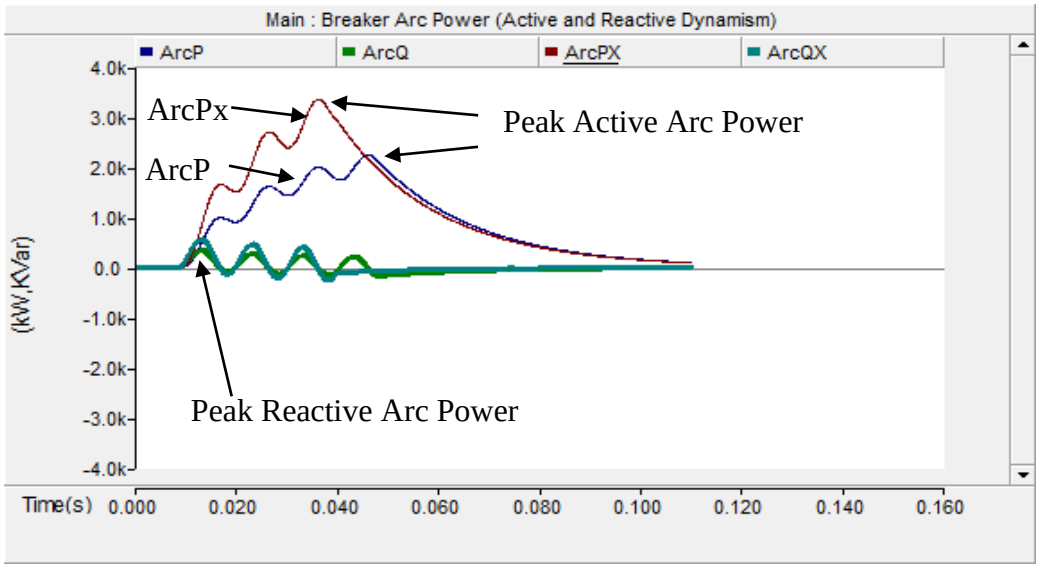

Figure 4.48: SN3 Controlled Switching Vs Conventional Arc Power

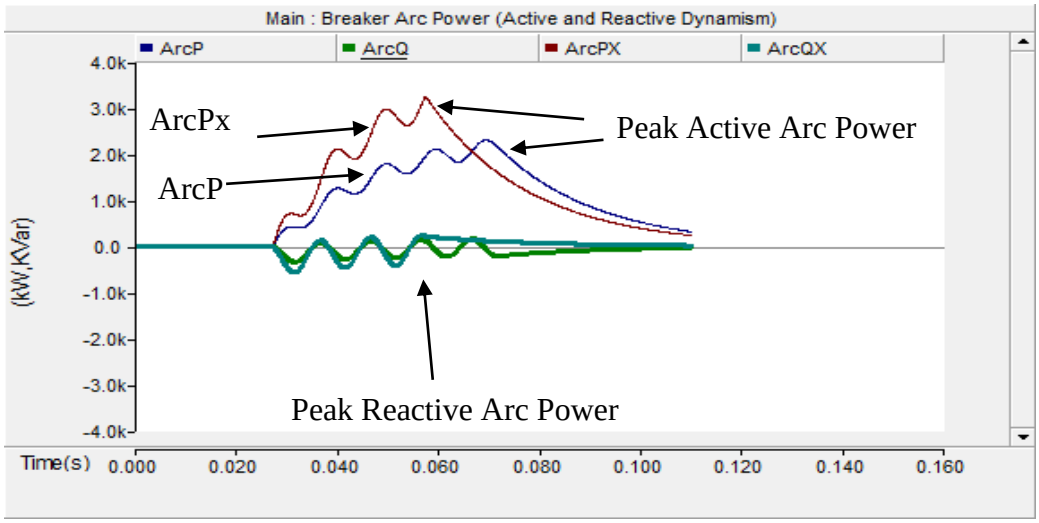

Figure 4.49: SN4 Controlled Switching Vs Conventional Arc Power

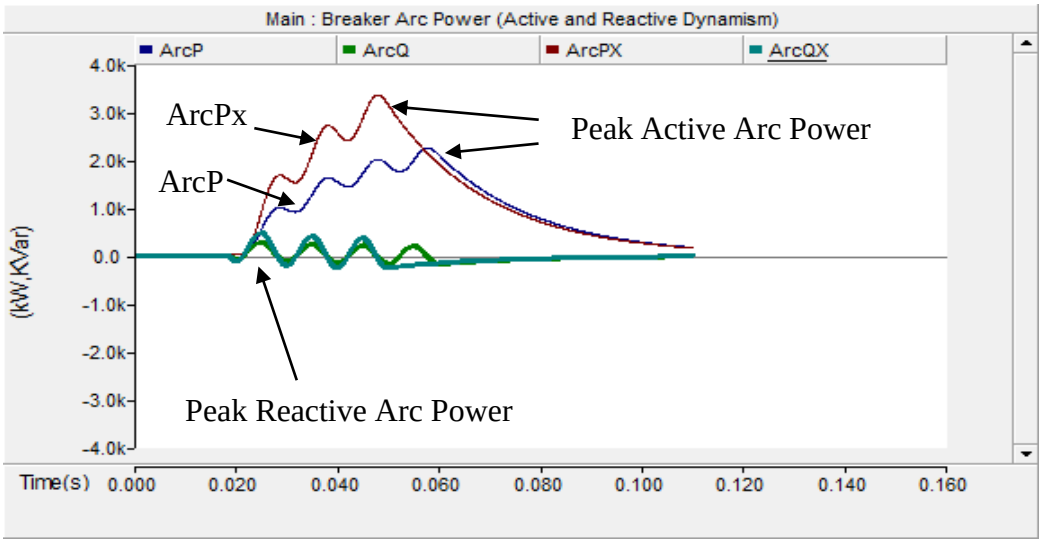

Figure 4.50: SN5 Controlled Switching Vs Conventional Arc Power

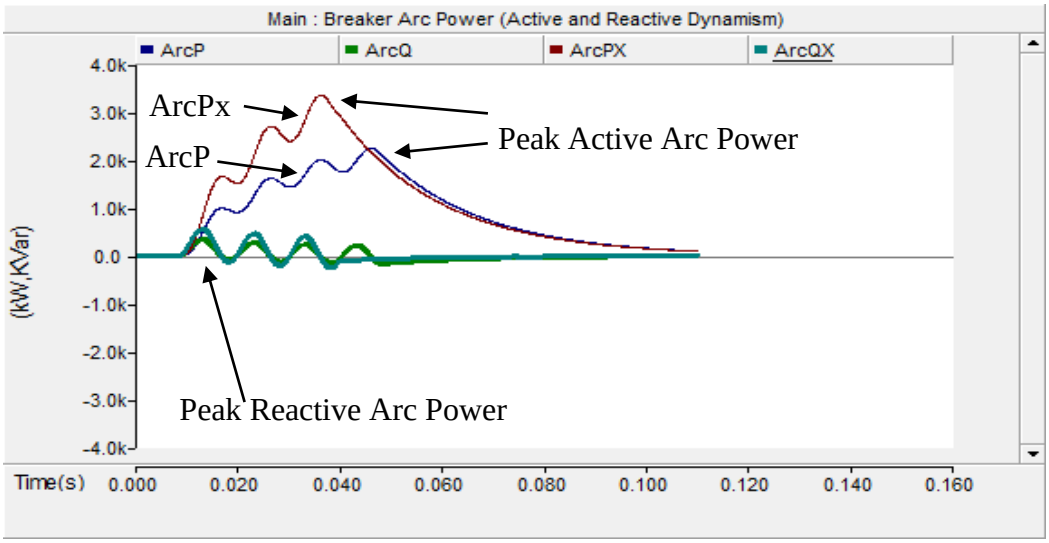

Figure 4.51: SN6 Controlled Switching Vs Conventional Arc Power

4.4.7.1 Conventional Switching Case

The power of the arc results from the simulation is inserted into equation (2.22) to determine the energy produced for SN1 to SN3 in Table 4.19. The power of the arc is proportional to the energy produced by the arc for all simulations. The noticeable trend for all simulations is of the active and reactive power of the arc which indicates a tapering of power to zero after current interruption due to the loss of energy and the loss attributed to the current starvation. The re-active power for SN2 and SN3 peaks at the start of the circuit breaker interruption cycle. However, the re-active power of the arc for SN1 peaks near current starvation. The reactive power tapers down in all simulations as it approaches the point of current starvation as shown in Figure 4.46 to 4.48. This indicates that at near current zero interruption for SN2 and SN3, the re-active energy is reduced significantly in the region of a $1/3^{rd}$ when compared to SN1. The current interruption instant for SN1 to SN3 shows that the angle of interruption on Figure 4.46 to 4.48 in terms of current starvation on the waveform makes an impact on the overall magnitude of arc power. SN2 and SN3 trips at its current peak with a high arc active power when compared to SN1. This is effectively the transient recovery arc voltage that is contributing to the increased arc power due to the difference in the energy from the source and load side which is higher when current interruption occurs at near current zero [100].

The peak arc instant (τ) in Table 4.19 indicates that the arc peaks for SN2 at 0.049 *s* is slower when compared to SN3 at 0.039 *s*. However, the Arc energy output peak for SN2 is lower at 138541.57 *J* in comparison to the arc energy produced for SN3 at 138635.71 *J*. This concludes that the arc energy produced which is the main contributor to stresses caused on the circuit

breaker contacts is proportional to the arc power. However, the energy produced is also influenced by the fault current angle and the rate of reaching the arc peak.

Table 4.19: Conventional Breaker Arc Power Output Results

Conventional Arc Power Output Results								
Simulation No. (SN)	**Arc Current (kA)**	**Arc Voltage (kV)**	**Arc Active Power (kW)**	**Arc Reactive Power (kW)**	**Energy of Arc Power (J)**	**Peak Arc Instant (s)**	**Trip Angle ($^\circ$)**	**Figure No.**
SN 1	24.76	9.95	3245	62	138834.18	0.057	275.4	4.46
SN 2	24.64	9.97	3351	14	138541.57	0.049	345.6	4.47
SN 3	24.89	9.93	3339	220	138635.71	0.039	216	4.48

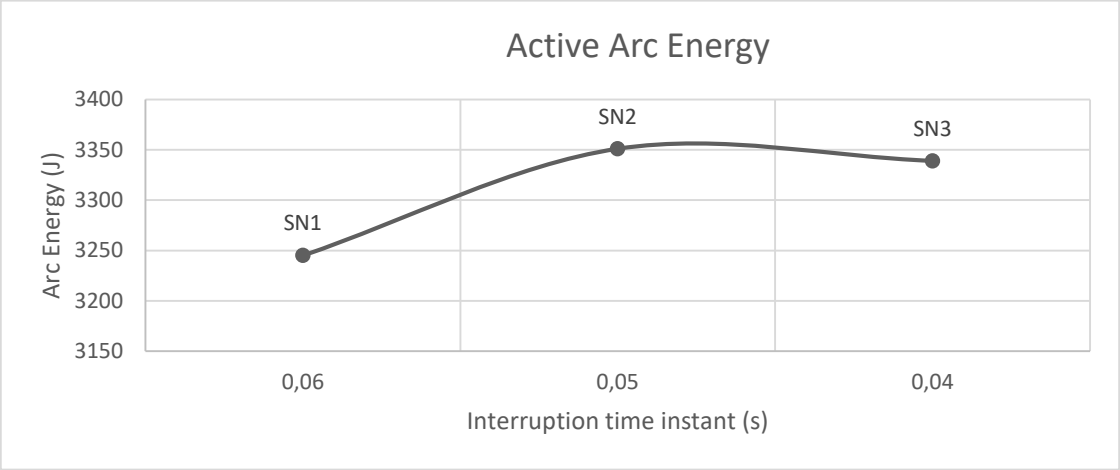

Figure 4.52: Arc Energy Vs Interruption Time

Figure 4.52 depicts that the angle of interruption in terms of the time instant where current starvation occurs indicating the non-linear relationship between the energy of the arc to the interruption time instant.

4.4.7.2 Advanced Controlled Switching Case

The power of the arc results from the simulation is inserted into equation (2.22) to determine the energy produced for SN1 to SN6 in Table 4.20. The average output arc current (i) is 22.26 *kA* and the average arc voltage(u) is 8.95 *kV* for all simulations. The peak active power of the arc for SN1 to SN3 occurs at 0.01 *s* prior to current starvation. However, when the input parameters relevant to the environmental changes, the active power peak occurs at the point of current interruption as indicated on Figure 4.46 to 4.51. The advanced controlled switching logic factors results in a change of the peak arc time instant (τ) occurrence while still ensuring the peak occurrence is regulating the magnitude of the arc power. The active power for all

simulations have proven to be regulated throughout all simulation within a tolerance of 3% with a constant arcing time. The current interruption instant for SN1 to SN6 indicated in Figure 4.46 to Figure 4.51 that current zero tripping produces a regulated arc active power output.

Table 4.20: Advanced Controlled Switching Arc Power Output Results

Advanced Controlled Switching Arc Power Output Results						
Simulation No. (SN)	**Arc Active Power (kW)**	**Arc Reactive Power (kW)**	**Energy of Arc Power (J)**	**Peak Arc Time Instant (S)**	**Trip Angle ($^\circ$)**	**Figure No.**
SN 1	2303.00	5.40	98476.21	0.065	405	4.46
SN 2	2245.00	39.30	92773.14	0.051	387	4.47
SN 3	2233.00	-40.00	93096.66	0.045	360	4.48
SN 4	2305.00	34.00	98456.21	0.068	405	4.49
SN 5	2243.00	65.00	92763.14	0.056	387	4.50
SN 6	2239.00	-62.00	93076.26	0.046	360	4.51

The re-active power rises as its progresses through the circuit breaker closing cycle for SN1 and SN3 while the re-active power for the remaining simulation follows a higher start and is subsequently reduced throughout the remaining circuit breaker closing cycle up until current interruptions. The peak re-active power results shown in Table 4.20 is not consistent during the simulations as its found to be influenced by the variable parameter change relevant to its environmental and fault interruption angle. The noticeable trend for all simulations is of the active and reactive power of the arc which indicates a tapering of power to zero after current interruption due to the loss of energy and the loss attributed to the current starvation.

The arc active power is found to be proportional to the energy of the arc throughout all simulations. The magnitude of the arc energy was found to deviate as the fault angle changed between simulations SN1, SN2 and SN3. The lowest fault angle at SN1 and SN4 produced the most arc energy at 98476.21 *J* and 98456.21 *J* respectively with the energy deviation between the remaining simulations not exceeding 6 %. The change in fault angle impacts the arc energy magnitude marginally. The energy magnitude of the arc is also impacted by the time it's able to reach its arc time instant (τ) and the active power (P) produced during fault interruption. In Table 4.20, it also indicates that the Peak arc time (τ) instant was marginally impacted by the change in input parameters relevant to environmental conditions change for the same fault current angle by slowing down the time it takes to peak as indicated in Figure 4.46 to 4.51 when comparing for the same fault interruption angle.

The tripping at current zero with the change in the environmental conditions have found to still regulate the overall energy of the arc output provided for the same fault angle with minimal deviations. The current interruption times are changed by half a cycle as the fault trip angle shifts by 30° between simulation. However, the duration of the arc is maintained at 0.11 *s*. The duration of the arc is also maintained when the environmental conditions are changed. This provides an indication that the advanced controlled switching logic which shifts the current interruptions time based on the fault angle is still able to regulate a low power arc and subsequently arc energy irrespective of the fault angle or environmental conditions by regulating the arc duration.

4.4.7.3 Case Comparison

The advanced controlled switching simulation effectively produces a regulated overall arc energy within a 1% tolerance throughout the simulations with a lower energy magnitude when compared to the conventional switching simulation. The peak arc instant was found to be the same for both simulations. However, the arc energy peaks early and starts to deteriorate earlier in conventional switching when compared to advanced controlled switching. This is due to the logic processing of advanced switching to achieve current zero interruption therefore a later current interruption at current zero produces a lower magnitude at interruption. This holistically reduces the overall energy within the circuit breaker.

4.4.8 Temperature of Arc

The Temperature of the Arc in the circuit breaker for the conventional and advanced controlled switching simulation SN1 to SN3 was completed by varying the fault current angle, with an additional variation of idle time and temperature being implemented for advanced controlled switching, for simulation SN4 to SN6.The temperature of arc for all simulations are shown in Figure 4.53 to 4.58. ArcTx represents the conventional graphs while ArcT represents the advanced controlled switching graph results.

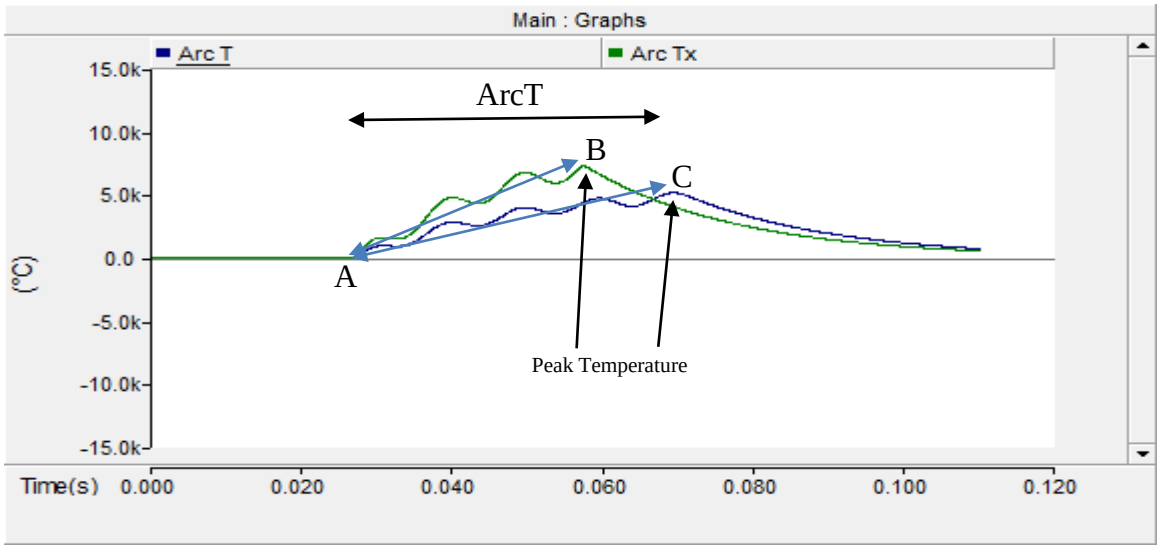

Figure 4.53: SN1 Controlled Switching Vs Conventional Arc Temperature

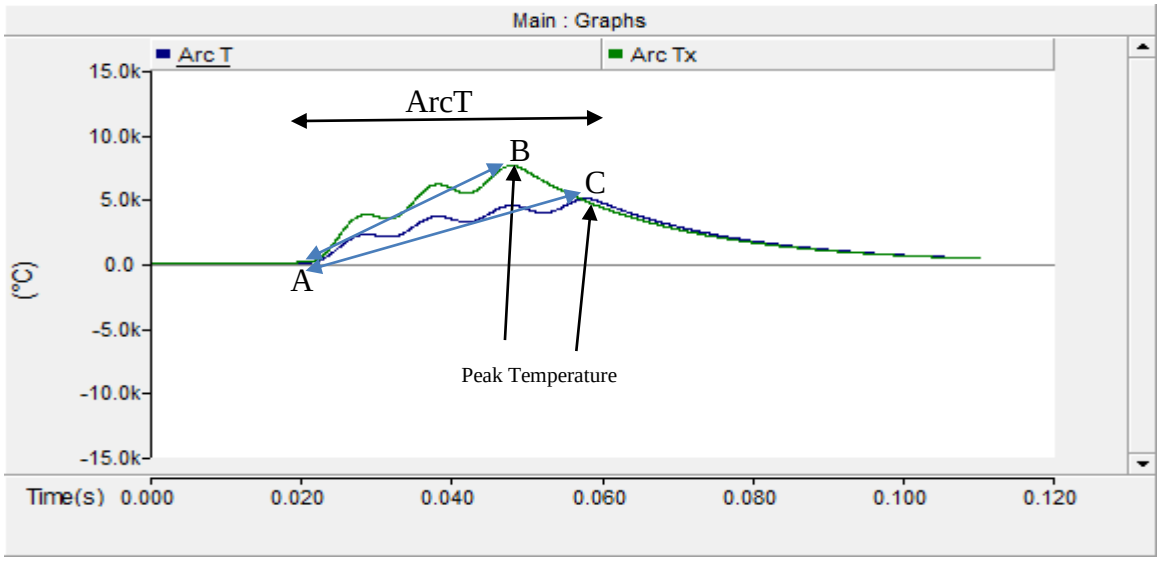

Figure 4.54: SN2 Controlled Switching Vs Conventional Arc Temperature

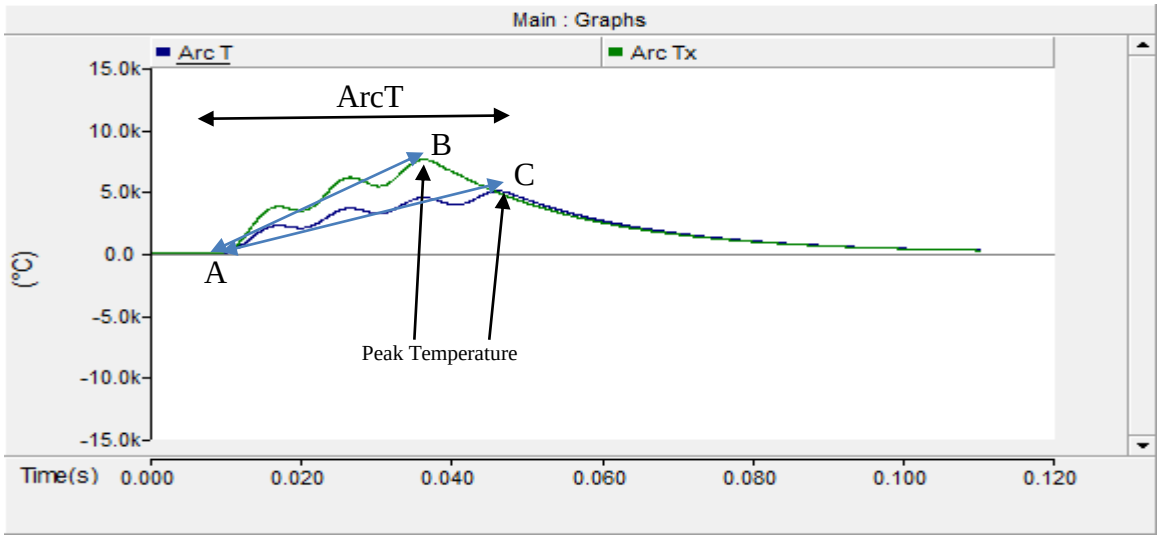

Figure 4.55: SN3 Controlled Switching Vs Conventional Arc Temperature

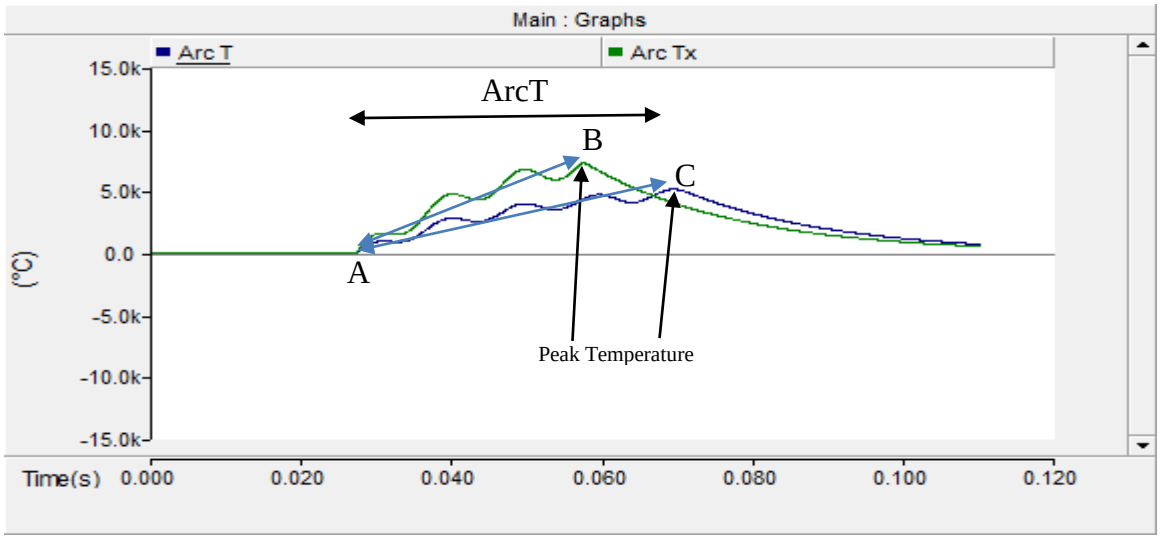

Figure 4.56: SN4 Controlled Switching Vs Conventional Arc Temperature

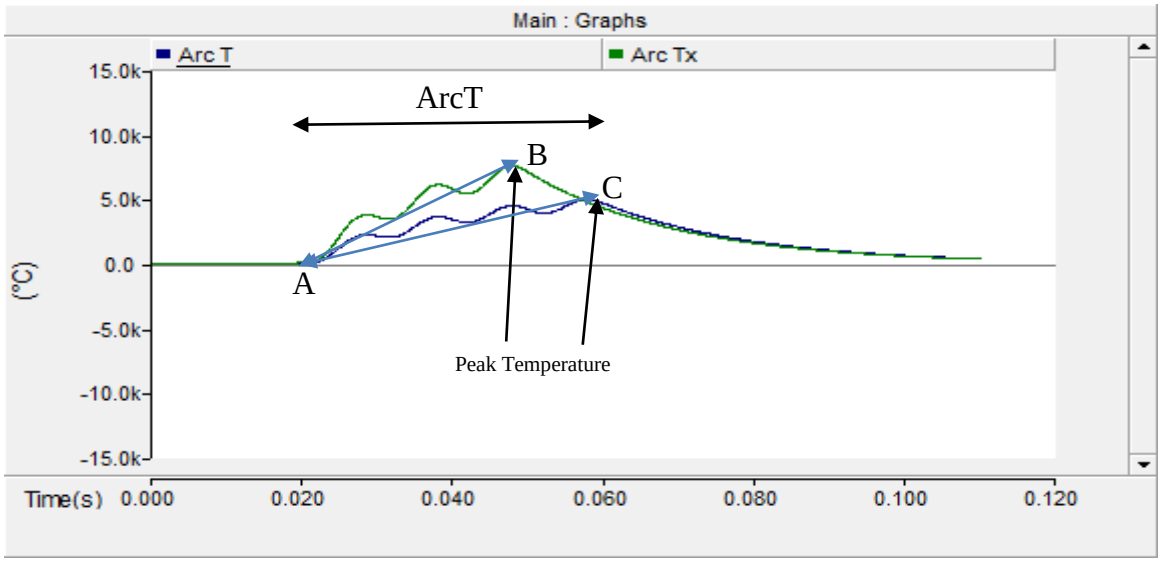

Figure 4.57: SN5 Controlled Switching Vs Conventional Arc Temperature

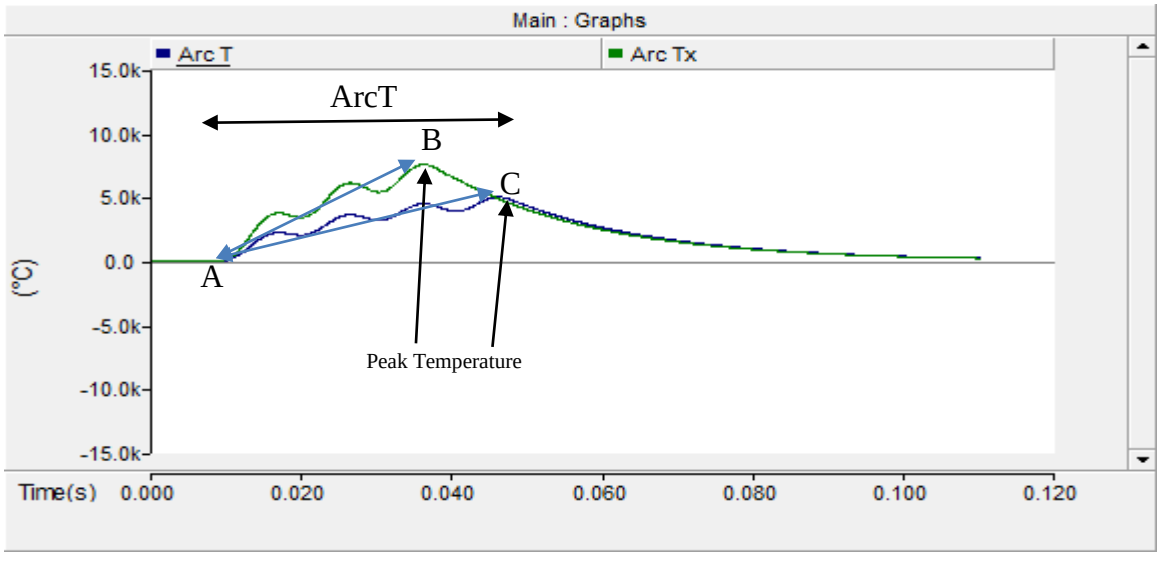

Figure 4.58: SN6 Controlled Switching Vs Conventional Arc Temperature

4.4.8.1 Conventional Switching Case

The peak arc time instant (τ) is found to almost co-inside with the current interruption time for all simulations. However, the arcing time duration through each simulation varies. In Table 4.21, the recorded temperature at SN1 which trips at current peak, deviates by $15°C$ when compared SN2 which trips at near current zero for a similar arcing duration. The results for SN2 and SN3 when compared indicates that the temperature at SN2 would have been higher than SN3 if only the arcing duration made an impact on the overall temperature magnitude.

Table 4.21: Conventional Breaker Temperature of Arc Output Results

Temperature of Arc Output Results				
Simulation No. (SN)	**Arc Temperature ($°C$)**	**Current Interruption time (S)**	**Peak Arc time Instant (S)**	**Figure No.**
SN 1	7287.64	0.057	0.0569	4.53
SN 2	7272.28	0.049	0.0470	4.54
SN 3	7277.23	0.039	0.0359	4.55

In SN3, The peak arc time instant (τ) is the lowest while the temperature produced by the arc is not the highest. Hence, this depicts that the peak arc time instant (τ) is not directly proportional to the temperature of the arc. Taking the above into consideration, the peak arc time instant (τ) and arc duration may not be directly proportional to the temperature of the arc but have an influence on the temperature of the arc stemming from the results in Table 4.21.

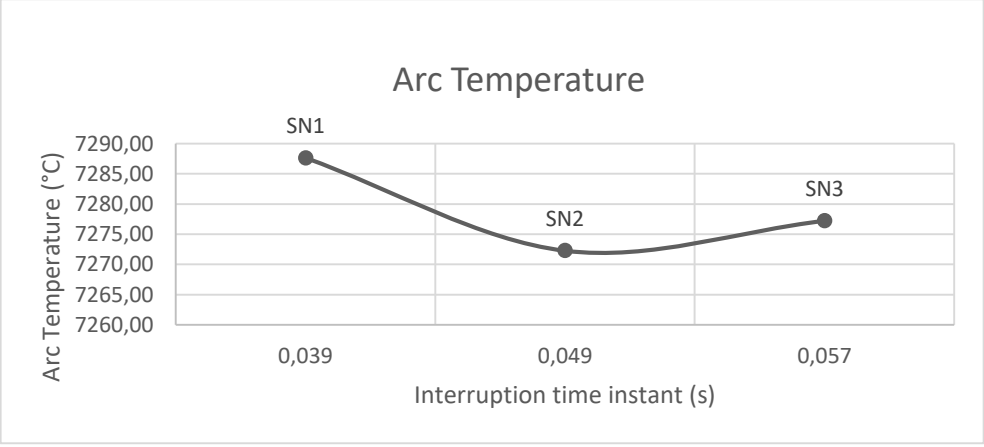

Figure 4.59: Conventional Breaker Arc Temperature Vs Interruption Time

The Figure 4.59 shows the rationality of the current interruption time relative to the temperature for SN1 to SN3. It's evident that the results in Table 4.21 shows that the delay in current interruption time does not necessary increase the temperature. The change in temperature is

also due to the influence of the current fault angle and peak arc time instant (τ).The results from SN1 to SN3 indicate that with a combination of an undesired fault current angle and current interruption angle, the temperature within the circuit breaker arcing chamber is hotter than the ions remaining within the arcing chamber raised from the arcing. This results in the ions tendency to vibrate more vigorously therefore colliding with neighboring ions consequently increasing the risk of restrikes and subsequently contact damaged.

The energy and power of the arc in the findings earlier reflected a proportional relationship to the current interruption angle. The temperature peak for all simulations in Figure 4.53 to 4.55 co-insides with the peak energy produced on Figure 4.53 to 4.55. Hence, the energy is also proportional to the rate of rise in temperature of the arc since the current interruption angle has a direct impact on the arcing temperature for the circuit breaker.

4.4.8.2 Advanced Controlled Switching Case

In SN1 to SN6, the highest temperature is recorded at $5169.19\,°C$ when the peak arc time instant (τ) reached 0.68 *s* for SN4 and the lowest temperature at $4867.72\,°C$ is recorded at a peak arc time instant (τ) of 0.56 *s* for SN5 as shown in Table 4.22 . However, these peak arc time instant (τ) results for SN1 and SN5 was not the highest or lowest respectively during the simulations hence the temperature of the arc is not directly proportional to the peak arc time instant (τ) but is impacted by its change. This impact is found when the fault angle of interruption is the same for SN1 and SN4 yet the temperature deviates by $4.5\,°C$ due to the input parameters. Evidently this indicates again that the peak arc time instant (τ) has a slight influence on the temperature change.

Since the current interruption for all simulations occurs at current zero yet the temperature vary by up to 6% between simulations , its deduced that the fault current angle is found to have up to a 6% change on the temperature while the temperature changes relevant to the input parameters relevant to the environment have up to a 0.1% change between simulations. The temperature of the arc for all simulations follow the same trend as the arc energy produced in Figure 4.53 to Figure 4.58 from the previous section. In essence, the arc power and arc energy are proportional to the rate of rise of temperature of the arc produced.

Table 4.22: Controlled Switching Temperature of Arc Output Results

Controlled Switching Temperature of Arc Output Results				
Simulation No. (SN)	**Arc Temperature (℃)**	**Current Interruption time (S)**	**Peak Arc time Instant (S)**	**Figure No.**
SN 1	5164.70	0.071	0.065	4.53
SN 2	4872.06	0.060	0.051	4.54
SN 3	4873.71	0.048	0.045	4.55
SN 4	5169.19	0.071	0.068	4.56
SN 5	4867.72	0.060	0.056	4.57
SN 6	4886.80	0.049	0.046	4.58

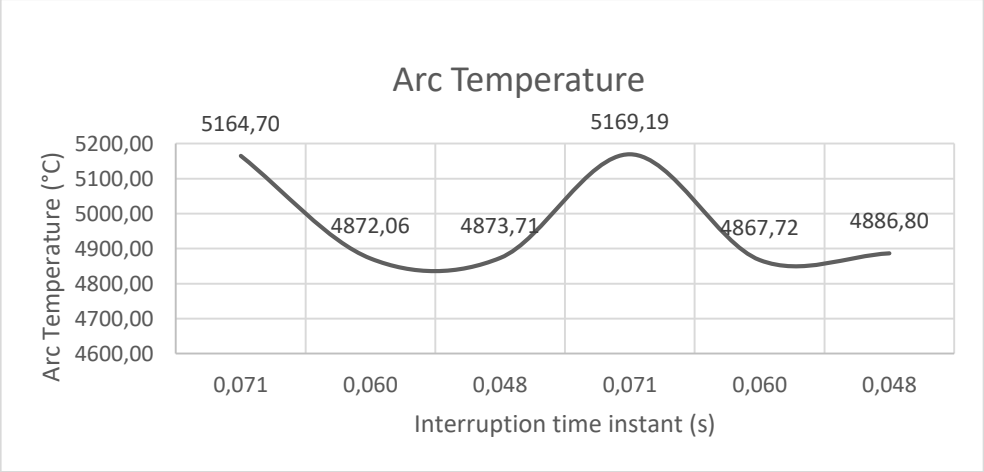

Figure 4.60: Controlled Switching Arc Temperature Vs Interruption Time Instant

4.4.8.3 Case Comparison

The temperature output results in Table 4.23 and 4.24 for SN1 to SN6 confirms that it is proportional to the energy of the arc produced as indicated in Figure 4.53 to 4.58 for both controlled and conventional switching. When the temperature for SN1 to SN6 for advanced controlled switching are compared to that of conventional circuit breaker switching, the temperature rises for advanced controlled switching is on average 32% lower than when conventional circuit breaker switching is implemented. The temperature of the arc follows similar trend as the arc energy produced, consequently the energy of the arc produced is found to be the major influence on the temperature of the arc due to its proportionality. The difference in temperatures recorded between simulations does not have an impact on the circuit breaker lifespan since the arc temperatures changes only contribute to the lifespan expectancy when the arc temperature results are greater than 1000 ℃ [101].

In SN4 to SN6 for advanced controlled switching, when the input parameters relevant to the environment changes, the temperature deviation remains at a 32% average decrease in comparison to the conventional switching simulations SN1 to SN3.The controlled logic adapts the change in environment parameters into its logic to regulate the temperature output. The peak arc time instant for SN1 to SN3 in the conventional simulations decreases as the fault current angle increase. This is also present in the advanced controlled switching simulations. The arc duration is on average 10 *ms* more for advanced controlled switching when compared to conventional tripping. However, when the Peak Arc time Instant (τ) is compared in SN1 to SN6, the conventional switching reaches its peak temperature on average of 0.02 *s* earlier but with a sharp rise as shown in line AB in Figure 4.53 to 4.58 when compared to the line AC of advanced controlled switching. The advanced controlled switching increase to the peak temperature is more regulated with a linear relationship as shown in line AC represented in Figure 4.53 to 4.58.

The lower temperature magnitude on the advanced controlled switching reduces the thermal rise of the arc within the circuit breaker when compared to conventional switching. The highest temperature produced is found for SN1 at 5164.70 $^{\circ}C$ when the power and the energy of the arc is at its highest. The arc temperatures are within the expected circuit breaker withstand capabilities rated for a period of 1 *s* [102]. When the power and energy of the arc is at its lowest point for SN5, the temperature is found to be at its lowest value at 4867.72 $^{\circ}C$ amongst all the simulations for advanced controlled switching. In essence, the arc power and arc energy are proportional to the rate of rise of temperature of the arc produced and the magnitude of the energy produced [103]. The arc energy is proportional to the temperature rise therefore for advanced controlled switching, a lower arc energy is produced due to the lower arc power resulting in the temperature output being lower. Refer to Appendix D for the percentage temperature reduction for each simulation with advanced controlled switching implemented.

Table 4.23: Conventional Arc Temperature Output Results

Conventional Output Results				
Simulation No. (SN)	**Figure No.**	**Arc Temperature ($^{\circ}C$)**	**Current Interruption Time (S)**	**Peak Arc Time Instant (S)**
SN 1	4.105	7287.64	0.057	0.056
SN 2	4.106	7272.28	0.049	0.047
SN 3	4.107	7277.67	0.039	0.035

Table 4.24: Advanced Controlled Arc Temperature Output Results

Advanced Controlled Output Results					
Simulation No. (SN)	**Figure No.**	**Arc Temperature ($^{\circ}C$)**	**Current Interruption Time (S)**	**Peak Arc Time Instant (S)**	**Percentage Temperature Reduction ($\%$)**
SN 1	4.105	5164.70	0.071	0.065	29
SN 2	4.106	4872.06	0.060	0.051	33
SN 3	4.107	4873.71	0.048	0.045	33
SN 4	4.108	5169.19	0.071	0.068	29
SN 5	4.109	4867.72	0.006	0.056	33
SN 6	4.110	4886.80	0.049	0.046	33

4.4.9 Circuit-breaker Lifespan Impact Diagnosis Between Simulations

The overall variance in results when using the advanced controlled switching in comparison to the conventional switching are summarized for all simulations in Appendix D. The difference is evaluated for the power of the arc, energy of the arc and temperature of the arc. The Arrhenius equation (2.23) is used to measure the rate of change relevant to the circuit breaker lifespan with reference to the temperature and energy of the arc.

Table 4.25: Conventional Circuit Breaker Lifespan Results

Conventional Circuit Breaker Lifespan Output Results				
Inputs to Arrhenius equation				**Output Results**
Simulation No. (SN)	**Arc Active Power (W)**	**Energy of Arc Power (J)**	**Peak Arc Temperature ($^{\circ}C$)**	**Rate Constant (k)**
SN 1	3245	138834.18	7287.64	0.109744
SN 2	3351	138541.57	7272.28	0.109750
SN 3	3339	138635.71	7277.23	0.109732

The results obtained from the simulation in Table 4.25 are based on the conventional circuit breaker operation that operates at an average of 40 times a year [91]. The energy of the arc and peak arc temperature in Table 4.25 for the conventional circuit breaker at an average circuit breaker lifespan of 20 years was used. This is a basis for transposition of values into the Arrhenius equation (2.23) to determine the kinetic rate constant (k) results [101] which is subsequently compared to the kinetic rate constant (k) for advanced controlled switching.

Table 4.26: Advanced Ccontrolled Circuit Breaker Lifespan Results

Advanced controlled Circuit Breaker Lifespan Results						
Simulation No. (SN)	**Peak Arc Temperature ($^{\circ}C$)**	**Rate Constant (k)**	**Energy of Arc Power (J)**	**% Change**	**Increased Lifespan (Days)**	**Increased Lifespan (Years)**
SN 1	5164.70	0.113336	98476.21	3.28%	240	0.7
SN 2	4872.06	0.100134	92773.14	8.69%	634	1.7
SN 3	4873.71	0.100208	93096.66	8.76%	647	1.8
SN 4	5169.19	0.113539	98456.21	3.47%	253	0.7
SN 5	4867.72	0.099940	92763.14	8.55%	615	1.7
SN 6	4886.80	0.100795	93076.26	8.94%	653	1.8

The results shown in Table 4.26 for SN1 to SN6 are for a advanced controlled switching circuit breaker that also operates at an average of 40 times a year [91]. The input energy of the arc for all simulations extracted from Table 4.20 and the peak arc temperature in Table 4.26 are transposed using the Arrhenius equation (2.23) to determine the kinetic rate constant (k) and is subsequently used a basis for comparison against the conventional circuit breaker for fault interruption in Table 4.25. The results in Table 4.26 for SN1 to SN6 for advanced controlled switching are produced by using a conventional circuit breaker average lifespan of 20 years as a reference to the conventional circuit breaker rate constant results with equation 4.1 This is to determine the rate of percentage change and increased lifespan results of the advanced controlled switching circuit breaker.

The Table 4.26 results produced in SN1 to SN6 shows an increase in lifespan expectancy of the circuit breaker relevant to the energy and temperature operation for advanced controlled switching. The Lifespan expectancy is also found to be dependent on the fault current angle that's imposed on a circuit breaker over a period of time. In each simulation, the results are based on the circuit breaker being imposed by the same fault current angle over its lifecycle to determine the improved lifespan expectancy. The best yields are for SN3 which is increased by 1.8 years lifespan when the fault angle for interruption is at 90°. The lowest improved Lifespan expectancy of 0.7 years was found for SN1 at a fault current angle of 30°. The remaining results in SN4 to SN6 also underwent a reduction in lifespan days when the environmental conditions changed which yielded the same results as SN1 to SN3 within a 0.1% tolerance when the same fault current angle was applied. Hence, the lifetime expectancy has improved significantly when compared to the conventional circuit breaker for all simulations. The benefits are prevalent of advanced controlled switching which has an increased lifespan average of 7% relating to an

average increase in useful life of 1.4 years. However, the fault current angle if possibly controlled and used together with advanced controlled switching could provide a guaranteed regulated lifespan increase of the vacuum circuit break

Chapter 5

Conclusion and Recommendations

5.1 Conclusion

The results were analysed by simulating the vacuum circuit breaker under a Line-to-Earth fault on a MV Power line, with no advanced controlled logic i.e. the conventional method and subsequently with the advanced controlled switching logic.

The conventional 11 *kV* vacuum circuit breaker without advanced controlled switching logic under fault interruption was simulated using the electromagnetic transient simulation software at variable fault current phase angles. The 11 *kV* vacuum circuit breaker using advanced controlled switching logic under fault interruption was thereafter simulated using the electromagnetic transient simulation software at variable fault current angles and variable input parameters relevant to its environment, namely the temperature, idle time and standard circuit breaker time. The predicted controlled trip time formulae as defined by equation (3.14), was used to verify the electromagnetic transient simulation results of the advanced controlled switching circuit breaker under fault operation. It was shown to be accurate within a 0.1% tolerance, therefore proving equation (3.14) to be effective for this application.

The results of the interruption time and various Interruption Phenomena during the circuit breaker fault interruption under the simulated conditions was captured and analyzed. The simulated results of the conventional circuit breaker under fault operations were then compared to the circuit breaker using an advanced controlled switching logic.

The advanced controlled switching had successfully tripped the circuit breaker at current zero for fault interruption for all simulations The average arc current had reduced by 9% and average arc voltage had reduced by 11% upon implementation of advanced controlled switching. The chopping currents was found to be almost negligible when compared to the non-controlled conventional circuit breaker. The reduction of the chopping currents for advanced controlled switching had triggered the reduction of the transient recovery voltage to an average of 29%. The advanced controlled switching restrike average peak ignition voltage produced for all simulation was constant with an average decrease of 250% which was aided by a lower transient recovery voltage. The overall power of the arc for advanced controlled switching had reduced by an average of 32% due to the reduction in arc current and reduction in restrike voltage.

The overall power interruption results for arc interruption which was dependent on the above-mentioned Interruption Phenomena had revealed the influence it had on the energy of the arc. The energy of the arc was found to be directly proportional to the power of the arc by yielding the same reduction of 32 % in energy produced by the arc. The temperature followed the same trend as the energy of the arc for advanced controlled switching by producing a 32 % decrease in temperature when compared to the conventional non-controlled circuit breaker.

It was concluded that the phenomena's that occurred was interdependent and produced the overall power reduction which was proportional to the arc energy output. This was effectively proportional to the arcing temperature. The analyzed arc temperature and energy results was subsequently transposed using the Arrhenius method for conventional and advanced controlled switching circuit breakers and the findings have indicated an average circuit breaker useful life improvement of 7 % for the advanced controlled switching circuit breaker. However, the useful life of the circuit breaker over and above the implementation of advance controlled switching, was still dependent on the current influence of the fault current angle and the environmental conditions of the circuit breaker. Overall, the application of the advanced control switching method was successful in increasing the useful life of the breaker by a short duration of time. The average useful life of a circuit breaker is 20 years and by extending the lifespan of the circuit breaker by an average of 1.4 years to a new lifespan of 21.4 years, supporting the viability of the hypothesis. The cost of replacement may be differed by 1.4 years which will have a significant impact on the total annual capital expenditure budget for power utilities. Differing capital budget allows for more available funds for maintenance and/or refurbishment of the power system.

5.2 Recommendations

The improved average useful life of 1.4 years successfully allows for a longer equipment lifecycle. However, the capex costs may not be realized due to the higher initial cost to purchase the advanced controlled circuit breaker. The improvement of 7 % in the circuit breakers useful life was determined not to be sufficient to offset the high initial costs for advanced controlled switching circuit breaker when compared to a conventional circuit breaker.

The advantage where its realized, is where the medium voltage controlled circuit breaker is installed on a power gird as it accounts for approximately 56 % of the power girds circuit breakers. The improved useful life time will thus allow power utilities more time in an average maintenance cycle to attend to other areas of maintenance.

The advanced controlled switching vacuum circuit breaker was implemented with the temperature and idle time coupled with standard circuit breaker time taken as the input variables to the environmental conditions to predict the desired interruption time delays to achieve current zero tripping. However, there are areas that may be researched and considered for development to allow for more logic integration with artificial intelligence. The recommendation for areas of development in this technology are as follows:

- Its recommend that the advanced controlled switching logic allow for a more wider variable environmental factors that include certain fluids and vapours namely sulphur hexafluoride and polychlorinated biphenyls asbestos to improve the impact on the circuit breakers efficiency and reliability.
- Investigation into developing logic that can also utilize the current information via fibre connection from the protection relays further upstream or downstream to assist the advanced controlled switching circuit breaker in predicting the fault currents probability earlier, therefore enabling it to achieve an earlier current zero interruption which can possibly compensate for the delays imposed to achieve the current zero tripping relevant to its environment
- Using machine learning to track the breakers reaction to a fault at a specified angle and magnitude and subsequently changing the logic for each fault interruption to adopt an earlier current zero tripping time could possibly improve the circuit breakers interruption times.
- Taxonomical survey on fault currents in power systems and effects on expenditure and power system performances viewpoints.

The research completed in this dissertation may be expanded using the methods above to increase the useful life of the vacuum circuit breaker significantly which will improve capital expenditure to a point that the increased useful life outweighs the higher capital costs required for advanced controlled switching.

References

[1] T. Agarwal (2009, Aug), *Types of Faults and Effects in Electrical Power Systems*, elprocus.com, Sept 19, 2020. [Online]. https://www.elprocus.com/what-are-the-different-types-of-faults-in-electrical-power-systems/.

[2] D. M. et al, "Worldwide reliability study of Intermediate results of Circuit Breakers," in *CIGRE WG A3.06 - Tutorial Course on Reliability of HV Equipment*, Seoul, 2008, pp. 4-15

[3] C. Puret (1992, Jan), *MV Public Distribution Networks Throughout the World*, se.com, Sept 8, 2021. [Online]. https://www.se.com/us/en/download/document/ECT155/.

[4] H. Ito, "Current status and future trend of controlled switching system," *Mitsubishi Electric Adance*, vol. 117, pp. 2-5, 2007.

[5] Gedeon, "The Effects of Arcing," *Material Branch Performance Alloys Technical Tidbits,* vol. 31, p. 2, 2012.

[6] R. Thomas, "Controlled switching of high voltage Sf6 circuit breakers," Chalmers University of Technology, Reproservice, Göteborg, 2004.

[7] V. Edvard (2017, Oct), *The Structure of Electric Power Systems (Generation, Distribution and Transmission of Energy)*, electrical-engineering-portal.com, Oct 19,2017. [Online]. https://electrical-engineering-portal.com/electric-power-systems.

[8] "*Why Generation Voltage in Power Plant is Low (11kVto 33kV)?*" Mar 15, 2014. Sept 8,2018.[Online].http://electricalquestionsguide.blogspot.com/2011/03/why-generation-voltage-in-power-plant.html.

[9] V. Mehta and R. Mehta, in *Principles of Power System*, NEW DELHI, S. Chand & Company LTD, 2004, pp. 50-62.

[10] I. Boci, in *Transmission Bus Configuration Design Philosophy The intent of this document is to provide bus configuration guidelines for new*, New York, Taylor & Francis, 2019, pp. 50-62.

[11] ABB South Africa (2016, Apr), "The problem of overheating inside LV switchboards," ee.co.za, Apr 12, 2016. [Online]. https://www.ee.co.za/article/problem-overheating-inside-lv-switchboards.html.

[12] P. S. R. Murthy, *Power System Analysis*, Hyderabad: BS Publications, 2007, pp 336.

[13] "*We make what matters work*,"eaton.com, Sept 9, 2021.[Online] https://www.eaton.com/us/en-us/company/news-insights/energy transition/buildings-as-a-grid.html.

[14] NRS 048-2, "Electricity Supply — Quality of Supply," NRS, Johannesburg, 2003.

[15] B. Chatterton et al., "Benchmarking distribution network reliability in the future electricity distribution industry (EDI) of South Africa: an international overview, discussion, and summary of key lessons learnt," in *IEEE Power Engineering Society Conference and Exposition in Africa, Power Africa*, Cape Town, 2005.

[16] E. Fahad "Faults in Power System and protection devices against faults," electroniclinic.com, Dec 9, 2020. [Online]. https://www.electroniclinic.com/faults-in-power-system-and-protection-devices-against

[17] "Types of Faults in Electrical Power Systems," electronicshub.org, Nov 12, 2015.Sept 9,2021[Online].https://www.electronicshub.org/types-of-faults-in-electrical-power-systems/.

[18] V. N. Ogar, D. N. Abara and E. J. Akpama, “Symmetrical and unsymmetrical faults analysis: Using Nigeria 330-KV grid as case study,” in *IEEE International Conference on Emerging & Sustainable Technologies for Power & ICT in a Developing Society (NIGERCON),* Owerri, 2017.

[19] H. Ali, S. Saif and F. Alam, “Short Circuit Current Calculation and Prevention In High Voltage Power Nets,” BTH, New York, 2014,pp. 13-17.

[20] I. Adam , “Fundamentals of Protection System,” New York, working paper , Nov.2018.

[21] “Worked example of cable calculation,” electrical-installation.org, Dec 20, 2019. Sept 9,2020[Online].https://www.electricalinstallation.org/enwiki/Worked_example_of_cable_calculation.

[22] A. Waqar, S. Ahmad and T. Yahya, “A communication-less protection strategy to ensure protection coordination of distribution networks with embedded DG,” in *2018 International Conference on Power Generation Systems and Renewable Energy Technologies (PGSRET),* Islamabad, 2018.

[23] R. Mariga (2016, Apr), “Balanced faults”, Sep 16, 2019. [Online]. https://www.slideshare.n et/rodgersmariga/balanced-faults.

[24] I. Kasikci, Short Circuits in Power Systems: A practical guide to IEC 60909-0, 2nd Edition, Hoboken: Wiley, 2018.

[25] V. Ogboh and T. Madueme, “Investigation of faults on the Nigerian power system transmission line using artificial neural network,” *Journal of Renewable and Sustainable Energy Reviews,* vol. 23, no. 2, pp. 342-351, 2015.

[26] V. Gevorgian, M. Singh and E. Muljadi, “Symmetrical and unsymmetrical fault currents of a wind power plant,” in *IEEE Power and Energy Society General Meeting,* 2012.

[27] M. D. Borkar and K. D. Thakur, “Analysis of unsymmetrical fault using symmetrical component for improvement of overcurrent protection scheme,” in *2013 International Conference on Computer Communication and Informatics, Jan 4-6,* New Delhi, 2013, p. 15.

[28] P. C. Sim, C. K. Lee and J. L. You, “A study of arc fault current in low voltage switchboard,” in *IEEE Conference on Sustainable Utilization and Development in Engineering and Technology (STUDENT),* Beijing, 2012.

[29] J. Kaumanns, “Influence of the arcing time on the interruption behaviour and current zero conditions of vacuum circuit breakers,” in *Proceedings ISDEIV. 18th International Symposium on Discharges and Electrical Insulation in Vacuum (Cat. No.98CH36073), Aug 17-21,* New York, 1998.

[30] B. K. Rao and G. Gajjar, “Development and application of vacuum circuit breaker model in electromagnetic transient simulation,” in *Power India Conference, IEEE, 2006,* Mumbai, 2006, p. 7.

[31] S. Wong, L. Snider and E. Lo, “Overvoltage’s and reignition behaviour of vacuum circuit breaker,” in *2003 Sixth International Conference on Advances in Power System Control, Operation and Management ASDCOM 2003 (Conf. Publ. No. 497) Nov 11-14. 2003,* Chicago, 2003.

[32] M. Binnendijk, W. F. H. Merck, R. P. P. Smeets, K. Watanabe and E. Kaneko, “High current interruption in vacuum circuit breakers,” in *Proceedings of 17th International Symposium on Discharges and Electrical Insulation in Vacuum, 21-26 July,* Washington, 1996, p. 281-285.

[33] J. Yan, Z. Ma and L. Jin, “Research on post-arc reignition phenomena for 40.5 kV vacuum interrupter,” in *in XXIst International Symposium on Discharges and Electrical Insulation in Vacuum, 2004. Proceedings. ISDEIV*, 2004, p. 371-373.

[34] C. Wadhwa, Electrical Power Systems Paperback, New Age International Publisher, 2009.

[35] H. Wang et al. “Prestrike Electric Field Characteristics when Switching on Inrush Current in 40.5kV VCB,” in *2018 28th International Symposium on Discharges and Electrical Insulation in Vacuum (ISDEIV), 23-28 Sept*, 2018, pp. 5-6.

[36] E. P. V. Lanen et al., “Vacuum circuit breaker current-zero phenomena,” in *IEEE Transactions on Plasma Science*, vol. 33, no. 5, pp. 1589-1593, 2005.

[37] B. Badrzadeh, “Transient recovery voltages caused by capacitor switching in wind power plants,” in *IEEE Industry Applications Society Annual Meeting, Oct 7-11*, London, 2012, pp. 1-8.

[38] “*Transient Recovery Voltage (TRV) In Interruption of Small Inductive Currents by Circuit Breakers*,” powerandcables.com, Sep 17,2019. [Online]. https://www.powerandcables.com/transient-recovery-voltage/.

[39] A. H. Soloot and H. K. Hoidalen, “Upon the impact of power system and vacuum circuit breaker parameters on transient recovery voltage,” in *2010 Asia-Pacific Power and Energy Engineering Conference, 28-31 March*, Tokyo, 2010, pp. 1-4.

[40] R. P. P. Smeets and W. A. v. d. Linden, “Current-zero measurements of vacuum circuit breakers interrupting short-line faults,” in *IEEE Transactions on Plasma Science*, London, 2003, pp. 12-13.

[41] A. Pertsev, A. Panibratets and L. Rylskaya, “About the prevention of restrike of vacuum circuit-breakers,” in *25th International Symposium on Discharges and Electrical Insulation in Vacuum (ISDEIV)*, Tokyo, 2012, pp. 469-472.

[42] D. Burger, W. K. S. Tenbohlen and W. Ebbinghaus, “Impact of multiple restrikes at vacuum circuit breakers on the EMC of medium voltage switchgear,” in *International Symposium on Electromagnetic Compatibility-EMC EUROPE*, 2012, p. 1-6.

[43] “*Power Circuit Breaker Theory and Design*,” Sep 10, 2021. [Online].: http://kinozoo.ru/pl/?q=power+circuit+breaker+theory+and+design.

[44] J. Ambier and P. Perdigon, “Fretting corrosion of separable electrical contacts,” *IEEE transactions on components, hybrids, and manufacturing technology*, vol. 8, no. 1, pp. 197-201, 1985.

[45] Z. Stanisic, “Method for static and dynamic resistance measurements of HV circuit breaker,” in *2011 2nd IEEE PES International Conference and Exhibition on Innovative Smart Grid Technologies*, 2011, pp. 1-5.

[46] “*What is Contact Resistance*,” carelabz.com, Aug 10, 2020. [Online]. https://carelabz.com/what-contact-resistance-test-why-contact-resistance-testing-done/.

[47] J. Andrea et al., “Model of an electric arc for circuit analysis,” in *International Conference on Electric Contacts*, Edinburgh, 2016, pp. 1-8.

[48] E. Nasrallah (2019), “Electricenergyonline.com,” Electric Energy, May, 2007. [Online]. https://electricenergyonline.com/energy/magazine/306

[49] M. B. Barbieri et al., “Transients due to multiple prestrike phenomenon when energizing Capacitor Banks with a Vacuum Circuit-Breaker,” in *2006 IEEE/PES*

Transmission & Distribution Conference and Exposition: Latin America, Aug 15-18, 2006, pp. 1-6.

[50] Z. Zhang, Y. Nie and W. Lee, "Arc voltage characteristics of medium-low voltage arc fault in short gaps," in *2018 IEEE Industry Applications Society Annual Meeting (IAS), 23-27 Sept,* Beijng, 2018, pp. 1-8.

[51] D. R. Doan, "Arc flash calculations for exposures to DC systems," in *IEEE Transactions on Industry Applications,* New York, 2010, pp. 2299-2302.

[52] A. Lamikiz and S. Martinez, "Thermal advanced machining processes," *In Journal Modern Machining Technology,* vol. 20, no. 2, pp. 15-19, 2011.

[53] "*What is Arc phenomenon in Circuit Breakers and Methods of Arc Extinction*," electricalengineeringinfo.com, Sep 10, 2021. [Online].https://www.electricalengineeringinfo.com/2016/03/what-is-arc-in-circuit-breakers-methods-of-arc-extinction.html

[54] E. Hoagland, M. et al., "Measurements, observations, and Implications of moving electrical-arc behaviour and effect of reclosure events on overhead lines and worker protection," ,*2016, pp. 3501-3507*

[55] S. Xiu et al., "The experimental study of long-gap vacuum arc," in *24th ISDEIV 2010,* 2010, pp. 308-311.

[56] Y. Niwa et al., "The characteristics of the vacuum arc and the interruption ability on the high-speed vacuum circuit breaker," in *20th International Symposium on Discharges and Electrical Insulation in Vacuum,* 2002, p. 435-438.

[57] "*Operating mechanism*," June 10, 2021. [Online]. https://megger.com/applications/circuit-breakers/operating-mechanism.

[58] USNRC, "Circuit Breaker Components and Operation," USNRC, USA, 2021.

[59] D. Chen, J. Z. R. Dai and W. Tong, "Dynamic simulation of operating mechanism for moulded case circuit breaker," in *Electrical Contacts - 2007 Proceedings of the 53rd IEEE Holm Conference on Electrical Contacts, Sept 16-19,* Tokyo, 2007, pp. 188-193.

[60] D. Serve et al., "Mastering all sub-assemblies of medium-voltage circuit-breaker and racking truck system ensures reliability and robustness," in *CIRED - Open Access Proceedings Journal, vol. 2017,* New Jersey, 2017, pp. 312-315.

[61] U. A. Bakshi and M. V. Bakshi, Protection and Switchgear, Pune: Technical Publication, 2009.

[62] R. D. Garzon, High Voltage Circuit Breakers, New York: CRC Press, 2002.

[63] National Standards Authority of Ireland (NSAI), "Electrical accessories - Circuit-breakers for overcurrent," CEN-CENELEC Management Centre, Brussels, 2015, pp. 1-45.

[64] W. Feiming et al. "Test analysis of dielectric recovery characteristic in high voltage SF6 circuit breaker," in *2017 4th International Conference on Electric Power Equipment - Switching Technology (ICEPE-ST), Oct 22-25,* Beijing, 2017, pp. 22-25.

[65] R. Yeckley and J. Perulfi, "Oil Circuit Breakers: A look at the earlier generation history," in *IEEE Power and Energy Magazine,* New York, 2018, pp. 86-97.

[66] D. C. Prince and W. F. Skeats, "The Oil-Blast Circuit Breaker," in *Transactions of the American Institute of Electrical Engineers,* Washington, 1931, p. 506-512.

[67] T. Wenzel, T. Leibfried and D. W. Retzmann, "Dynamical simulation of a vacuum switch with PSCAD," *IEEE T POWER DELIVER,* pp. 1-11, 2008.

[68] D. Goldsworthy et. al, “Controlled switching of HVAC circuit breakers: Application examples and benefits,” in *Protective Relay Engineers, 2008 61st Annual Conference IEEE*, 2008, pp. 520-535.

[69] C. Cereda, “Synchronous medium voltage circuit-breakers: ABB solution based on magnetic drive and electronic control,” in *CIRED 99-15th Conference on Electricity Distribution, Nice, June*, London, 1999, pp. 100-120.

[70] C. Cao and X. Lin, “Dynamic simulation and closing bouncing analysis on the 12kV vacuum circuit breaker with permanent magnetic actuator,” in *2013 2nd International Conference on Electric Power Equipment - Switching Technology (ICEPE-ST)*, Pune, 2013, pp. 20-23.

[71] E. Boghiu, at al. “Aspects regarding controlled switching of the vacuum circuit breaker,” in *2017 International Conference on Electromechanical and Power Systems (SIELMEN), Oct 11-13*, New York, 2017, pp. 11-13.

[72] M. L. Eng and A. G. Eng, “Controlled switching and circuit breaker monitoring,” in *2017 IEEE 37th Central America and Panama Convention (CONCAPAN XXXVII), 15-17 Nov*, Washington, 2017, pp. 1-5.

[73] Abhilash and K. S. Smitha, “Reduction of transformer inrush current by controlled switching method,” *International Journal of Scientific & Engineering Technology*, vol. 7, no. 4, pp. 628-635, 2019.

[74] M. André at al., Controlled switching of HVAC CBs - Guidance for further applications including unloaded transformer switching, New York: ELECTRA, 2004.

[75] C. E. Solver at al., “First results from on-going CIGRÉ enquiry on reliability of high voltage equipment,” in *Present and future of high voltage equipment and substation technologies*, Chicago, 2005.

[76] T. Olsen (2005, Jan), “Electrical equipment lifespan: watt in the world,” new.siemens.com, Jan 2, 2020. [Online]. https://new.siemens.com/us/en/products/energy/product-support/t-d-guardian-articles/electrical-equipment-lifespan-watt-in-the-world-.html.

[77] J. Clark (2002, Oct), “Rate constants and the Arrhenius equation,” chemguide.co.uk, Oct 13, 2002. Sept 02, 2021 [Online]. https://www.chemguide.co.uk/physical/basicrates/arrhenius.html.

[78] K. Jeong, et al., “A study on the statistical life span estimation of aged low-voltage circuit breakers,” *Journal of Electrical Engineering & Technology*, vol. 15, no. 6, pp. 2833-2839, 2020.

[79] R. Thomas, “Three phase controlled fault interruption using high voltage Sf6 circuit breakers,” in *Doctorate, Department of Energy and Environmental, School of Electrical Engineering, Chalmers University of Technology*, Goteborg, 2007, pp. 51-170.

[80] A. I. Aio, “Modelization and analysis of the electric arc in low voltage circuit breakers,” Universidad del País Vasco - Euskal Herriko Unibertsitatea , 2013.

[81] L. Yuan, L. Sun and H. Wu, “Simulation of fault arc using conventional arc models,” *Energy and Power Engineering*, vol. 5, no. 4, pp. 833, 2013.

[82] Y. Eshaf et al., “Simulation of switching arc using modified mayr arc model,” *IEEE Transactions on Power and Energy*, vol. 122, no. 1, pp. 40-45, 2002.

[83] P. H. Schavemaker and L. V. d. Slui, “An improved Mayr-type arc model based on current-zero measurements,” *IEEE Transactions on Power delivery*, vol. 15, no. 2, pp. 580-584, 2000.

[84] L. D. Wright and C. R. Wetter, “Mayr's Model of the arc applied to 50-and 60-Hz Interruption in Low-Voltage Devices,” *IEEE Transactions on Industry Applications,* vol. 21, no. 6, pp. 1343-1348, 1985.

[85] X. Zhang, J. Zhang and G. Pietsch, “Estimation of the arc power during a three-phase arc fault in MV electrical Installations,” *IEEE Transactions on Plasma Science,* vol. 35, no. 3, pp. 724-730, 2007.

[86] K. Nowak, J. Janiszewski and G. Dombek, “The possibilities to reduce arc flash exposure with Arc,” *Energies,* vol. 14, pp. 1-25, 2021.

[87] K. C. P. Wong, H. M. Ryan and Tindle, “Power system fault prediction using artificial neural networks,” *ORO,* vol. 5, no. 1, pp. 1181-1186, 1996.

[88] “*8h.wasaskolana.online*”, “P438 Relay Manual,”, Jun 23,2017. May 12 , 2019 [Online].: https://8h.wasaskolan1a.online/mbo2.

[89] “*How hot can circuit breakers get*?” se.com, Sep 10, 2021. [Online].: https://www.se.com/us/en/faqs/FA173839/

[90] Z. Huang at al., “Improvement of breaking capability of vacuum circuit breaker using controlled fault interruption,” in *2013 2nd International Conference on Electric Power Equipment - Switching Technology (ICEPE-ST), Oct 20-23,* Beijing, 2013, pp. 1-4.

[91] J. Tobias et al., “Impact of operating mechanism type on MV vacuum circuit-breaker reliability,” in *CIRED Conf,* 2015.

[92] M. Edla et al., “An improved rectifier circuit for piezoelectric energy harvesting from human motion,” *Applied Science,* vol. 11, no. 5, pp. 790-810, 2008.

[93] “*PSCAD Knowledge Base*,” pscad.com, Aug 10, 2019. [Online]. Available: https://www.pscad.com/knowledge-base.

[94] “*More information from the unit converter*,” convertunits.com, Sep 10, 2021. [Online]. Available: https://www.convertunits.com/from/celsius+heat+unit/to/joule.

[95] K. M. Dantas et al., “On applying controlled switching to transmission lines: Case studies,” in *International Conference on Power Systems Transients (IPST),* Zurich, 2009, p. 9.

[96] “*Power Point Arc 2*,” May 2, 2021. [Online].: https://www.scribd.com/document/35312530/Power-Point-ARC-2.

[97] “Sample records for switches circuit breakers,” 10 Sep 10, 2021. [Online].: https://worldwidescience.org/topicpages/s/switches+circuit+breakers.html

[98] K. Kamei and H. Kohyama, “Field experience of controlled switching system used for transformer switching,” *Mitsubishi Electric Advance,* vol. 117, pp. 18-21, 2007.

[99] H. Bahirat, M. Ali and K. Praveen, “Effects of transient recovery voltages on circuit breaker ratings,” *Instructor,* pp. 1-8, 2008.

[100] S.C. Kam, “Assessing of circuit breaker restrike risks using computer simulation and wavelet analysis,” Queensland University of Technology, Queensland, 2012.

[101] S. S.Chandankar and A. A.Bhole, “Review: to investigate impacts of various factors on the Characteristics of Transient Recovery Voltage,” *International Journal of Advanced Research in Electrical Electronics and Instrumentation Engineering,* vol. 5, no. 12, pp. 8821-8825, 2016.

[102] F. Ledbetter and D. Waltershied, “Medium voltage vacuum circuit breaker life Medium-Voltage Vacuum CIrcuit Breaker Life Extention,” vdocument.in, Jun 16,2020. [Online].https://vdocument.in/medium-voltage-vacuum-circuit-breaker-life-medium-voltage-vacuum-circuit-breaker.html.

[103] P. Kumar et al., “Internal arc fault simulation in medium voltage panel for thermal and structural withstand,” in *2018 IEEE Holm Conference on Electrical Contacts*, Delhi, 2018, pp. 405-411.

Appendices

Appendix A

Table A-1 :Advance Controlled Switching Calculated Results

Advanced controlled switching calculated results								
Input Parameters into $T_{If} = I_F . [sin(\omega \cdot t + \alpha - \varphi) - sin(\alpha - \varphi) \cdot e^{(-t/\tau)}]$								**Output Results of** T_{If}
Simulation No.	***α (deg)-Pf Curve (0,30, 60,90)***	***φ(deg)***	***Cycle (s)***	***ωL/R***	***τ = L/R***	***[sin (ω ·t + α – φ)***	***sin (α – φ) · e (–t/τ)***	***Tif (s)***
1	30	77.73	0.08	4.59	0.015	0.74002182	-0.373759544	0.02727713
2	60	77.73	0.17	4.59	0.015	0.304586264	-0.153836036	0.01865665
3	90	77.73	0.25	4.59	0.015	-0.212462935	0.107307714	0.00842043
4	30	77.73	0.08	4.59	0.015	0.74002182	-0.373759544	0.02727713
5	60	77.73	0.17	4.59	0.015	0.304586264	-0.153836036	0.01865665
6	90	77.73	0.25	4.59	0.015	-0.212462935	0.107307714	0.00842043

Appendix B

Table B-1 : Input to Predicted Controlled Trip Equation for Advance Controlled Switching

Inputs to Predicted Controlled Trip Equation $T_{co} = \lfloor (T_{If}) + (\Delta T_{temp} + \Delta T_{Idle} + T_{std})] \rfloor [(T_{If}) + (\Delta T_{temp} + \Delta T_{Idle} + T_{std})] + 0.01 \rfloor$			
CB Std operating time (open + Arc) - Tstd in (s)	**CB Temperature time delay (s) - ΔTtemp**	**CB Idle time delay (s) - ΔTIdle**	**Fault Time instant ΔIF(s)**
0.03505	0.00054	0.000031	0.02727713
0.03505	0.00054	0.000031	0.018656648
0.03505	0.00054	0.000031	0.00842043
0.03505	0.00048	0.000031	0.02727713
0.03505	0.00054	0.000077	0.018656648
0.03505	0.00138	0.000155	0.00842043

Table B-2 :Output Results from Equation for Advanced Controlled Switching

Output Results Predicted Controlled Trip Equation $T_{co} = \lfloor (T_{If}) + (\Delta T_{temp} + \Delta T_{Idle} + T_{std})] \rfloor [(T_{If}) + (\Delta T_{temp} + \Delta T_{Idle} + T_{std})] + 0.01 \rfloor$		
Arcing Time (s)	**Total Delay Time (s)**	**Predicted Current Zero Trip Time (s) Tco**
0.0427	0.0629	0.0710
0.0413	0.0543	0.0600
0.0416	0.0440	0.0490
0.0427	0.0628	0.0700
0.0413	0.0543	0.0590
0.0416	0.0450	0.0049

Appendix C

Table C-1: Conventional Switching Simulated Results

Conventional Simulation Results				
Simulated Tco	**Peak Simulated Ps (kW)**	**Peak Simulated Qs (kVar)**	**Peak Energy (J)**	**Conventional Temp (°C)**
0.057	3245	77.00	138834.18	7287.6
0.049	3351	0.000	138541.67	7272.3
0.039	3339	255.00	138635.71	7277.2
0.0623	3245	77.00	138834.64	7287.6
0.0573	3351	0.000	138541.28	7272.3
0.0435	3339	255.00	138635.23	7277.2

Table C-2: Advanced Controlled Switching Simulated Results

Advanced Controlled Switching Results				
Simulated Tco	**Peak Simulated Ps (kW)**	**Peak Simulated Qs (kVar)**	**Energy (J)**	**Controlled Temp (°C)**
0.070	2303.00	5.40	98476.21	5164.70
0.060	2245.00	39.30	92773.14	4872.06
0.050	2233.00	-40.00	93096.66	4873.71
0.071	2305.00	34.00	98456.21	5169.19
0.060	2243.00	65.00	92763.14	4867.72
0.049	2239.00	-62.00	93076.26	4886.80

Appendix D

Table D-1: Results Difference – (Conventional Vs Controlled)

Result Differences - (Conventional Vs Controlled)				
TCO (Conv Vs Controlled) - (ms)	**PS (kw)**	**QS (kVar)**	**TCO (Simulated Vs Calc)**	**% Temp Decrease**
13.0	942.0	71.6	0	29%
11.0	1106.0	-39.30	0	33%
11.0	1106.0	295	0	33%
8.7	940.0	43.00	-1	29%
2.7	1108.0	-65.00	0	33%
5.5	1100.0	317.00	1	33%

Table D-2: Advanced Controlled Switching Energy and Temperature Efficiency Results

Advanced Controlled Switching - Energy and Temperature Efficiency				
Difference in Energy(J)	**Temp Decrease (°C)**	**System Power Ps - (kW)**	**System Fault Power - (kW)**	**System Energy (J)**
40443.41	2,122.94	3,843.00	427,336.36	164,183.99
45725.75	2,400.22	3,843.00	427,336.36	158,882.50
45788.53	2,403.52	3,843.00	427,336.36	159,790.29
40357.97	2,118.46	3,843.00	427,336.36	164,183.99
45808.43	2,404.56	3,843.00	427,336.36	158,882.50
45539.05	2,390.42	3,843.00	427,336.36	159,790.29